Control of the ICE-Harvest System using an Advanced Multi-Agent Framework

Control of the ICE-Harvest System using an Advanced Multi-Agent Framework

By Joshua Fitzpatrick, B.Eng.

A Thesis Submitted to the School of Graduate Studies in Partial Fulfilment of the Requirements for the Degree Master of Applied Science

Master of Applied Science (2022) McMaster University

(Electrical & Computer Engineering) Hamilton, Ontario, Canada

TITLE: Control of the ICE-Harvest System using an Advanced Multi-Agent Framework

AUTHOR: Joshua Fitzpatrick

B.Eng., (Electrical Engineering)

McMaster University (Hamilton, Ontario, Canada)

SUPERVISOR: Dr. Mehdi Narimani and Dr. James Cotton

NUMBER OF PAGES: xiii, 139

Abstract

This thesis presents the development of an advanced control structure for the novel Integrated Community Energy and Harvesting (ICE-Harvest) system. The ICE-Harvest system is similar to a District Energy (DE) system in many ways and is different in others. It consists of a set of energy producing and storage units coupled to a thermal network which connects residential and commercial buildings of various types. Its operation is geared towards addressing challenges associated with the current energy landscape in Ontario, with potential to be applicable elsewhere in Canada. The control of this system is based on the implementation of a Multi-Agent System (MAS) combined with Sequential Logic Controllers (SLCs). Results demonstrate the capability of the developed control framework to operate the ICE-Harvest system while ensuring the thermal and electrical energy supply to the different consumers. Based on the results presented, the operation of the ICE-Harvest system by the developed control framework is compared with that of a Business-As-Usual (BAU) scenario. This comparison demonstrates the capability of the developed control framework to operate the ICE-Harvest system in a way that also increases the energy utilization and reduces emissions.

Acknowledgements

I would like to extend my deepest gratitude to my supervisors, Dr. James Cotton and Dr. Mehdi Narimani, for their leadership and support. I would like to thank you for the opportunity of further education in topics that I am passionate about. I hope to use the knowledge and skills I have developed through your guidance to make a positive impact in my career. It has truly been a pleasure to work with you.

I also wish to express my gratitude to Dr. Jorge Chebeir for his mentorship throughout my graduate studies. I appreciate the time and effort you have put towards assisting me on this journey. Working with you has been fantastic. I would also like to thank my colleagues at McMaster University and HCE Energy for their support and words of encouragement. Thank you all for making this a more positive experience.

My utmost appreciation goes to my family and those closest to me. Without you, I would not be who I am today, and would not have accomplished what I have up to this point, let alone reach this milestone. I can never repay you for all you have done for me.

This work was supported by the Natural Sciences and Engineering Research Council of Canada [CRDPJ 401203143-2018]; and the Ontario Centre of Excellence [27851-2018]. I would like to acknowledge the McMaster Energy Research Cooperative partners for their contributions: HCE Energy Inc., GridSmartCity, GeoSource Energy Inc., s2e Technologies Inc., Siemens Canada Limited, Enbridge Gas Inc., and Alectra Utilities Corporation. Lastly, I would like to thank Modelon Inc., and Lawrence Berkeley National Laboratory for their contributions in the form of the Modelica libraries used in this work.

Table of Contents

List of Tables

List of Figures

Notations and Abbreviations

Nomenclature

T	Temperature (°C)
Q	Thermal Power (kW)
P	Electrical Power (kW)
η	Efficiency (unitless)
τ	PID Controller Time Constant (s)
K_P	PID Controller Gain (unitless)
$\dot{m}$	Mass Flow Rate (kg/s)
V	Voltage (V)
f	Electrical Frequency (Hz)
E	Electrical Energy (kWh)
C	Cost (tCO2eq)
p	Price per W of Fuel Consumed (tCO_2eq/W)

Subscripts

max	Maximum value of parameter or number in set
min	Minimum value of parameter or number in set
CHP	Quantity pertaining to CHP
HP	Quantity pertaining to Heat Pump
NGB	Quantity pertaining to Natural Gas Boiler
H	Quantity pertaining to Heat Pump Condenser

C	Quantity pertaining to Heat Pump Evaporator
EMC	Quantity pertaining to Energy Management Center
MTN	Quantity pertaining to Micro-Thermal Network
STES	Quantity pertaining to Short-term Thermal Energy Storage
BTES	Quantity pertaining to Borehole Thermal Energy Storage
EES	Quantity pertaining to Electrical Energy Storage
HH	Quantity pertaining to Hot Header
WH	Quantity pertaining to Warm Header
AC	Quantity pertaining to Low-Voltage AC Network
DC	Quantity pertaining to Low-Voltage DC Network
el	Quantity pertaining to electrical energy generation or storage
th	Quantity pertaining to thermal energy generation or storage
inl	Quantity pertaining to heat exchanger inlets
r	Quantity which is a ratio of other parameters
P	Quantity pertaining to Proportional Part of PID Controller
I	Quantity pertaining to Integral Part of PID Controller
D	Quantity pertaining to Derivative Part of PID Controller
Rated	Quantity which Corresponds to Operation at Full Capacity
Set	Referring to a Setpoint

Abbreviations

ICE-Harvest	Integrated Community Energy & Harvesting
DE	District Energy

MAS	Multi-Agent System
SLC	Sequential Logic Controller
BAU	Business-As-Usual
GHG	Greenhouse Gas
ETS	Energy Transfer Station
PID	Proportional-Integral-Derivative
SISO	Single-Input Single-Output
CHP	Combined Heat & Power
UTN	Unidirectional Thermal Network
COP	Coefficient of Performance
NGB	Natural Gas Boiler
STES	Short-term Thermal Energy Storage
BTN	Bidirectional Thermal Network
PV	Photovoltaic
BTES	Borehole Thermal Energy Storage
ATES	Aquifer Thermal Energy Storage
PLC	Programmable Logic Controller
EMC	Energy Management Center
MTN	Micro-Thermal Network
EES	Electrical Energy Storage

Chapter 1

Introduction

1.1 Motivation

In recent years, climate change has become an impending and serious issue facing humanity. The tangible effects of climate change can be seen worldwide and have resulted in a variety of devastating phenomena on a global and local scale [1], [2]. In order to reverse its detrimental effects on the environment and prevent long-term irreparable damage, there is a greater need to make efficient use of resources and limit the emission of greenhouse gases (GHGs) [3], [4]. In accordance with the Paris Agreement of 2015, collective action must be taken by an increasing number of countries to reduce global GHG emissions to a net zero level. Currently, 131 of the world's nations have implemented policies and targets to accomplish the climate goals established in the Paris Agreement [5]. As such, the

Government of Canada has set an emissions reduction target of 40% by 2030, followed by a target of net-zero emissions by 2050 [6]. In 2018, human activity accounted for 52 $GtCO_2eq$ of emissions, 34% of which was attributed to the energy sector [7]. As such, targeting GHG emissions reduction in the energy sector is a pathway that can make a significant impact toward reaching overall targets. There are a wide variety of approaches to accomplish this, and GHG reduction measures can be implemented anywhere between source and end use.

Replacing fossil fuels in power generation with synthetic fuels or biofuels can reduce GHG emissions while providing benefits such as increased ease of storage and transport [8]–[11]. Plant-based biofuels also have the additional benefit of removing carbon dioxide from the air during the production process, offsetting GHG emissions from use of the fuel [8]. As old power plants are retired and new energy infrastructure is built, opting for carbon-free power generation technologies, such as wind and solar, can contribute to lowering grid emissions over time. Effective storage technologies and advanced operating schemes will be required to overcome the challenges associated with renewable generation and increase their share in the grid electricity mix [12], [13]. Reducing energy consumption at the end users can also significantly decrease GHG emissions. Buildings have been a target for GHG emissions reductions for a number of years, and there are many methods to improve building energy use [14]. Improvements in building design have led to increased thermal energy efficiency and decreased energy consumption [15]–[17].

There are a variety of techniques to accurately model building properties. This makes it possible to predict changes in the indoor thermal conditions in response to various factors [18]–[21]. These predictions can then be utilized by building automation systems

to manipulate thermal or electrical loads and reduce energy consumption [22]–[26]. In turn, emissions associated with electricity consumption and thermal conditioning are reduced. These improvements are primarily focused on reducing thermal losses of buildings and usage of heating, cooling and electrical equipment, rather than the ways in which energy is generated and delivered.

It is widely recognized that buildings occupy a large portion of energy use and resulting GHG emissions [14], [27]. Furthermore, 29% of worldwide energy use came from buildings in communities (Residential, Commercial and Public Service sectors) in 2018 [28]. In Canada, community buildings represent an even larger share of total energy consumption at 37% [29]. Natural gas is the most-used source of energy in communities, representing approximately 48.1% of energy consumption in the residential and commercial sectors. In addition, electricity represents 36.1% of energy consumption in the residential and commercial sectors. In 2020, communities used approximately 1444.8 PJ of natural gas and 1086.2 PJ of electricity, which represented an increase of approximately 5.3% and 18.9% respectively in the last 15 years [29]. Additionally, natural gas is used in power generation, most often to meet the increased demand during peaks. As annual electricity consumption rises, it is predictable that the magnitude of electrical peaks and associated natural gas use will increase as well. Therefore, improving energy efficiency and utilization at the community level can significantly reduce primary energy consumption and GHG emissions.

District Energy (DE) systems have shown enormous potential to deliver thermal energy to community buildings while accomplishing these objectives. This is especially true for 4^{th} and 5^{th} Generation DE systems, due to their low operating temperature. This

development has facilitated the reduction of heat loss in distribution pipes, incorporation of a variety of renewable and non-renewable energy producers and integration of thermal and electrical energy networks [30]–[36]. Furthermore, key improvements have been performed in 5th generation systems including the ability to provide both heating and cooling with the same equipment, and operating temperature that follows the ground temperature to minimize thermal loss [31].

As is the case with all energy distribution systems, it is necessary to ensure the continuity of service to the consumer. This turns the integrated control structure of these systems and their components into a critical issue for successful operation. In conventional DE systems, the control structures are designed to meet the thermal needs of buildings by maintaining supply water temperature and differential pressure of the network heating and cooling lines, by controlling heating and cooling equipment and pumps at a central energy plant [31]. A building controls its mass flow rates using pumps and valves installed in the Energy Transfer Station (ETS) connecting it to the network, adjusting thermal energy flow and influencing building temperature [37]. In most modern DE systems, control is distributed, with local controllers at the connection points of the producers and consumers with the network. Each of the distributed controllers maintains the required temperature for the producer/consumer, while the network temperature varies according to the action of each controller [31]. Typically, a proportional-integral (PI) or proportional–integral–derivative (PID) controller is implemented to control the mass flow rate and in turn the temperature of a fluid stream. When using multiple single-input single-output (SISO) controllers such as PIDs, the interaction between controllers as they act on the same system. The action of one controller will affect the input conditions of the next and so on. As a

thermal network becomes large and the number of local controllers increases, it becomes increasingly difficult to analyze the system and tune each controller accordingly [38]. Therefore, the proper tuning of the control structure for a large thermal system may represent a challenging task. An alternative control approach is needed to maintain the reliable supply of thermal energy. Unfortunately, there is little research done on the control of state-of-the-art DE systems [31]. As DE systems integrate a wider variety of integrated technologies to generate, transfer and store thermal and electrical energy, increasingly sophisticated control systems will be necessary. Advanced control structures will also be required to implement desirable features and operational strategies that further reduce energy consumption and GHG emissions for DE systems.

1.2 Contribution

This thesis presents the conception and development of an advanced multi-level control framework proposed for operation of the Integrated Community Energy and Harvesting (ICE-Harvest) system. This system aims to improve the utilization of energy and reduce the GHG emissions of communities. It consists of a centralized set of energy generation and storage units which are connected to a thermal network or a low-voltage electrical network. These provide the energy required to meet the heating, cooling and electricity demands of several buildings connected to the networks. The ICE-Harvest system incorporates many features from the 4th and 5th generations of DE systems, such as low temperature operation and the use of a diverse mix of thermal and electrical energy sources. However, there are also key differences between the ICE-Harvest system and 4th and 5th generation DE systems. The ICE-Harvest system employs a unique operational

strategy in which different thermal energy sources are operated depending on the current state of Ontario's electricity grid. During periods of peak electrical demand, the ICE-Harvest system harvests thermal energy from on-site electricity generation. Conversely, during off-peak periods, the system utilizes electrical power in heat pumps at the connected buildings to harvest thermal energy rejected from cooling processes. The thermal energy harvested through these methods is utilized to meet heating demands of buildings, or is stored seasonally in a geothermal borehole field. The operation of the ICE-Harvest system in this manner results in a complex control problem and system dynamics. The developed control structure utilizes the concept of a Multi-Agent System (MAS) in addition to Sequential Logic Controllers (SLCs) and conventional control techniques to effectively manage the aforementioned effects.

1.3 Thesis Structure

The remainder of this work is organized as follows:

Chapter 2 presents a comprehensive review of the literature related to DE and similar systems, the control of such systems and Multi-Agent control frameworks. This includes a brief history of DE systems and their development over time, as well as discussion of various other traditional and modern control techniques.

In Chapter 3, the structure and capabilities of the ICE-Harvest system, as well as the thermal and electrical components are described. Chapter 3 also provides a detailed explanation of each facet in the developed control structure, and their interaction.

In Chapter 4, the case study is introduced and its input parameters and scope are defined. A detailed description of the methodology used to model the ICE-Harvest physical system and control structure is also presented in this chapter.

Chapter 5 presents the results obtained from simulation of the model, and the analysis of the control system performance over short-term and long-term periods. The cumulative results for the case study and corresponding analysis are also presented in Chapter 5.

In Chapter 6, conclusions from the work are presented and potential future work is discussed. These include future developments for the control framework presented in this thesis, as well as for future iterations of the ICE-Harvest system.

Chapter 2

District Energy and Control

2.1 Development of District Energy

Since their conception in the late 19th century, DE systems have changed significantly. These systems have been categorized into five generations in the literature based on the time period and technologies utilized [32]. Despite these distinctions, all DE systems deliver thermal energy to buildings through an underground piping network. Typically, production of thermal energy is centralized, however modern DE systems can employ a combination of centralized and distributed generation. Additionally, modern DE systems typically include both renewable and non-renewable sources of thermal and electrical energy [31]. This diverse energy mix is crucial to the success of DE and similar energy systems in facilitating a zero-carbon future. By utilizing a diverse set of generation

technologies, energy systems can reduce their usage of fossil fuels at a gradual pace to reach long term goals. Over the next decades, DE systems will continue to evolve; therefore, it is also important to understand the evolution of DE from the first generation to now.

The first generation of DE systems was established in the United States in the 1880s. These systems centralized the generation of heating by producing and delivering pressurized steam at temperatures up to 200 °C. Similarly, centralized cooling generation was provided by distributing refrigerant from a central plant to building cooling systems [32]. This centralization of generation was the key value of the early DE systems, since a fleet of large steam boilers can be operated with greater efficiency than individual building units operating at part load. Dedicated boilers and furnaces in buildings are sized to meet expected peak heating demand, therefore they operate at a significantly lower output level for the majority of the heating season. This results in lower energy efficiency since thermal energy producing units are typically most efficient when operating at full capacity. This issue becomes magnified with a greater number of buildings with this configuration of heating system.

In the centralized production of thermal energy in DE systems, multiple boilers are operated simultaneously to meet the total heating demand of the system. This allows the output of individual boilers to be controlled in order to keep the energy efficiency of the fleet as high as possible. This is accomplished by operating an appropriate number of boiler units at full capacity and at partial loads. If the heating demand is sufficiently low, some of the boiler units can shut down since not all of the boilers are needed to meet the demand. Unfortunately, these systems still suffer from significant thermal energy loss from

distribution pipes to the ground due to their high operating temperature, nullifying some of the efficiency gain from centralizing generation. The benefits of the early DE systems outweighed this drawback, and they were utilized in a variety of places until the beginning of the second generation [32].

In the 1930s, DE systems began to utilize pressurized water instead of steam to provide heating. This transition marked the beginning of the second generation of DE systems. The operating temperatures utilized in this period were significantly lower than during the first generation, but still greater than 100 °C [32]. The reduction in temperature led to an increase in system efficiencies, however the operating temperatures of second generation DE systems still resulted in significant energy loss in distribution pipes. Cooling remained largely the same until the 1960s when cold water from mechanical chillers was used to provide cooling instead of refrigerant [32]. Due to the significant improvement over the first generation, the second generation became the dominant technology for DE systems.

The third generation of DE systems began in the 1970s. This advancement in technology allowed for heating delivery at temperatures less than 100 °C and to incorporate other sources of heat such as combined heat and power (CHP), solar and geothermal energy. In the 1990s, DE systems began to incorporate different cooling sources. In addition to the mechanical chillers already in operation, absorption chillers and natural cooling sources were being utilized. Another key feature of the third generation was the transition from in situ construction to pre-fabricated components [32]. These trends would continue into the next generations and set the foundation for the modern DE systems in operation all over the world.

The first three generations of DE systems can be considered conventional DE technology, since these types of systems are no longer used. Modern DE technology includes both the fourth and fifth generations, which represent a shift toward a more versatile and sustainable approach to energy systems. The vast majority of new and existing systems utilize these technologies and have demonstrated the ability to further reduce capital and operating costs, as well as GHG emissions in a variety of ways [31], [34], [36], [39]. Although there are grey areas and overlaps in the fourth and fifth generations, there are defining characteristics that provide some distinction between the two.

The trend of decreasing temperature continues into the fourth and fifth generations; the difference between the two lies in their typical ranges of supply temperatures. Fourth generation systems operate with distribution pipe temperatures ranging between 30 °C and 70 °C, while fifth generation systems utilize lower distribution temperatures, often close to that of the ground. Both types of DE system provide further reduction of thermal energy loss in distribution pipes and allow for the inclusion of low-grade heat sources such as solar-thermal energy and waste heat [31], [32]. Modern DE systems also represent a movement towards a more diverse energy mix, which involves the integration of heating, cooling and electricity, and an increase of renewable energy sources. The energy producers in modern DE systems can be utilized in a centralized or decentralized approach, or some combination thereof [31], [32], [34], [40], [41]. As a result of these factors, modern DE systems are highly flexible compared to conventional systems, and produce significantly less GHG emissions.

Improved energy efficiency due to the reduction of pipe losses leads to significant reduction in energy consumption. Therefore, a modern DE system can provide the same

amount of energy with reduced fuel and electricity usage compared to a conventional system. This reduces GHG emissions, while simultaneously decreasing the operating costs of the system. Increasing the energy efficiency of the system can also allow for reduction in the size of the energy producing equipment, which leads to a reduction of the associated capital cost.

Further reduction of cost and GHG emissions are achieved through the diverse energy mixes which modern DE systems utilize. Naturally, the inclusion of carbon-free renewable energy sources will decrease the GHG emissions produced by a DE system. Utilizing various sources of waste heat also results in lower GHG emissions by offsetting thermal energy production from the other units in the system. Waste heat and renewable energy sources can contribute to reducing operating costs, since they both offset the use of fuels which need to be purchased. Additionally, as carbon taxes continue to increase, the reduction in fossil fuel use provided by these alternatives becomes more valuable financially. Although the installation of renewables and waste heat recovery systems represent an increase in capital cost, the resulting decrease in operating cost can offer a reduction of total cost of the system over its lifetime.

Thermal energy produced can be delivered to buildings in the DE system using a variety of distribution piping network configurations. Modern network topologies can facilitate the reduction of cost and GHG emissions. However, modern DE systems can also utilize the four-pipe topology of traditional thermal networks, which could be preferrable in a retrofit scenario. This is because the capital cost of the network piping represents the majority of the capital cost associated with the construction of a DE system [39]. Therefore, it can be financially advantageous to leave existing pipes in the ground, provided they are

not approaching end of life. In a conventional four-pipe thermal network, heating and cooling are provided by two-pipe systems, each with a supply and return line. In this configuration, thermal energy is transferred to and from buildings via heat exchangers connected to the respective supply and return lines. The structure of a DE system with a typical four-pipe thermal network is depicted in Figure 2.1.

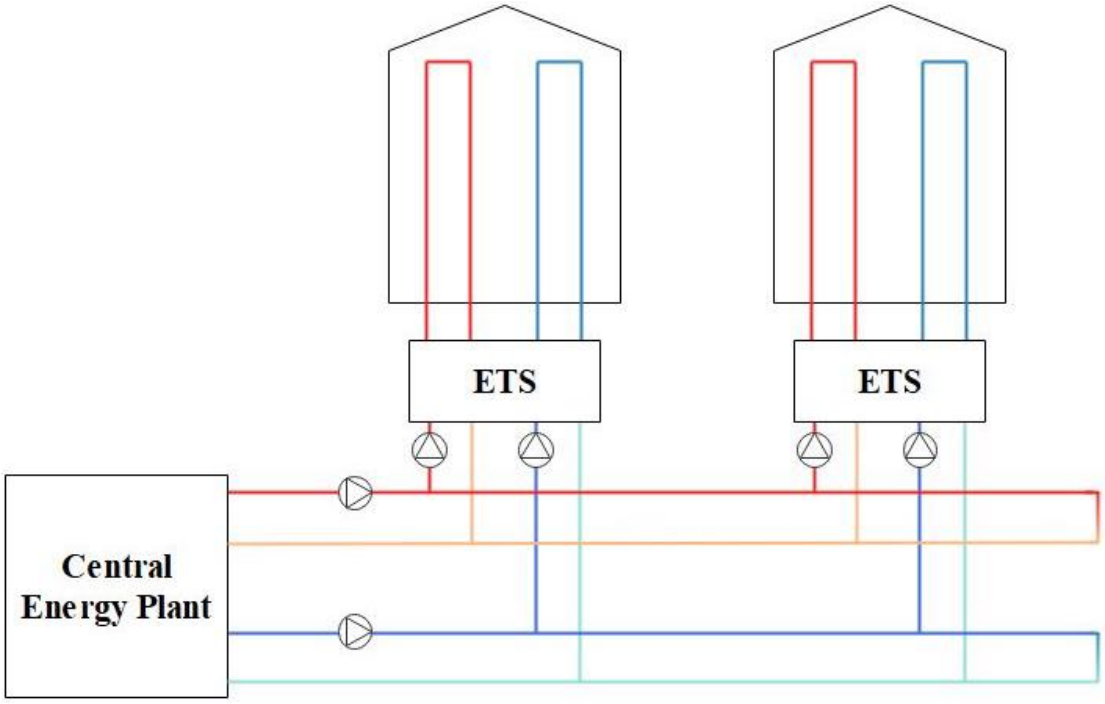

Fig.2.1: Schematic representation of a DE system with a conventional four-pipe thermal network.

In the case where a four-pipe thermal network is retrofitted, the DE system would be updated to allow for operation at lower temperatures. The heat exchangers at each ETS would be replaced by heat pumps since they are typically utilized in modern DE systems for thermal energy transfer between buildings and the network. This is due to the decreased supply temperatures which are not suitable for direct heat exchange. The typical ETS utilized by buildings in conventional four-pipe thermal networks is depicted in Figure 2.2.

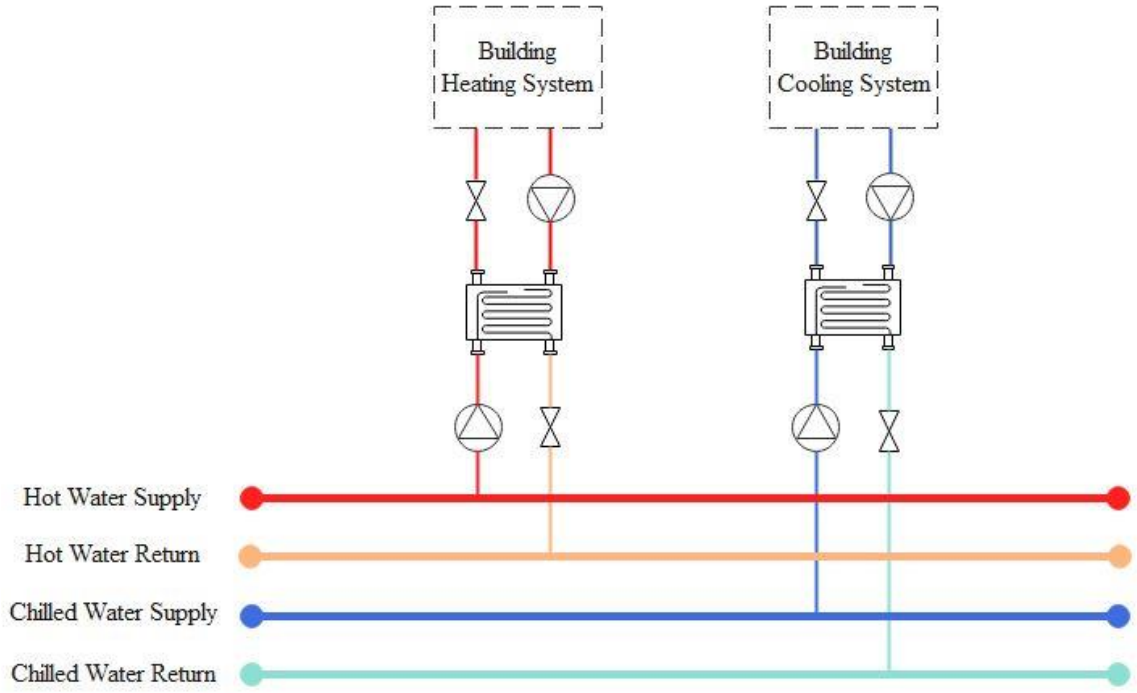

Fig.2.2: Schematic representation of a building ETS in a conventional four-pipe thermal network.

The use of heat pumps in modern thermal networks allows for heating and cooling demands of a building to be met with reduced piping requirements compared to their conventional counterparts. Modern thermal networks typically exist in either a low-temperature unidirectional or bidirectional configuration. These types of thermal networks utilize one or two pipelines at moderate temperatures to provide a thermal energy source or sink for the distributed heat pumps at buildings.

In a unidirectional thermal network (UTN), thermal energy is delivered with a single distribution pipe. This type of DE system utilizes heat pumps at buildings to interface with the network and provide both heating and cooling [31], [41]. In this configuration, the system can deliver thermal energy for heating and cooling with a variable network temperature. This is due to the use of heat pumps to transfer thermal energy to and from

buildings, since they can operate with variable condenser and evaporator temperatures. The structure of a DE system with a typical UTN topology is depicted in Figure 2.3.

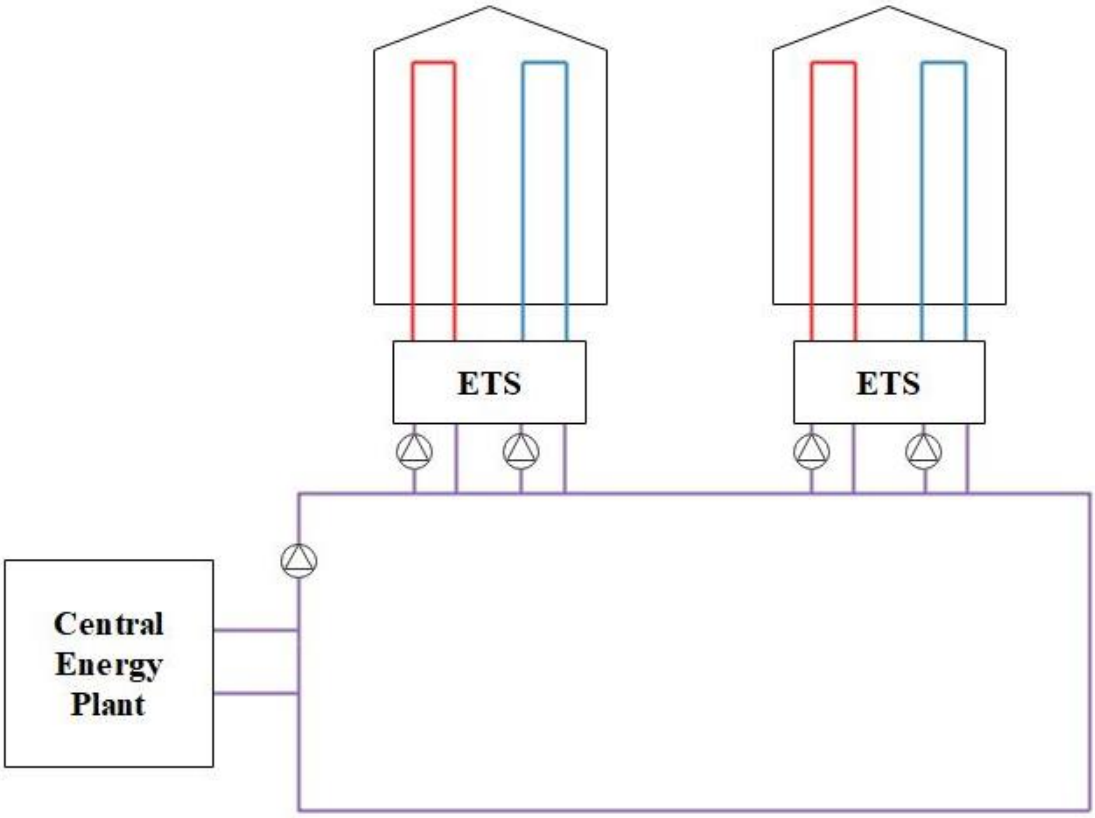

Fig.2.3: Schematic representation of a DE system with a UTN.

Variation of the network temperature is a critical factor affecting the operation and energy consumption of a UTN. This is because the temperatures at the condenser and evaporator of a heat pump affect its coefficient of performance (COP). Variation of COP influences the electric power consumption of heating and cooling heat pumps, potentially leading to an extreme increase of system electrical load. During on-peak periods on the electrical grid, an increase in electrical load will cause peaking power generators to come online. In most cases, these are natural gas burning power plants due to their ability to quickly ramp up and down to match highly variable grid demands. These only operate at

34 - 38% efficiency, compared to typical natural gas boilers (NGBs) at 70 - 80% efficiency [42]–[44]. Therefore, an increase in electrical energy consumption of a unidirectional thermal network can actually increase the amount of GHG emissions produced in comparison to status quo heating systems.

Increasing temperature of the network improves the COP of heating heat pumps, while reducing the COP of cooling heat pumps. Decreasing network temperature results in the opposite trend for the heating and cooling heat pumps. Since both types of heat pumps share the same pipeline, the optimal temperature of the network is highly situational and represents a complex problem affected by multiple factors. Generally, at times when the heating demand is higher than the cooling demand, a higher network temperature is more favourable. The opposite is true during periods when cooling demand is greater than heating demand. However, this connection between thermal energy and the electricity grid can also be advantageous. Since heat pumps consume electrical power to meet thermal energy demands, they can be operated in conjunction with onsite thermal and electrical power generation and the grid to reduce peak heating demands and mitigate the variable nature of renewable electricity sources [32]. For example, during off-peak periods on the electrical grid, carbon-free electricity sources are often curtailed, meaning they are shut down due to low electrical demand. Heat pumps in DE systems can be operated during these times to increase electricity demand and avoid curtailment of renewables and other carbon-free generation. Any excess thermal energy generated by the heat pumps can be stored in short-term thermal energy storage (STES) tanks at buildings or shared between them by transferring it back to the network and supplementing the thermal energy source of other heating heat pumps. Thermal energy stored during this period can be utilized to

offset NGB use in times of peak heating demand. In this way, a UTN can facilitate the decarbonization and electrification of heating. The typical ETS utilized by buildings in a UTN is depicted in Figure 2.4.

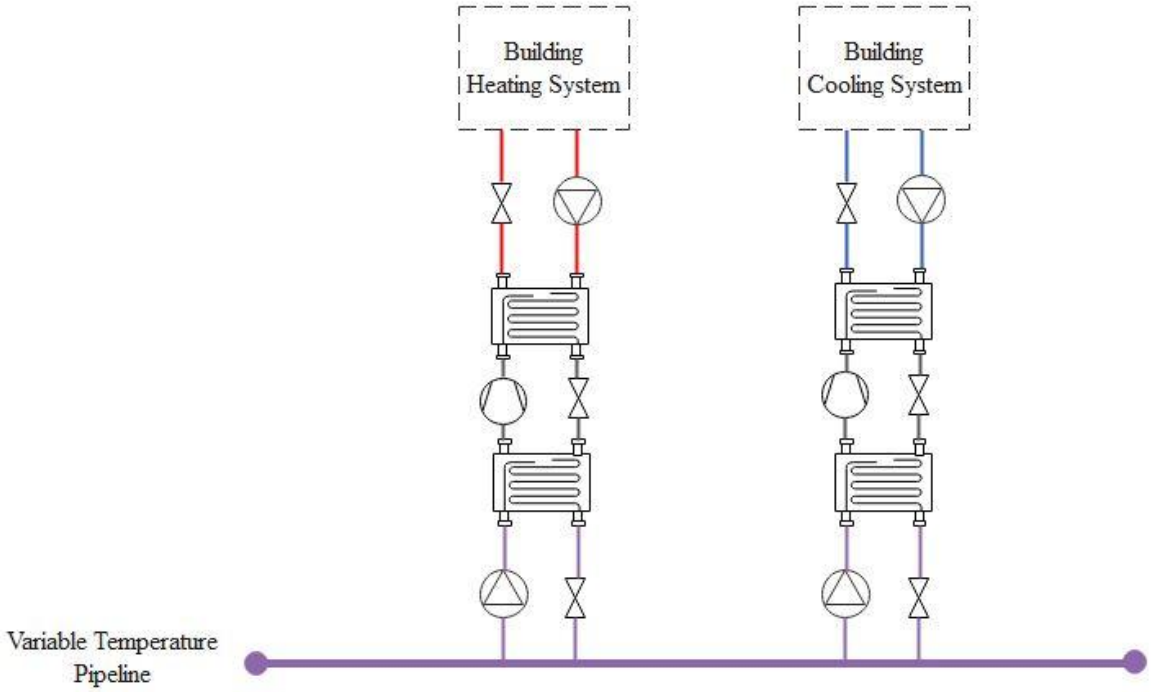

Fig.2.4: Schematic representation of a building ETS in a UTN.

Bidirectional thermal networks (BTNs) are similar to UTNs in many ways. In both configurations, thermal energy is delivered at low temperatures and heat pumps are utilized to provide the appropriate temperatures to building heating and cooling systems. In a BTN, there are two thermal distribution pipelines, each with low supply temperatures that differ by only a few degrees Celsius. The temperature of each pipeline can vary within a small range, though the temperature difference between the two pipelines is held approximately constant [41]. The structure of a DE system with a typical BTN topology is depicted in Figure 2.5.

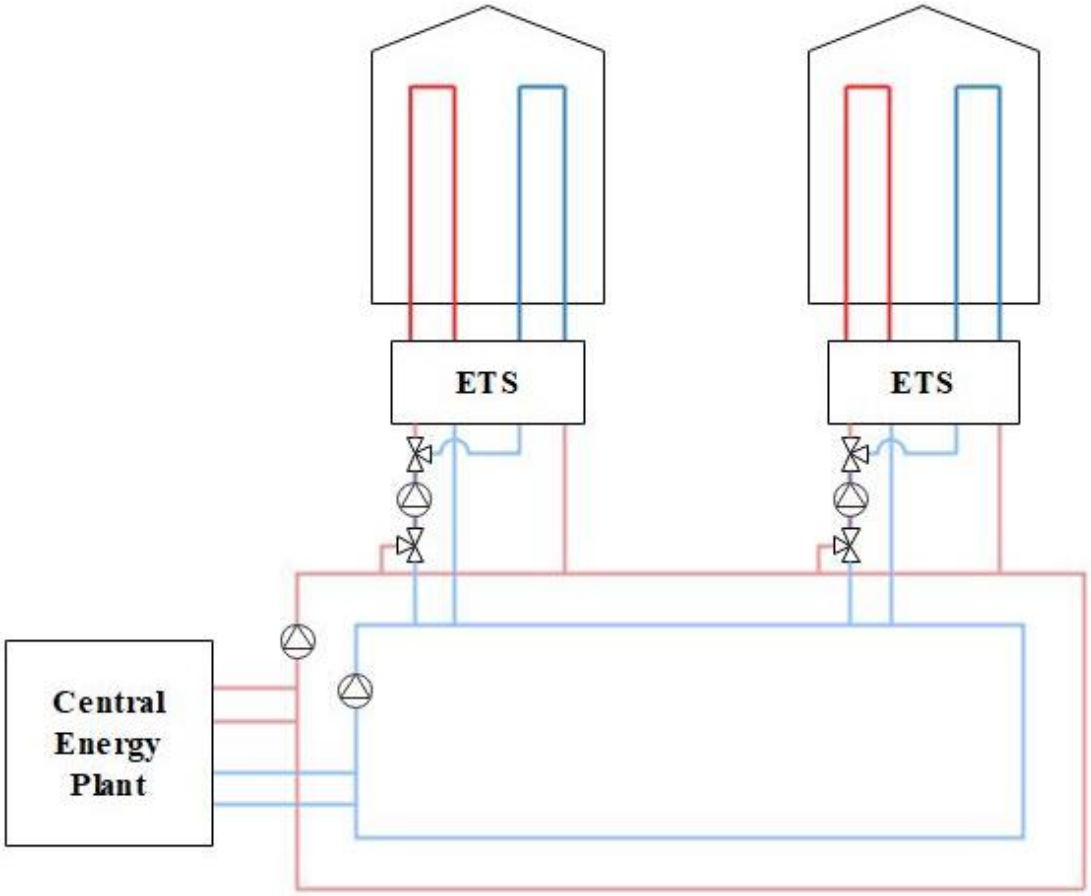

Fig.2.5: Schematic representation of a DE system with a BTN.

Similar to the case of a UTN, the variation of temperature in either pipeline will influence the COP of the heat pumps connected to it. However, in a BTN, thermal energy is transferred to and from buildings differently than in a UTN. The heating heat pump uses the warm pipeline as its source, increasing the temperature of the fluid in the building heating system, and returns the cooled water to the cool pipeline. Conversely, the cooling heat pump decreases the temperature of the fluid in the building cooling system, and the rejected heat is transferred to the warm pipeline [41]. The typical ETS utilized by buildings in a BTN is depicted in Figure 2.6.

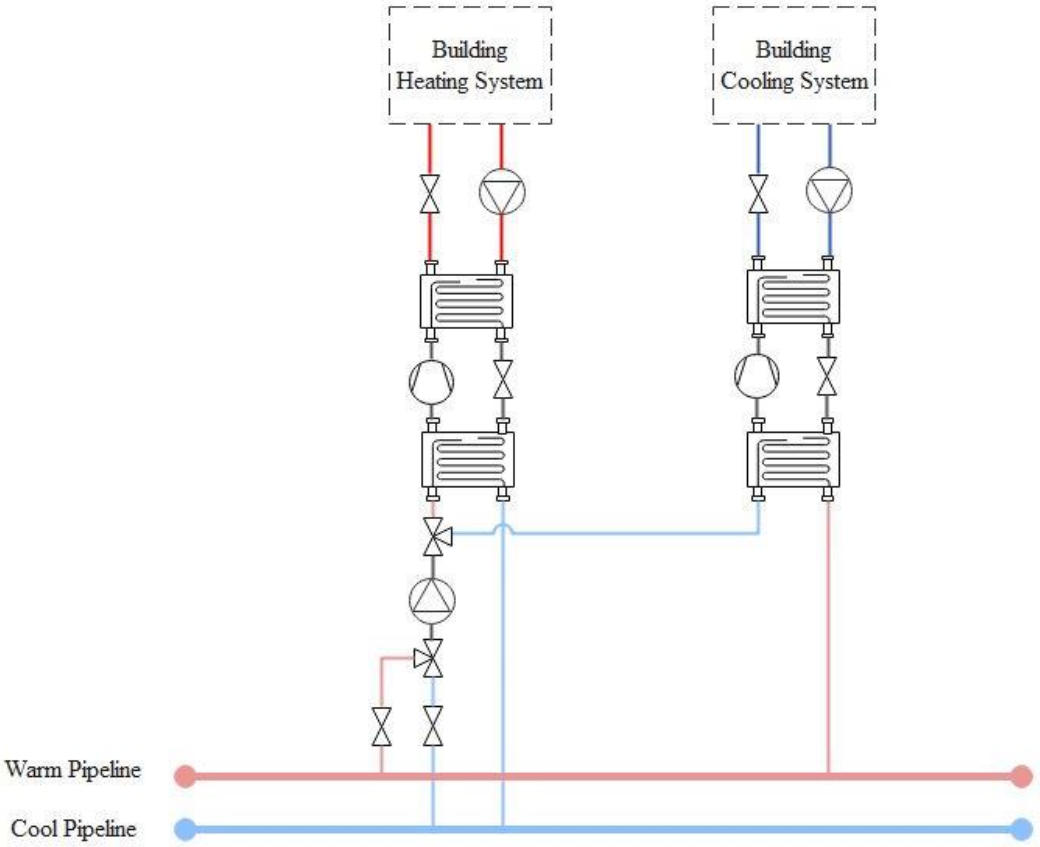

Fig.2.6: Schematic representation of a building ETS in a BTN.

In the literature, the buildings connected to a BTN are most often considered with only one fluid circulation pump. This means that the buildings can only operate in heating or cooling mode, albeit independently from the operation of other buildings connected to the network. Therefore, some buildings in the network can operate in cooling mode, while others are operated in heating mode. This is not necessarily the optimal way in which to operate a BTN, and little research has been published regarding this type of DE system [31], [41]. There is no reason why buildings connected in this configuration cannot accomplish simultaneous heating and cooling with the use of individual circulating pumps for the building heating and cooling systems. An improved ETS design for buildings in a BTN is depicted in Figure 2.7.

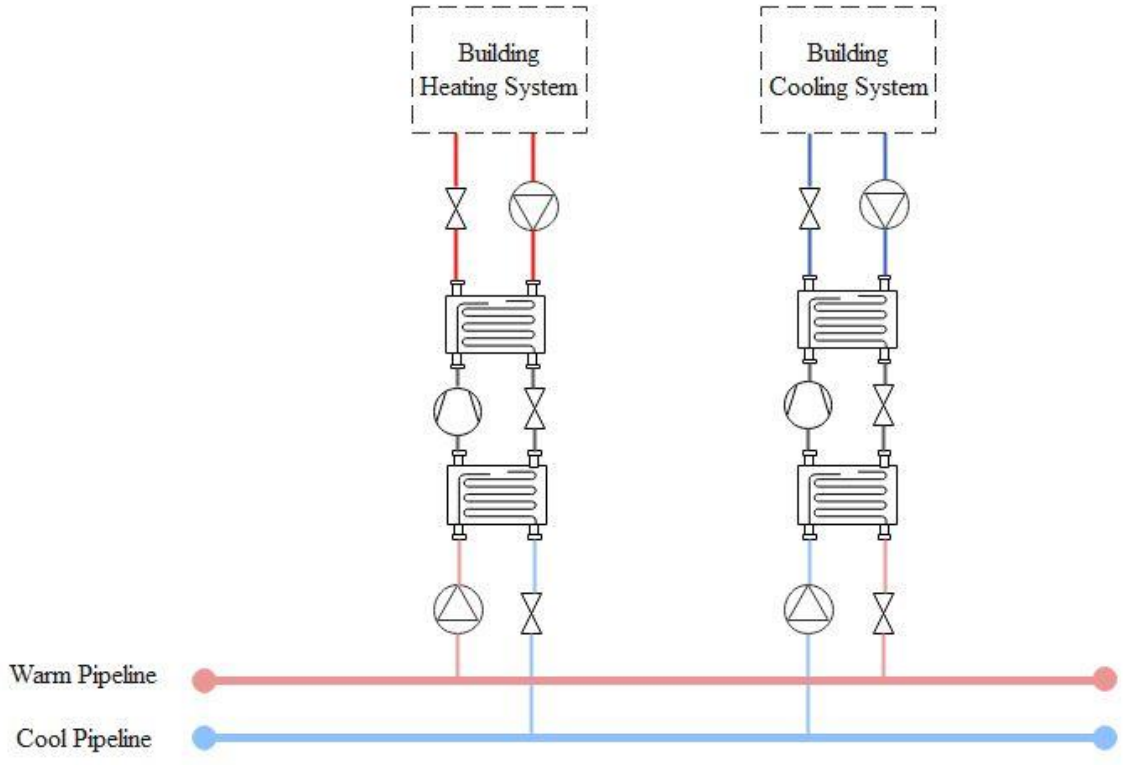

Fig.2.7: Schematic representation of an improved building ETS in a BTN.

Modern DE systems can utilize a wide variety of generation and storage units to deliver energy. Many buildings utilize individual CHP units to offset site electrical demands and provide thermal energy for space heating and hot water [45], [46]. The same concept can be applied to centralized generation. Thermal and electrical energy produced by CHP units can be delivered to multiple buildings in a DE system through the thermal network and transmission lines. Modern DE systems can also incorporate various renewable electricity sources such as solar photovoltaics (PV) and wind turbines to further diversify their electricity mix [47]. Thermal energy resources such as solar thermal heating and geo-exchange systems can also accommodate heating and cooling needs. These

technologies can be utilized at individual buildings or at a central facility, the difference being the total generation capacity or size of the system.

In addition to the various methods of thermal energy generation, modern DE systems can incorporate significant quantities of waste heat from various sources. Waste heat can be harvested from industrial processes at a wide range of temperatures and used as a thermal energy input to a DE system. These sources of industrial waste heat are not necessarily located in close proximity to existing or planned DE systems, therefore connecting pipelines are needed to transport thermal energy. Recovered thermal energy would then be transferred to the heating supply line or the central energy facility of a DE system to be utilized [48]. Additionally, rejected heat can be recovered from cooling processes to meet heating demands or be stored. In a bidirectional thermal network, low grade heat rejected from centralized cooling can be harvested and utilized in the warm pipeline of the same system, provided that the temperature is sufficiently low. Since unidirectional thermal networks supply thermal energy for both heating and cooling in the same distribution pipe, there is typically no centralized cooling generation. To accomplish centralized heat recovery from cooling, thermal energy must first be transferred to the network by cooling heat pumps and utilized to charge centralized short-term or seasonal storage units. It is then supplied back to the network to be utilized by the heating heat pumps during periods of high heat demand.

Both bidirectional and unidirectional thermal networks can incorporate heat recovery from distributed cooling heat pumps. In a unidirectional thermal network, rejected heat from cooling heat pumps can be utilized directly by building heating systems, either as a source for the heating heat pumps or to charge short term storage tanks. If there is no

use for it, the heat can be rejected to the network to supplement the source of other heating heat pumps. Rejected heat can still be utilized directly within buildings in a bidirectional thermal network, however if there is no need for it, the heat is rejected into the cool pipeline of the network. From there it returns to the central plant where it used, stored or rejected to the atmosphere.

Due to the intermittent nature of renewable electricity generation and seasonal variation of thermal energy demands, effective short and long term storage options are necessary to mitigate fluctuations in energy supply and reduce peak energy demand [47], [49], [50]. Short term thermal energy storage is usually accomplished with hot or cold water tanks, while other methods are typically used for long term thermal energy storage. Borehole thermal energy storage (BTES) and aquifer thermal energy storage (ATES) are two alternatives that are often utilized in modern DE systems [31]. Excess heat from processes such as solar thermal generation or CHP is stored during the summer, and used during the winter to meet building heating demands [49]–[51]. Utilizing this otherwise wasted thermal energy offsets the use of natural gas furnaces or boilers, reducing the GHG emissions associated with building heating. Electrical energy storage presents more of a challenge than thermal energy storage, due to the limitations of current technologies. Despite being costly and short-lived, batteries and fuel cells are currently the most viable alternatives for electrical energy storage in modern DE systems due to ease of implementation and scalability. Other mature technologies such as compressed air or pumped hydro energy storage require the existence of suitable geographical formations and construction of large facilities, while a bank of batteries or fuel cells can be housed within a building [47], [52]. Since batteries and fuel cells only last for a certain number of charge-

discharge cycles, they must be periodically replaced, which presents a cost-benefit problem. Depending on the opportunity cost of curtailing renewable electricity generation during periods of low demand, it is possible that electrical energy storage is not economically feasible.

As DE systems have continued to evolve, greater emphasis is being placed on flexibility, variety and efficiency. Much of this can be attributed to the ongoing threat of climate change, and the recognition that mitigating action must be taken to avoid catastrophic damage. To reduce their environmental impact, energy systems must be able to effectively utilize renewable energy technologies, minimize wasted energy and respond to the demand patterns of the communities they service. As a result, DE systems are becoming more and more complex. Increasingly sophisticated control structures are necessary to manage the complexity of integrating multiple sources of energy and exploiting synergies that exist within thermal and electrical energy systems. Therefore, the control structures utilized in DE systems must undergo a similar transition away from the conventional generations.

2.2 Conventional Control and District Energy

Conventional DE control structures utilize a combination of controllers located at the building ETSs and the central plant. In most cases, the control strategy is focused on the control of relevant temperatures in the system. Temperatures in the network are controlled by manipulating the mass flow rate in fluid streams that transfer thermal energy. Typically, different variations of PID controllers are utilized to manipulate the mass flow rates of various pumps and valves based on the corresponding temperatures. Changes in

flow rate result in greater or lower thermal energy transfer, which increases or decreases temperature to reach the setpoint [37]. At each heating and cooling ETS, PIDs manipulate the mass flow rates on the primary or secondary side of heat exchangers to ensure that building supply temperatures are sufficiently high for heating and low for cooling. This affects the return temperature to the network as well. The control systems at each ETS have only one objective - to ensure the thermal energy demands of a specific building are met. Therefore, in periods of high demand, buildings located first in the network may be able to satisfy their demands, while subsequent buildings may not. To prevent this, the central plant control system ensures that the supply temperature is sufficient to meet the thermal demands of all buildings in the network [37]. This is accomplished by adjusting the thermal power output of the heating and chilling units located in the central plant.

Typically, PID controllers at each thermal energy producer are used to manipulate the rate of conversion to thermal energy from some other form. For example, the thermal power output of a NGB is manipulated by varying the rate of fuel injection for combustion. The fuel injection rate is adjusted by the PID controller based on the temperature of the fluid passing through the NGB. Temperature control with other types of thermal energy producers is accomplished in a similar fashion depending on the method of energy conversion. As is the case with the ETS controllers, the objective of each PID in the central plant is to manage the output of a thermal energy producer. The output temperature of each unit is critical to the operation of the subsequent units, since it affects the temperature supplied to them. For example, if the temperature supplied to a heat producing unit is too high, then it is unable to transfer all of the thermal energy it produces. This causes an increase of temperature inside the unit, which begins to reject heat through its radiators or

shuts down to avoid damage. As a result, thermal energy is wasted and energy efficiency is reduced. To avoid this situation, the thermal energy producers were connected to conventional DE systems in the appropriate hydraulic sequence [37]. This means that the heat carrier fluid returning from the consumers to the central plant enters the thermal energy producer requiring the lowest inlet temperature first, followed by the producer which requires the next lowest temperature and so on.

Similar methods of control are utilized in modern DE systems; however, the aforementioned issues are less prevalent. The reduced operating temperature and technologies utilized make the issue of supply and return temperatures less critical to the successful delivery of heating and cooling. Since modern DE systems often utilize low temperature thermal networks and heat pumps to deliver thermal energy, they can tolerate some variation in temperature throughout the network. For example, if the supply temperature of a heating heat pump decreases, it is still able to transfer heat to the building. Here, the only difference is that the electrical energy consumption of the heat pump increases. This situation is acceptable if it occurs infrequently and in short durations since increasing electricity consumption is generally undesirable. Additionally, it is inadvisable during electrical peaks since the increased electricity consumption can cause fossil fuel based peaking power plants to increase their output. These effects are in direct conflict with the goals of DE systems - to deliver energy with reduced primary energy consumption and GHG emissions. PID controllers are still used for the same purposes as in conventional systems. At central energy plants, they are utilized to adjust the output of energy producing units and control the temperature supplied to the network. At the ETS of each building, they adjust the flow rates through pumps and valves, and the thermal power output of heat

pumps, to control the temperature supplied to building heating and cooling systems. In both conventional and modern DE systems, there is typically some form of communication between the controllers and a central control room which coordinates their actions. From the control room, a human operator can monitor the system, adjust the setpoints of controllers and open or close control valves if necessary [38].

Despite the increased flexibility in temperatures utilized in modern DE systems, they still suffer from some of the same issues as conventional systems resulting from the control strategies utilized. Each controller has some effect on the system through the piece of equipment they are controlling. Since they are all connected to the same system, each controller's action has an impact on all the other controllers. This is referred to as process interaction and occurs when the output of one controller affects the input conditions of the remaining controllers in the system. This can affect the performance of the other controllers for better or worse depending on their respective control objectives and how their input conditions are affected by the interactions [38].

Process interactions between controllers occur in both steady state and transient situations. For example, a building heating system controller in steady state is tracking its setpoint and returning water to the thermal network at a temperature based on its supply temperature and heating load. The return temperature affects the supply temperature of the next building in the network, and this interaction occurs between each building. When a building heating system controller detects a deviation from setpoint, it responds by manipulating the rate of heat transfer to the building to reach the setpoint again. Depending on the tuning of the controller, there can exist some overshoot and oscillation in temperature until the controller settles. As a result, the overshoot and oscillations are also

present in the return temperature from that building, and in the supply temperature of the next. The control system of the next building then responds to this transient in a similar fashion; however, depending on the tuning of its controller, the impact of the transient on this building's temperature can be greater than that of the previous building.

The greater the number of buildings in a thermal network, the process interactions between them become increasingly significant due to the number of controllers. As a result, the tuning methodology for controllers in this type of system is a more holistic approach. Control tuning for each controller is done based on the performance of the system as a whole in response to adjustment in the tuning parameters [38]. Tuning in this case becomes an extremely complicated endeavour which takes an exorbitant amount of time to complete. This process also does not necessarily result in adequate control performance.

Furthermore, the use of multiple PID controllers must involve careful coordination. Since they are SISO controllers, every PID receives and targets a single setpoint. Therefore, appropriate setpoints must be chosen for each controller to accomplish their control objectives. Determining appropriate setpoints for multiple controllers in the same system represents a challenging task for a control room operator. It would require extremely detailed knowledge of the system and nearly constant monitoring of the control variables. This is not feasible in most cases due to the size and complexity of the system, interaction of controllers and potential for human error. It is clear that the conventional control methods utilized in DE systems can result in sub-optimal performance. Additionally, it is difficult to implement any decision-making capability beyond manual adjustment of the control system by human operators. Therefore, it is necessary to use more intelligent and

advanced control strategies wherever possible, especially as DE moves toward a sustainable future.

2.3 Multi-Agent Systems and District Energy

A promising control strategy for DE systems is the Multi-Agent system (MAS). It is a methodology in which agents communicate with each other to accomplish their own control objectives and those of the overall system [53]–[55]. An agent in a MAS is an entity that is part of a larger environment, and can control its actions within a limited scope based on the sensory input it receives [56]. In a real system, an agent is a combination of software and hardware which has some control over the output of a piece of equipment acting on the system. Typically, agents are software programs contained on Programmable Logic Controllers (PLCs) or system computers that communicate with their assigned piece of equipment. The agents are part of a larger object-oriented software algorithm that governs their interactions.

In a DE system, agents represent the energy producers and consumers within the network, and the MAS satisfies consumer energy demand by balancing it with energy supply from the producers [41], [53], [57], [58]. The producer agents attempt to provide the least amount of energy to meet consumer needs, and the consumer agents attempt to satisfy their own thermal demands. Another type of agent defined in the literature is called a redistribution agent, which communicates with producers and a group of consumers to ensure energy is fairly distributed [59]. Since MASs are largely based on software, there are many more potential types of agents that can be defined. It is up to the designer to

conceptualize new types of agents, and to program them to accomplish the functionalities envisioned.

The MAS is a suitable method of control for modern DE systems as it is able to effectively manage the complex nature of modern DE systems and provide robust control [58], [60]. MASs are also relatively simple to implement and do not require the same complicated tuning as using multiple PIDs. They have shown promise in controlling a variety of energy generation and storage units in centralized or decentralized configurations. Some of these include CHPs, NGBs, solar thermal and PV, heat pumps, thermal storage tanks and geothermal energy storage [61]–[64]. Multi-Agent frameworks have also been proposed that provide valuable services such as peak shaving and demand management. These systems utilize building thermal mass and flexible temperature setpoints to reduce average and peak thermal energy required from producers [65], [66]. Thermal mass is the ability of a system to store thermal energy or hold its temperature for some time in the absence of a source of heating or cooling [67]. The larger a building's thermal mass, the longer it takes to heat up or cool down the space to reach the desired temperature. This behaviour can be taken advantage of by control systems for early shutdown and late start-up of thermal energy generation for peaks, since the temperature will not change significantly over that time frame. This strategy requires adequate modelling of building thermal mass to predict when thermal comfort goals will be impacted by reducing thermal energy generation and respond accordingly.

Due to their object-oriented nature, MASs are versatile and can be applied to energy systems of various sizes and configurations. These can range from a single building with onsite thermal and electrical generation to many buildings connected in a large DE system.

Single-building MASs typically focus on thermal comfort and satisfaction of occupants with lower cost or GHG emissions [61], [68], [69]. In larger DE systems, consumer demands are directly met by the ETS at each building. In this case, the MAS is utilized primarily to control the thermal and electrical generators that provide the source of energy for building systems. The goal of the MAS is to deliver energy with improved efficiency and reduced cost or GHG emissions [62], [70]. In addition to these consumer-centric and producer-centric approaches, there exist Multi-Agent frameworks that manage producers and consumers simultaneously, as well as those in which multiple MASs are utilized in the same DE system. These MASs work together to facilitate the transfer of energy between producers and consumers, often employing a transactive energy approach in which energy is traded in some sort of virtual market structure [41], [71].

MASs have also been combined with various other algorithms to provide enhanced control structures. Optimization, model predictive control and artificial intelligence techniques have all been applied to MASs, typically to provide the system with some form of supervisory control. These determine the values of critical parameters such as thermal network temperature and building indoor temperature, and provide them as inputs to the MAS [41], [68], [70]. Similar to the programming of the agents themselves, there are many possibilities for the design of the software algorithms that drive the overarching Multi-Agent frameworks. The designer can write the algorithm for any type of operational structure that is feasible for the system and implement any desirable features that the system should be able to perform.

Most Multi-Agent frameworks applied to DE systems target the same temperature setpoints in the network and central plant year-round. As mentioned previously, this can

result in sub-optimal performance at times due to the seasonal variation in weather conditions, outdoor air temperature and consumer demand. The optimal operating temperature can vary significantly, so the ability to adjust temperature setpoints in real-time has the potential to improve energy efficiency and consumption of these types of systems. Variable operating temperature can also improve the flexibility of DE systems. The flexibility of the system comes from its total thermal capacity, which consists of thermal storage units, building thermal mass, and the thermal network itself [72]. In order to utilize thermal energy storage at all, the system must be able to increase and decrease its temperature in a controlled fashion.

Thermal energy storage units are utilized in mainly two ways, as storage or as a thermal buffer. When used as storage, energy is stored, held and then released at a later time when needed. This storage time can vary anywhere from a few hours to a few months [51]. For example, distributed thermal storage tanks are used over several hours at a time while storage over several months is typically accomplished using much larger water tanks or borehole thermal energy storage [49], [62], [63], [73]. On the other hand, when used as a buffer, storage units continually absorb and release thermal energy, and mitigate the temperature fluctuations of the system [74], [75]. This mode of operation requires that the unit is constantly connected to the system and circulating fluid so thermal energy can be transferred. Energy is stored when the system temperature is above that of storage, and immediately released when the system temperature falls below that of storage, without any holding phase. Both modes of operation provide different benefits to a system. Buffers keep the temperature in the system from fluctuating excessively, thereby improving the reliability of the system. Storage allows the system to make use of otherwise wasted energy

by saving it until there is demand for it [51]. These benefits are both desirable in DE systems, however they are not often accomplished simultaneously.

As DE systems continue to evolve, MASs can similarly adapt and continue to provide advanced control solutions. MASs have demonstrated great potential for innovation and as new strategies for mitigating GHG emissions are developed, MASs can begin to utilize them. As such, MASs are a promising tool for DE systems to utilize in moving toward a sustainable future.

Chapter 3

ICE-Harvest System and Methodology

3.1 Description of ICE-Harvest System

The control framework developed in this thesis is applied to the ICE-Harvest system which utilizes features of both the fourth and fifth generations of DE technology at a community scale. In this system, energy requirements of the customers are met by a set of interconnected thermal and electrical generators and storage units, while the system harvests as much waste heat from cooling as possible. The system is divided into two thermally and electrically connected sections, the Energy Management Center (EMC) and the Micro-Thermal Network (MTN). The EMC contains all of the energy producers and storage units of the system, and the MTN contains all of the energy consumers of the system. The sizes of the various equipment and the parameters of the system are selected

based on those of the ICE-Harvest research facility at McMaster University. Some of these parameters are scaled up for the proposed case study. The detailed operation of the EMC and MTN, as well as their interaction are described throughout this chapter.

3.1.1 Energy Management Center

In the EMC, thermal energy producers are connected to a small thermal network with two pipelines - one at higher temperature than the other. The higher temperature pipeline is referred to as the hot header, and the lower temperature pipeline is referred to as the warm header. The hot header operates between 50 °C and 80 °C, and the warm header operates between 10 °C and 50 °C. The mass flow rate of both headers is 150 kg/s. The electrical energy producers are connected to either a low-voltage AC network which operates at 60 Hz, or a low-voltage DC network. The AC network operates at 600 V and the DC network operates at 240 V. These AC and DC networks are connected together through a bidirectional power converter so that electrical energy can be transferred between them. The low-voltage network also provides the electrical energy required to power the water pumps and heat pump in the EMC. The hot header is connected to the MTN through a heat exchanger to deliver thermal energy to the consumers, while the low-voltage AC network delivers electrical energy to consumers directly through low-voltage transmission lines.

The EMC contains a CHP unit, which is the primary energy producer in both the thermal and electrical parts of the system. The CHP is connected to the hot header and the low-voltage AC network. It is capable of supplying up to 600 kW of electrical power and 1000 kW of thermal power to the system. To supplement the thermal energy provided by

the CHP, there is a NGB also connected to the hot header, with a maximum thermal power output of 3000 kW. The system also contains a heat pump that is connected to both pipelines, with its condenser connected to the hot header and its evaporator connected to the warm header. The heat pump uses electrical power from the low-voltage network to remove thermal energy from the warm header and add it to the hot header. The heat pump will consume at most 220 kW of electrical power, to provide up to approximately 1000 kW of thermal power. Since the heat pump removes thermal energy from the warm header, it requires a source of heat to continue operating. This is accommodated by energy from a BTES system at the EMC or waste heat from cooling processes, harvested from the buildings during periods of low heating demand. The BTES discharges thermal energy to the warm header which the heat pump utilizes to provide thermal energy to the hot header for meeting the heating demand from the MTN. The BTES is also connected to the hot header for charging, which results in the heat pump instead utilizing the waste heat recovered from buildings in the MTN as its source to provide thermal energy. In this case, the heat pump is used to meet the thermal demand of the MTN and charge the BTES.

Excess thermal energy generated by the CHP is also transferred to the hot header and stored in the BTES. STES tanks are also connected to both headers. Each tank stores and provides small amounts of thermal energy at times and mitigates temperature fluctuations in their respective headers. The thermal energy storage tanks are fully mixed and their temperature follows their respective headers, varying between approximately 50 °C and 80 °C for the hot header storage and between 10 °C and 50 °C for the warm header storage. The electrical portion of the system is able to import from the power grid to supplement the electrical energy provided by the CHP. There is also a battery electrical

energy storage (EES) system which stores off-peak electricity from the grid, and releases it during peaks when more energy is needed. The EES also stores electrical energy from the grid during off-peak periods and discharges during the peak times to reduce the amount of on-peak electricity imported from the grid. Its maximum rate for both charging and discharging is 200 kW and its storage capacity is 800 kWh. The energy producers and storage units in the system are managed by the developed control framework to provide energy to meet consumer demands. The structure of the EMC and the interconnection of the various components is depicted in Figure 3.1.

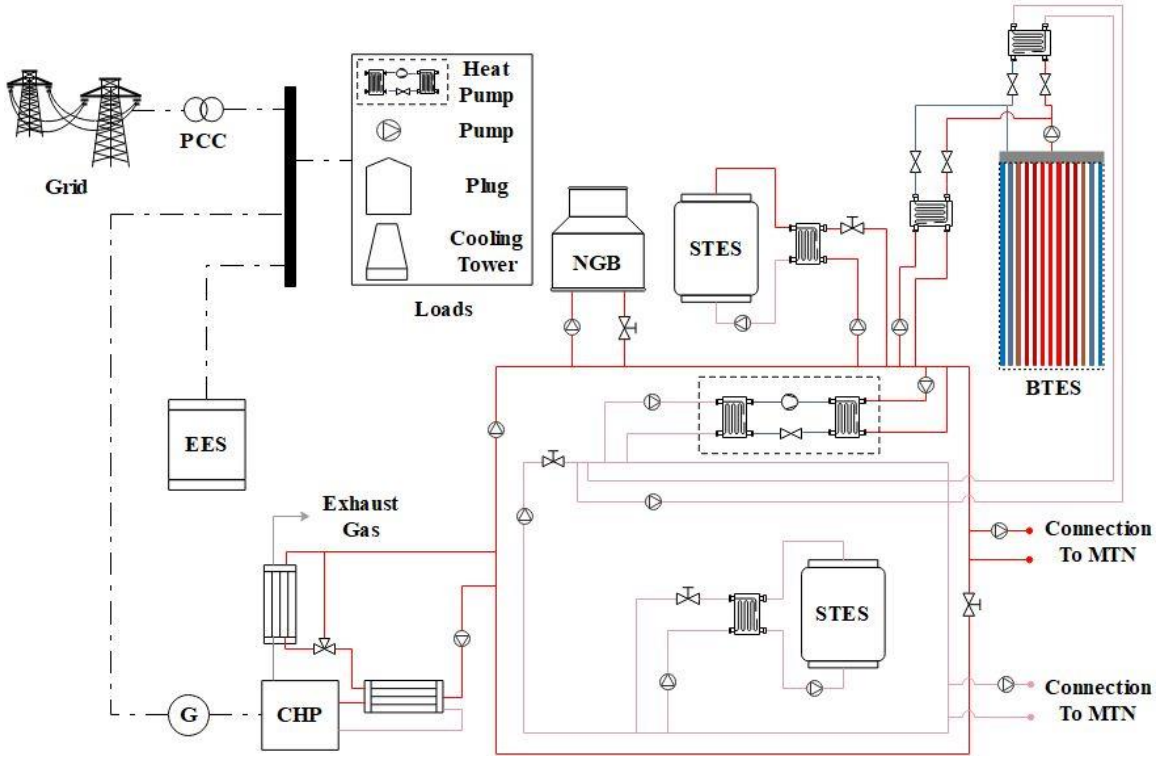

Fig. 3.1: Schematic representation of the EMC and its different components.

3.1.2 Micro-Thermal Network

In the MTN, the energy consumers are a set of buildings located in Ontario, Canada, connected together in a unidirectional thermal network. This network consists of a single pipeline to transport thermal energy which operates at a constant temperature of 35 °C, and mass flow rate of 150 kg/s. Each building is connected to the network through two heat pumps - one for heating and one for recovering heat from building cooling processes. These cooling processes are also accommodated by a heat pump at each building. The heat pumps accommodate the thermal energy needs of the buildings by taking heat from the pipeline and rejecting heat to it or the ambient environment. In this configuration, the heating and cooling needs of the buildings are satisfied simultaneously and buildings are able to share energy with one another. For example, a building that predominantly requires cooling will reject more thermal energy than it consumes. This thermal energy can then be rejected by the heat recovery heat pump to the network and used by an adjacent building to accommodate its heating requirements. Cooling towers at each of the buildings are able to reject any heat that could not be recovered and cool the return water for building cooling systems. The detailed connection of a building in the network is depicted in Figure 3.2.

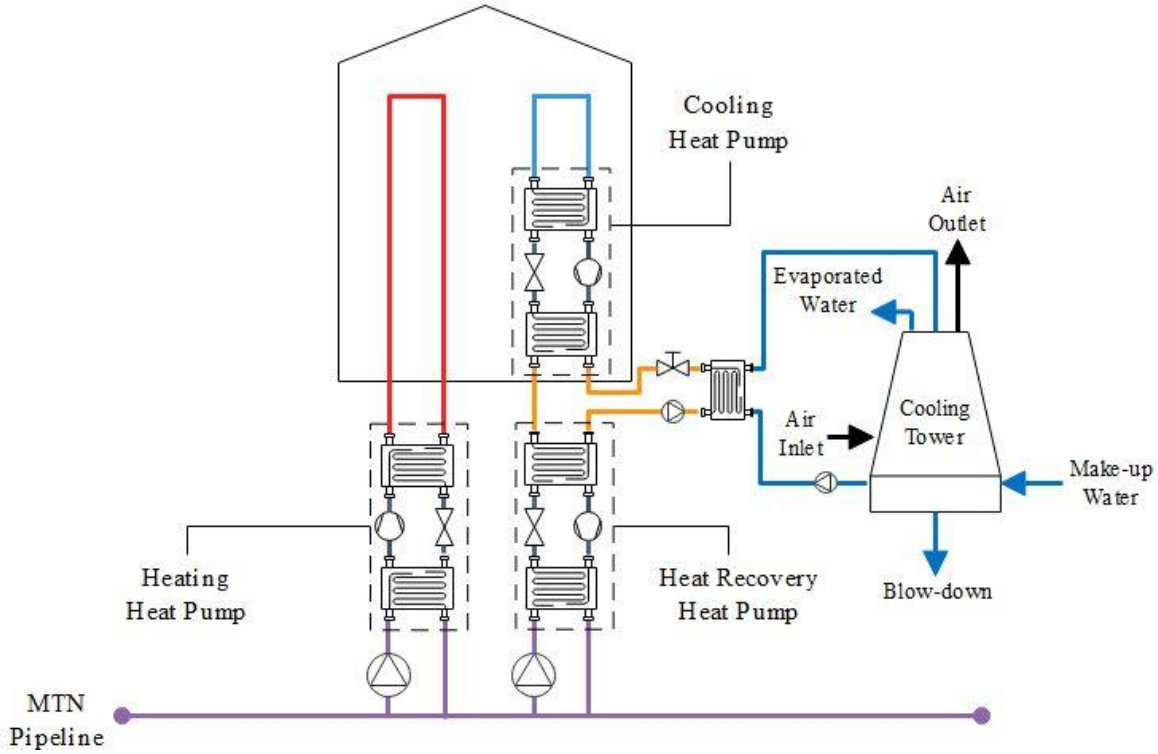

Fig. 3.2: Schematic representation of building thermal system.

The MTN is also equipped with a heat recovery system to handle the situations when the amount of cooling process heat available is greater than can be shared between buildings. In this case, the temperature of the network at the outlet of a building is greater than the inlet. As a result, the temperature of the heat carrier fluid rises as it traverses the network and reaches the heat recovery system. The heat recovery system is a heat exchanger which connects the MTN to the warm header of the EMC. It transfers heat rejected by cooling dominated buildings from the MTN back to the EMC and reduces the temperature of the pipeline. The buildings are also electrically connected to the low-voltage network of the ICE-Harvest system. The electrical energy provided to the buildings is used to power their heat pumps and flow pumps, and to meet their non-thermal electrical

demands, such as lighting and appliances. The layout of the buildings in the MTN, as well as its connection to the EMC is depicted in Figure 3.3.

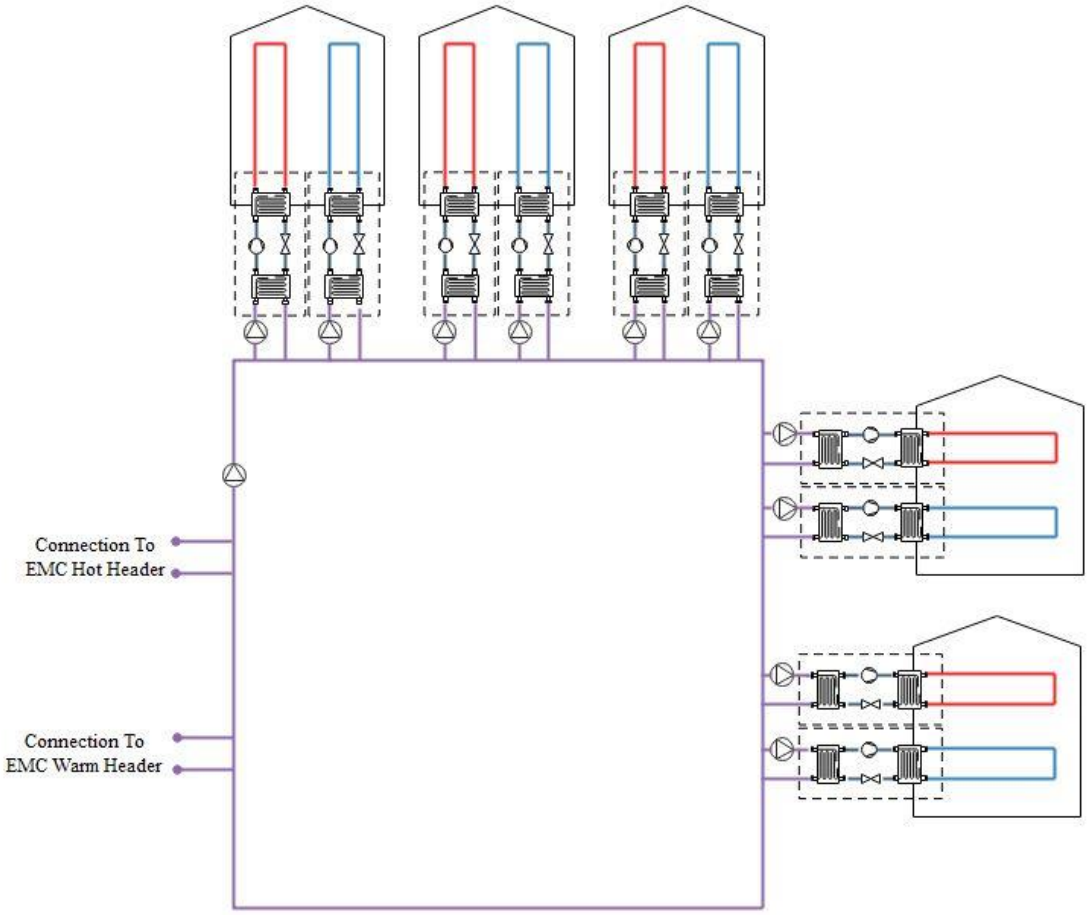

Fig. 3.3. Schematic representation of the MTN and its different components.

3.2 Proposed Control Framework for ICE-Harvest

The proposed control structure is a self-regulating closed loop between the ICE-Harvest system and a three-part control framework. The first part of the control framework is the MAS, which determines the amount of thermal power required by the MTN based on deviations of temperature from the setpoint, and controls the energy producers in the EMC to accommodate the demand. It ensures that consumer demands are met at all times,

by continually balancing the supply and demand of thermal energy. The second part of the control framework is the set of SLCs, which utilize sequential logic to determine the appropriate temperature setpoint for the system and provide it as an input to the MAS. The SLCs monitor the current state of the system and change the temperature setpoint when specific conditions are met. The last part of the developed control framework is the set of Auxiliary Controllers which control temperatures and thermal power flows within the MTN. The action of the Auxiliary Controllers influences the net thermal energy demand of the MTN which is accommodated by the MAS. The operational strategy implemented by the Auxiliary Controllers results in a change in dynamics of the system, which the remaining parts of the control framework respond to. The overall structure of the control framework is depicted in Figure 3.4 and the detailed operations of the MAS, SLCs and Auxiliary Controllers, as well as their interactions, are presented in the following sections.

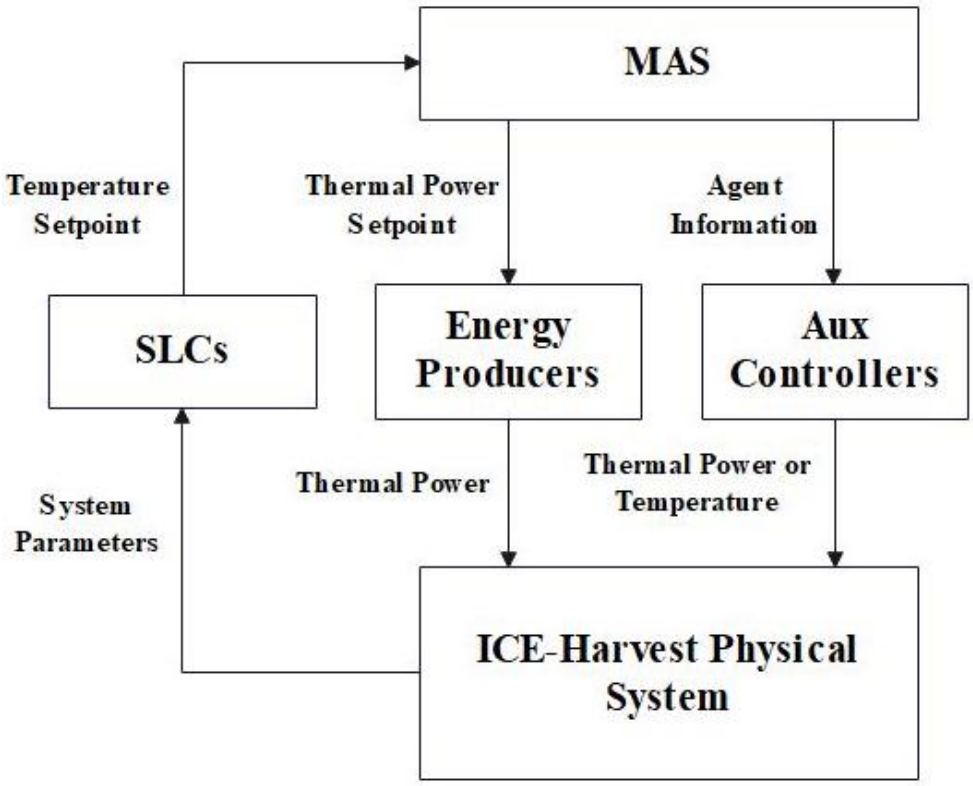

Fig. 3.4. Block diagram representation of overall control framework.

3.2.1 Multi-Agent System

The MAS consists of a set of agents which interact to meet the energy needs of consumers and keep the system at the desired operating temperature. The agents represent selected energy producers in the system, as well as the consumers. There are energy producer agents for the CHP, NGB and heat pump in the EMC, and one energy consumer agent which represents the net thermal demand of buildings connected to the MTN. There is also a central agent called the broker, which facilitates the interaction between the other agents in the system. The producer and consumer agents interact with each other and the broker in a negotiation process which is repeated every 5 minutes to determine how the energy producers in the system are controlled. The negotiation process begins with the

consumer agent, which measures the temperature of the hot header just ahead of the heat exchanger that connects it to the MTN. If the measured temperature is different than the setpoint, the consumer agent will request the corresponding increase or decrease of power to return to the setpoint. The amount of thermal power requested is determined by a PID controller which operates based on the difference between the current temperature and the setpoint. The broker then relays this request to each of the producer agents, who respond by either accepting or refusing, and stating their cost of processing it. An agent will refuse the request if the equipment they are controlling cannot physically accommodate it due to being at its maximum or minimum output already, or if it is unavailable. The broker then selects the agent with the lowest cost to process the request, and the agent signals the energy producing unit to increase or decrease its output accordingly. The cost in this system is stated in terms of the GHG emissions per W of fuel consumed by the producer. The fuels utilized are natural gas in the CHP and NGB, and electricity consumed by the heat pump compressor. The repetition of this process ensures continuity of service to the buildings, by continually restoring the balance of supply and demand.

Since the process is driven by a measured temperature difference, the temperature of the hot header typically fluctuates in a small range around the setpoint. These fluctuations are mitigated by the STES connected to the hot header which acts as a temperature buffer. Operation of the storage tank in this way also prevents the energy producers from having large swings in their output power, resulting in more consistent operation of each piece of equipment. Each energy producer’s availability to operate is an input to their agent, given by a predetermined schedule.

The schedule of the ICE-Harvest system is based on a unique operating principle in which the thermal and electrical energy producers in the system operate based on the peaks of the electrical grid. The CHP is only available to operate during the electrical peaks, since the natural gas peaking power plants are operational. In this manner, the ICE-Harvest system reduces the amount of power imported from the grid and replaces natural gas generators that would be utilized during peak times. Therefore, the operation of the CHP produces no additional GHG emissions compared to the status quo when operating in this way. The thermal energy generated by the CHP is then used to accommodate heating requirements and charge thermal energy storage units. This reduces the need for heating with the NGB and results in a reduction of the GHG emissions associated with meeting thermal demands. Since the CHP is part of the MAS which controls thermal energy output, it produces electrical power up to the point at which it can use the thermal energy produced. This is because the goal of the proposed system is to reduce GHG emissions while harvesting as much thermal energy as possible, without rejecting any to the ambient environment. Therefore, the role of the CHP in the ICE-Harvest system is to replace natural gas peaking power generation on Ontario´s grid with an alternative that provides greater system efficiency and the additional benefit of harvesting thermal energy.

Conversely, the heat pump is only available during the off-peak periods of the electrical grid. This is because the heat pump consumes electrical energy to provide thermal energy. The heat pump exclusively utilizes off-peak electricity from the grid to provide heat to the system to avoid contributing to peak electrical demand. Additionally, the heat pump is able to add electrical load to the system during the off-peak periods when curtailment of renewable generation is typically occurring. The NGB is always available,

and acts as a backup to the CHP or heat pump depending on which one is currently operating. Additionally, it accommodates any additional heating requirements beyond the capability of the CHP or heat pump. Therefore, the operation changes significantly depending on the availability of the CHP. When the CHP is available, the MAS will dispatch the CHP and NGB to meet the net thermal energy demand from the MTN, and when the CHP is unavailable, the MAS mainly relies on stored heat and grid electricity. The structure of the MAS and the interactions between the different agents and the physical system are depicted in Figure 3.5.

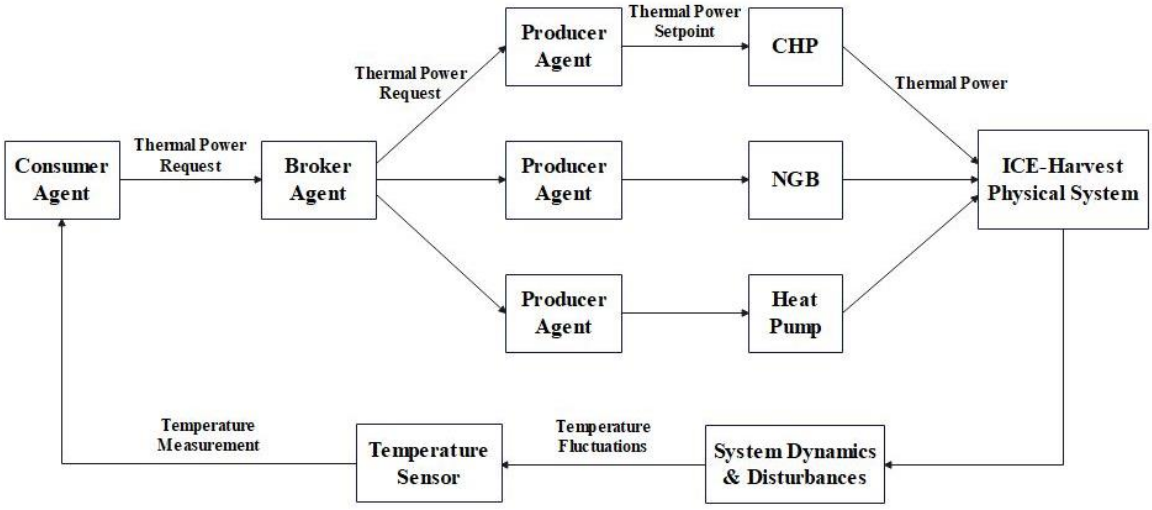

Fig. 3.5. Block diagram representation of MAS.

3.2.2 Sequential Logic Controllers

There are three SLCs in the system which work together to facilitate the operation of the STES and BTES. They are used to measure the current status of the system and provide the appropriate temperature setpoint to the MAS for charging and discharging of the storage units, and to connect the BTES with the appropriate header. Each SLC consists of several distinct states, each with a unique output value. Only one state can be active at a

time, therefore the output of the controller is determined by the active state. Transition between states is governed by a predefined set of conditions, which are based on measurements of the system. When the conditions are met, the current state is deactivated and the new state becomes active. In this way, the SLCs take measurements of the system and determine the appropriate output for the storage units' operation.

The first SLC is referred to as SLC 1, and prioritizes the charging and discharging of the STES. SLC 1 consists of seven states which represent the possible temperature setpoints. There is a 5 °C difference between each one, and they occupy the entire temperature range of the hot header. To charge the storage tank, the controller increases the temperature of the hot header by transitioning to higher temperature states. The controller repeatedly changes states until it reaches the maximum temperature or the conditions are no longer met. To discharge the storage tank, the same process occurs in reverse, with the controller repeatedly transitioning to lower temperature states until it reaches the minimum or no longer meets the conditions. Therefore, the charging and discharging processes are similar; the difference lies in the conditions for each. The set of conditions for transitioning between states during charging are the following:

- CHP must be active.
- CHP is operating at less than 800 kW thermal (~80% capacity).
- Temperature of the system must be at or above the current setpoint.

The set of conditions transitioning between states during discharging are the following:

- CHP must be inactive.
- NGB must be active.

The overall strategy of the controller can be observed from the conditions for charging and discharging. The system charges the STES with additional thermal energy available from the CHP, since it is not operating at its maximum output. The STES then imposes a thermal load on the EMC hot header, which causes the MAS to increase the output of the CHP, taking advantage of the fact that the CHP has the capacity to provide more energy. The storage is discharged when the CHP becomes unavailable and the energy from storage is used to offset some usage of the NGB. This is because the CHP is preferred over the NGB to provide thermal energy, since it provides electrical energy as well. The structure of SLC 1 is depicted in Figure 3.6.

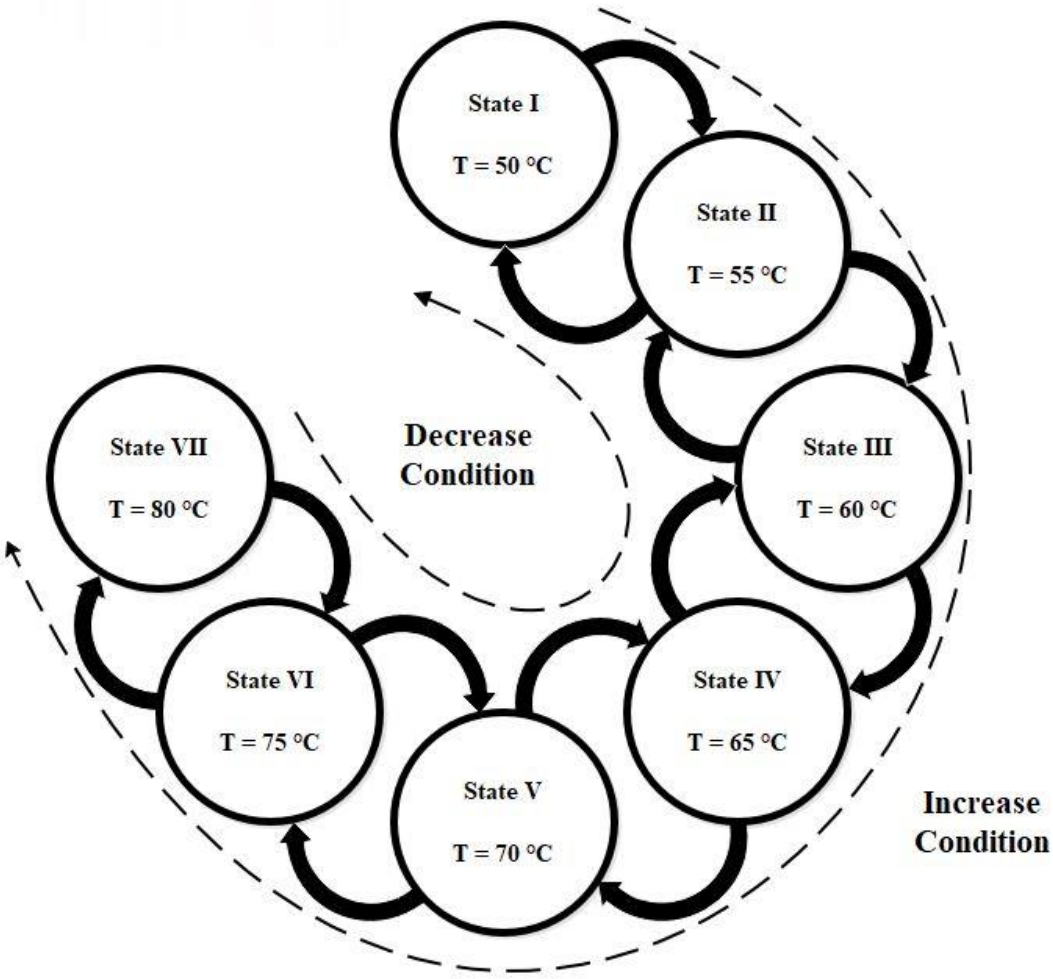

Fig. 3.6. SLC that determines temperature setpoint of the EMC hot header.

The second of the three SLCs is SLC 2, which prioritizes the charging of the BTES. It consists of seven states that represent the same temperature values as SLC 1, resulting in the same structure depicted in Figure 3.4. This controller is used to increase the temperature setpoint of the hot header to prevent the charging rate of the BTES from falling too low. As the seasonal storage is charged and its temperature increases, the temperature setpoint is increased. The transition to the next higher temperature state occurs when the temperature of the seasonal storage has increased by 5 °C. For example, when the temperature of the BTES is 20 °C, the temperature of the EMC hot header is 50 °C. Once the BTES temperature reaches 25 °C, the temperature setpoint of the EMC hot header is changed to 55 °C. Therefore, the sequential logic controller is restoring the temperature difference between the BTES and the hot header back to 30 °C to maintain a desirable charging rate.

The last of the controllers is referred to as SLC 3. It consists of two states, which represent the charging and discharging modes of the BTES and is used to manage the connection of the BTES to the EMC. In the discharging state, the seasonal storage is connected to the warm header. In this state, it discharges thermal energy to the warm header, and the heat pump extracts heat from it to add to the hot header. This is because the maximum temperature of the BTES is 60 °C, and the minimum temperature of the hot header is 50 °C. This means that for much of the discharging period, the temperature of the BTES is too low to transfer enough heat to the hot header. In the charging state, the BTES is connected to the hot header. It then imposes a thermal load on the hot header that is equivalent to the additional energy the CHP or heat pump can provide beyond the current demand of the consumers. This causes the MAS to increase the output of the CHP or heat

pump to provide the energy required to charge the storage. Transition from discharging to charging states occurs when the BTES reaches its minimum temperature of 20 °C. Similarly, transition from the charging to discharging state occurs when the BTES reaches its maximum temperature of 60 °C. When the controller changes state, it opens and closes the corresponding valves to connect the BTES to the appropriate header. The structure of SLC 3 is depicted in Figure 3.7.

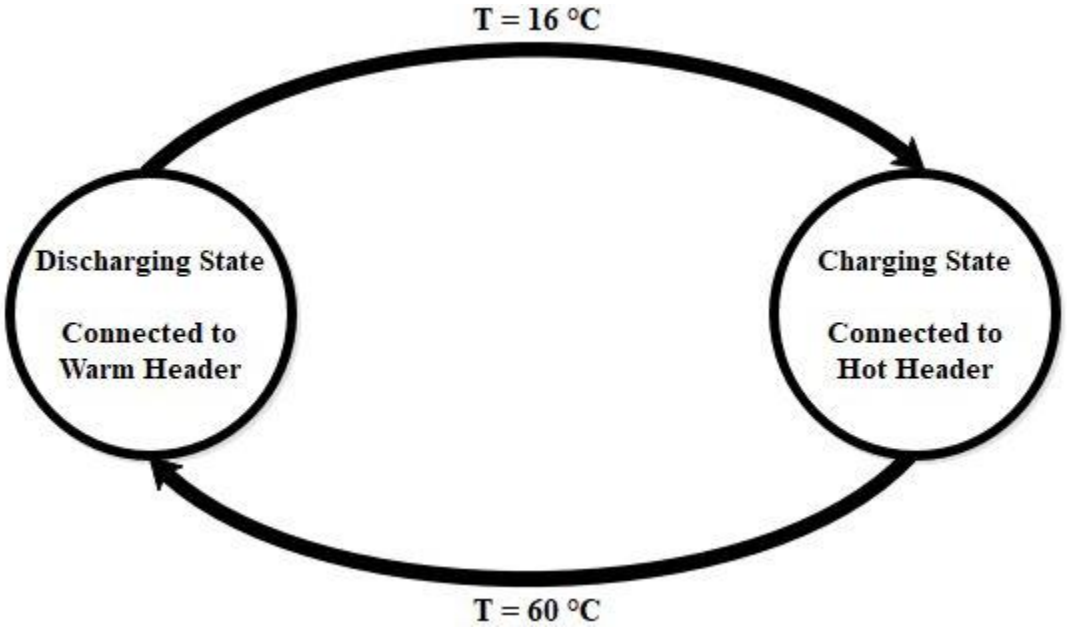

Fig. 3.7. SLC that determines mode of operation for the BTES.

The three sequential logic controllers work together in an integrated fashion to control the operation of the system to effectively utilize the STES and BTES. Since the BTES is connected to the warm header while discharging and the hot header while charging, SLC 3 is needed to switch between these two operating modes for the BTES. The operation of the ICE-Harvest system changes significantly based on this, resulting in two distinct phases for the control framework corresponding to the charging and discharging of the BTES.

During the discharging phase, the BTES is connected to the warm header and provides thermal energy to the system through the heat pump. At the same time, SLC 1 determines the appropriate temperature for the hot header to accommodate the operation of the STES. During the charging phase, the BTES is connected to the hot header and stores excess thermal energy produced by the CHP and heat pump. SLC 2 then increases the temperature setpoint of the header at the appropriate times to continue charging the BTES. To avoid providing conflicting inputs, SLC 1 and 2 must alternate their operation with the changing of the BTES operating mode. Therefore, SLC 3 is also utilized to switch between SLC 1 and 2, depending on which of the two should determine the temperature setpoint of the hot header. When SLC 3 is in the charging state, it sends a signal to SLC 2 to become active. At the same time, another signal is sent to SLC 1 to become inactive. In the charging state, there is little need for energy to be stored in the STES since thermal energy demand is low, and charging of the BTES is prioritized. In the discharging state, thermal energy demand is high and the BTES is no longer connected to the hot header. In this case SLC 3 signals for SLC 1 to become active again to control the temperature of the hot header and utilize the STES to help meet the increased demand for thermal energy.

3.2.3 Auxiliary Controllers

In addition to the MAS and SLCs which focus on operation of the EMC, the developed control structure also involves controllers which focus on operation of the MTN. These are referred to as Auxiliary Controllers and are located in the ETSs of each building and the heat exchangers connecting the EMC and MTN. Each controller is used to control the temperature or thermal power flow at specific points within the corresponding ETS or

heat exchanger. The collective action performed by the set of controllers is to maintain the temperatures supplied to building ETSs, and to facilitate waste heat recovery and thermal energy sharing between buildings. This will affect the net thermal energy demand from the MTN which is observed in the EMC by the MAS. Therefore, the MAS must respond to a thermal energy demand pattern which not only fluctuates based on the time of day or the season, but also based on the actions of the Auxiliary Controllers.

The heat exchanger which supplies thermal energy from the hot header to the MTN is controlled by a PID controller. As mentioned previously, the outlet temperature of this heat exchanger on the MTN side is maintained a constant 35 °C. This is done to provide consistent supply temperatures to the building ETSs. The action of this controller mitigates some of the natural fluctuation in the hot header temperature due to the operation of the MAS. Additionally, the high mass flow rate of the MTN results in relatively small changes in the temperature from inlet to outlet for any building ETS. This means that each building ETS typically receives a supply temperature that is only slightly higher or lower than 35 °C. Therefore, the heat pumps at each building ETS do not have drastically different COPs and electricity consumption from each other due to variation of temperature over the course of the MTN.

In order to accommodate heating and cooling demands, the heat pumps within building ETSs provide the required temperature to the heating and cooling systems. These heating and cooling heat pumps are controlled by PID controllers which manipulate the output power of the heat pump compressors based on the deviation from the temperature setpoint. The greater the output power of the compressor, the more thermal power the heat pump can transfer between its evaporator and condenser. Since mass flow rates within the

buildings are held constant, the changing of thermal power provided by the heat pump will alter the temperature provided to the heating and cooling systems and maintain it at the setpoint. It should be noted that the heating and cooling heat pumps must operate regardless of the status of natural gas peaking power plants on the electrical grid. This is because the heating and cooling demands of the buildings are paramount and must be satisfied at all times. Since the MTN is maintained at a constant temperature not suitable for direct heat exchange and it is a UTN, the only possible method of transferring thermal energy is utilizing heat pumps. As a result, the system must consume some electrical power during peak periods on the grid.

The heat recovery heat pumps at each ETS are controlled using a different method compared to their heating and cooling counterparts. Rather than tracking a temperature setpoint, they are controlled to provide a given amount of thermal power, which is equal to a desired portion of the heat rejected by the cooling heat pumps. PID controllers are used for this purpose as well, manipulating the output power of the heat pump compressors to control the thermal power transferred between evaporators and condensers. In order for the controller to provide an output signal to the compressor, the required electrical power must be calculated from the measured value and setpoint for thermal power. This relationship is influenced by the COPs of the heat recovery heat pumps; however, the effect on the performance of the controllers is minimal. Since the temperatures on either side of the heat recovery heat pumps are maintained in a small range, their COPs are also maintained in a small range. Therefore, the COP of each heat pump is assumed to be constant, which results in a small error in the calculated values, relative to the true electrical power required. This

is akin to noise in measurement instrumentation, which is suppressed by proper tuning of the PID controllers.

Similar to the heat pump in the EMC, the heat recovery heat pumps are operated according to the electrical peaks. The heat recovery heat pumps are only operating during off-peak periods to avoid increasing grid demand and the resultant GHG emissions during peak times. This means that thermal energy sharing between buildings only occurs during the off-peak periods. During the electrical peaks, the waste heat from cooling processes is rejected to the ambient environment through building cooling towers instead. Therefore, the amount of thermal energy shared fluctuates based on the electrical grid.

Thermal energy sharing also fluctuates due to the seasonal variation of heating and cooling demands within buildings. During the winter, the total heating demand is typically much greater than the total demand for cooling. Therefore, it is likely the amount of waste heat that can be recovered from cooling processes is not enough to satisfy all of the heating demand through thermal energy sharing. This means that when sharing occurs, the net demand of the MTN is only reduced, which results in a decrease of thermal energy that the MAS must provide. Moving toward the summer, the total heating demand diminishes while the total cooling demand increases. As a result, thermal energy sharing can accommodate an increasingly large portion of the total heating demand. During the summer, the heat recovered from cooling processes can meet or even exceed the total demand for heating. In this case, the MAS is not required to meet thermal energy demand of the MTN, and instead dispatches the thermal energy producers entirely for the purpose of charging the BTES. If the amount of thermal energy recovered at the buildings is greater than the total heating demand, the temperature at the inlet of the heat recovery system begins to rise due

to the surplus of thermal energy in the MTN. In this case, the heat recovery system is used to transfer the recovered waste heat to the warm header. The heat recovery system is controlled by another PID controller, which maintains the outlet of the heat exchanger at the same constant temperature setpoint as the MTN supply, cooling the fluid down as it passes through and returns to the supply heat exchanger. As a result, the supply temperature of the MTN is unaffected and no thermal energy is transferred to the MTN from the hot header.

The sets of Auxiliary Controllers work together to facilitate the bidirectional thermal energy flow between buildings and MTN, as well as MTN and EMC. This part of the control framework ensures the needs of consumers are always satisfied, and provides the system with demand management and heat recovery capabilities. Furthermore, the ability to perform heat recovery in the MTN is part of what facilitates the seasonal storage of thermal energy in the ICE-Harvest system. The thermal energy recovered in excess of the sharing between buildings is stored in the BTES during the off-peak times on the electrical grid. This allows the geothermal field to continue storing thermal energy when the CHP is not available to operate. Without this, the geothermal field would not be fully charged for the following winter season when it is a critical thermal energy producer that the MAS needs to reliably meet consumer demand. Therefore, the Auxiliary Controllers support the operation of the MAS in addition to accomplishing their aforementioned goals.

Chapter 4

ICE-Harvest Case Study and Model

4.1 Description of Case Study

To assess the performance of the developed control framework in a realistic ICE-Harvest application, a case study was performed using historical building data and a detailed model of the entire ICE-Harvest system. Historical heating, cooling and electrical energy consumption data over one year was collected for several existing buildings in an Ontario community to represent the thermal and electrical energy demands of consumers. Each is a different type of building with occupancy and load characteristics that vary significantly between them. The set of buildings consists of a library with a data center, a senior center, a community center, an arena and a residential condominium complex. These were selected to create a realistic scenario in which buildings are in close proximity and

the overall energy demand from the buildings is representative of independent consumers connected to the same energy system. This ensures that the case study accurately represents a real system and the control framework is robust enough to handle unpredictable load patterns and transient events. Data on the operation of natural gas peaking power plants in Ontario was collected for the same one-year period, and utilized to determine the availability of the energy producing units in the system - in particular, the CHP and heat pump [76]. These case study parameters which will be defined hereafter, are summarized by tables 4.1 – 4.3 at the end of this chapter.

The sets of data collected were used as input parameters within the system model. These data sets also provide the time-based events which form the dynamic conditions that cause perturbations in the physical system, and subsequent response by the control system. The model was developed using Dymola, which is an equation-based modelling software that utilizes the object-oriented programming language, Modelica. The Dymola software was chosen primarily due to its ability to model multi-energy systems, but also because there are many open-source libraries of validated component models available for use. The libraries used in this work are the Modelica Standard Library, Buildings Library, AIXLib and Microgrid Library from Modelon [57], [77]–[79]. The entire ICE-Harvest system model is depicted in Figure 4.1.

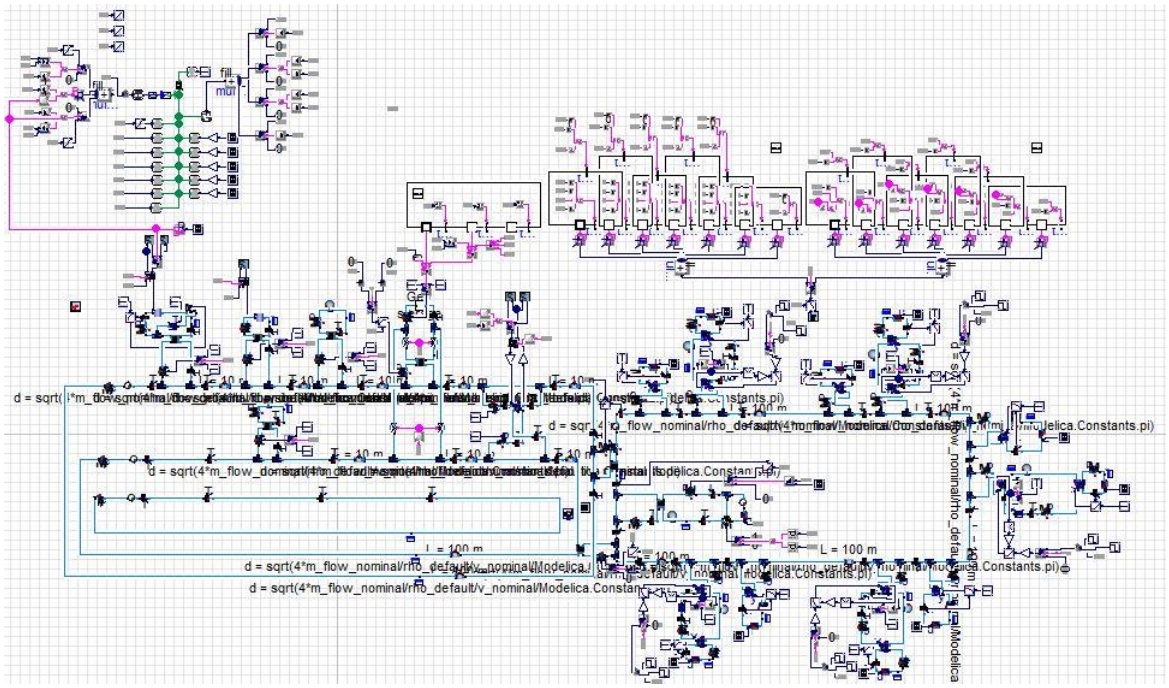

Fig. 4.1. Screen capture of entire system model within Dymola software.

A model was first developed for the physical system, which includes all of the interconnected thermal and electrical components. The model of the control framework was then developed, which consists of the various controllers that interact with components of the physical system. These two interconnected parts form the model of the entire system, which is simulated for one year in accordance with the case study. Within the model, the control system interacts with the physical system, reading state variables and adjusting control variables at each timestep. The development of the models for both the physical system and the control framework are discussed in detail in the proceeding sections.

4.2 ICE-Harvest Physical System Model

The physical part of the ICE-Harvest system model consists of the EMC and MTN. These are composed of various interconnected component models for the pieces of thermal and electrical equipment which make up the ICE-Harvest system. The EMC and MTN are connected by two heat exchangers which utilize the same plate heat exchanger model from the Buildings library [77]. The model is based on the effectiveness-NTU method which determines the amount of heat transferred by the heat exchanger [80]. At each timestep the thermal power transferred is calculated using equation 4.1:

$$\boldsymbol{Q = Q_{max}\varepsilon} \tag{4.1}$$

Where $\boldsymbol{\varepsilon}$ is the effectiveness of the heat exchanger and $\boldsymbol{Q_{max}}$ is the instantaneous maximum thermal power that can be transferred. The quantity $\boldsymbol{Q_{max}}$ is related to the mass flow rates and temperatures at the inlets of the heat exchanger according to equation 4.2:

$$\boldsymbol{Q_{max} = C_{min}\Delta T_i} \tag{4.2}$$

Where $\boldsymbol{C_{min}}$ is the lower heat capacity rate between the two heat exchanger streams, and $\boldsymbol{\Delta T_i}$ is the difference in temperature between their inlets. The heat capacity rate of a fluid stream is given by the product of its mass flow rate and specific heat capacity of the heat carrier fluid. The effectiveness of the heat exchanger depends on the heat capacity rates and temperatures of both streams, as well as the geometry and flow arrangement of the heat exchanger (i.e. counter-current or parallel flow). The heat exchangers within the system model utilize counter-current flow, whose effectiveness is given by equation 4.3:

$$\boldsymbol{\varepsilon = \frac{1 - exp[-NTU(1 - C_r)]}{1 - C_r exp[-NTU(1 - C_r)]}} \tag{4.3}$$

Where $\boldsymbol{C_r}$ is the ratio of heat capacity rates between the two streams and $\boldsymbol{NTU}$ is the number of transfer units, for which the NTU method gets its name. These are determined by equations 4.4 and 4.5:

$$\boldsymbol{NTU} = \frac{\boldsymbol{UA}}{\boldsymbol{C_{min}}} \tag{4.4}$$

$$\boldsymbol{C_r} = \frac{\boldsymbol{C_{min}}}{\boldsymbol{C_{max}}} \tag{4.5}$$

Where $\boldsymbol{U}$ is the overall heat transfer coefficient, $\boldsymbol{A}$ is the area of heat transfer, and $\boldsymbol{C_{max}}$ is the greater heat capacity rate of the two streams. The heat transfer coefficient is dependent on the materials from which the heat exchanger is constructed, the mechanism by which heat is transferred (i.e. conduction, convection or radiation), and the temperatures of the passing fluids. The value of the product $\boldsymbol{UA}$ is determined by the model and used to calculate the value of $\boldsymbol{NTU}$ at each timestep.

As described in Chapter 3, one of these heat exchangers is connected to the hot header and MTN supply, and the other is connected to the warm header and MTN return. The models of these two heat exchangers and their respective controllers determine the flow of thermal energy from the hot header to the MTN and from the MTN back to the warm header. This is elaborated upon in the proceeding subsections on the detailed description of the EMC and MTN models.

4.2.1 Modelling of Energy Management Center

In the modelling of the EMC, the energy producing units are connected to the headers in the arrangement depicted in Chapter 3, and are separated by small pipe segments, each 10 m in length. These pipe segments utilize the plug flow pipe model from AIXLib [78]. This model can incorporate thermal energy loss; however, this is neglected for the purposes of the case study. The EMC piping totals only 50 m in length and it is assumed that the pipes are sufficiently insulated and the EMC is housed within a climate-controlled building. These factors reduce the pipe losses to a negligible level.

The mass flow rate in each header is maintained at a constant value by their respective header pumps which use the flow-controlled pump model, also from AIXLib [78]. At each timestep, this model provides the desired flow rate and calculates the resulting pressure drop and efficiency from the pressure and efficiency curves provided to the model. These can be defined by manufacturer datasheets for a particular pump, or can be defined by the nominal mass flow rate and pressure drop values, which are input parameters of the model. To reduce the complexity of the ICE-Harvest system model, the latter method is utilized to define the pressure and efficiency curves of the pumps. This is also because the mass flow rates provided by the pumps are critical for the performance of the control system. It is assumed that in a real system, the pumping arrangements would be designed so that they have enough pumping power and can provide the required pressure to achieve desired mass flow rates.

The model of the CHP utilizes several components from AIXLib [78]. Firstly, the CHP is connected to the hot header by a heat exchanger which uses the same plate heat exchanger model mentioned previously. The thermal and electrical parts of the CHP are

modelled separately, and the energy produced in each is determined by the piece-wise function in equation 4.6:

$$\boldsymbol{P_{CHP}} = \begin{cases} \boldsymbol{Q_{CHP}}\left[\boldsymbol{\eta_r} - \boldsymbol{\Delta\eta_r}\left(\dfrac{\mathbf{501.9} - \boldsymbol{Q_{CHP}}}{\mathbf{501.9}}\right)\right], & \mathbf{0} < \boldsymbol{Q_{CHP}} \leq \mathbf{501.9}\ \boldsymbol{kW} \\ \boldsymbol{Q_{CHP}}\left[\boldsymbol{\eta_r} - \boldsymbol{\Delta\eta_r}\left(\dfrac{\mathbf{666.4} - \boldsymbol{Q_{CHP}}}{\mathbf{666.4} - \mathbf{501.9}}\right)\right], & \mathbf{501.9} < \boldsymbol{Q_{CHP}} \leq \mathbf{666.4}\ \boldsymbol{kW} \\ \boldsymbol{Q_{CHP}}\left[\boldsymbol{\eta_r} - \boldsymbol{\Delta\eta_r}\left(\dfrac{\mathbf{843.3} - \boldsymbol{Q_{CHP}}}{\mathbf{843.3} - \mathbf{666.4}}\right)\right], & \mathbf{666.4} < \boldsymbol{Q_{CHP}} \leq \mathbf{843.3}\ \boldsymbol{kW} \\ \boldsymbol{Q_{CHP}}\left[\boldsymbol{\eta_r} - \boldsymbol{\Delta\eta_r}\left(\dfrac{\mathbf{1025} - \boldsymbol{Q_{CHP}}}{\mathbf{1025} - \mathbf{843.3}}\right)\right], & \mathbf{843.3} < \boldsymbol{Q_{CHP}} \leq \mathbf{1025}\ \boldsymbol{kW} \end{cases} \quad (4.6)$$

Where $\boldsymbol{P_{CHP}}$ is the electrical power generated by the CHP and $\boldsymbol{Q_{CHP}}$ is the thermal power generated by the CHP. The parameter, $\boldsymbol{\eta_r}$ is referred to as the efficiency ratio, which is the ratio of the electrical ($\boldsymbol{\eta_{el}}$) and thermal ($\boldsymbol{\eta_{th}}$) efficiencies of the CHP. The value of these parameters for each partial load condition are given in table B.2 in Appendix B. The range of values for $\boldsymbol{Q_{CHP}}$ in each part of the piece-wise function are based on the measured data for partial load conditions of a real CHP unit. Between each of the given partial load operating points, the efficiency ratio is assumed to vary linearly with increasing thermal power output. Therefore, each part of the piece-wise function is a quadratic relationship between two partial load operating points.

The thermal energy production of the CHP is modelled with the non-controlled heat generator model from AIXLib [78]. This model simply provides the desired amount of thermal power at each timestep, which is transferred to the fluid passing through it. The CHP model also contains internal controls and a radiator to prevent the fluid inside from exceeding its temperature limit. If the temperature of the water entering the CHP reaches 90 °C, part of the fluid flow is diverted through the radiator by a three-way valve until the temperature decreases to 85 °C. This protection system seldom becomes active because the

temperature on the EMC side of the heat exchanger is typically too low to cause the internal temperature of the CHP to approach 90 °C.

Since the developed control framework is focused on thermal energy production, the electrical power produced by the CHP at each timestep is determined by the desired thermal power output according to equation 4.6. The electrical portion of the CHP model utilizes components from the Modelon Microgrid library. The electrical energy production of the CHP is modelled by the generic generator component. This model provides the desired electrical power at each timestep and calculates the amount of fuel consumed in kW based on the type of fuel selected in the model. This output from the model is ignored for the case study and the fuel consumption of the CHP is instead calculated according to the derived relationships for partial load efficiencies. The electrical power output of the generator is connected to a low-voltage bus model, which models the low-voltage AC network for the ICE-Harvest system.

The NGB is modelled in a similar fashion to the thermal portion of the CHP. It utilizes the same uncontrolled heat generator model and is connected to the EMC by the same effectiveness-NTU heat exchanger model. Unlike the CHP, the NGB is not equipped with an overheat protection system. This is because the temperature limit of the NGB is greater than that of the CHP, and is beyond the operating temperature limit of the EMC itself. Therefore, the fluid entering the NGB cannot become hot enough to cause it to exceed its temperature limits.

The heat pump located at the EMC is connected between the hot header and warm header. It utilizes the heat pump model based on Carnot efficiency from AIXLib [78]. The

electrical power consumed by the heat pump compressor is determined by a parameter $\boldsymbol{y}$ and the rated power of the compressor at each timestep. This is given by equation 4.7:

$$\boldsymbol{P_{HP} = P_{Rated} y} \tag{4.7}$$

Where $\boldsymbol{P_{HP}}$ and $\boldsymbol{P_{Rated}}$ are the output power and rated power of the compressor, respectively. The value of $\boldsymbol{y}$ can vary between 0 and 1, and represents a partial output percentage for the compressor. The respective amounts of thermal power removed from the warm header and added to the hot header by the heat pump are related to its instantaneous heating and cooling COPs and the output power of the compressor. The COPs of the heat pump are determined by the temperatures at the inlets of the evaporator and condenser, as well as the Carnot effectiveness. These relationships are given by equations 4.8 through 4.11:

$$\boldsymbol{COP_{Heat} = \frac{Q_H}{P_{HP}}} \tag{4.8}$$

$$\boldsymbol{COP_{Cool} = \frac{Q_C}{P_{HP}}} \tag{4.9}$$

$$\boldsymbol{COP_{Heat} = \eta \frac{T_H}{T_H + T_C}} \tag{4.10}$$

$$\boldsymbol{COP_{Cool} = \eta \frac{T_C}{T_H + T_C}} \tag{4.11}$$

Where $\boldsymbol{COP_{Heat}}$ and $\boldsymbol{COP_{Cool}}$ are the heating and cooling COPs, $\boldsymbol{Q_H}$ and $\boldsymbol{Q_C}$ are the thermal power flows of the condenser and evaporator, and $\boldsymbol{T_H}$ and $\boldsymbol{T_C}$ are the temperatures of the condenser and evaporator, respectively. The parameter $\boldsymbol{\eta}$ is the Carnot effectiveness of the heat pump, which is assumed to be constant.

The heat pump operates in conjunction with the geothermal storage field in the EMC and the heat recovery system in the MTN, since the heat pump requires a source of thermal energy to continue to operate. The geothermal storage field uses a simplified model

containing components for a storage volume, a heat exchanger and a heat loss to the outer field. The temperature of the storage volume is determined at each timestep based on the temperature at the previous timestep and the net thermal energy loss or gain from the heat exchanger and outer field loss. The amount of heat loss to the outer field is determined by the difference in temperature between the core and perimeter of the field. It is assumed that the perimeter of the field remains at a constant temperature. The model of the geothermal field is connected to the hot and warm headers of the EMC, through a pair of valves for each. These valves utilize the binary valve model which are either fully open or fully closed, depending on the input they receive.

4.2.2 Modelling of Micro-Thermal Network

The model of the MTN is constructed with many of the same component models that are used in the modelling of the EMC. Models of the consumer buildings and their ETSs are connected together by pipes that also utilize the plug flow model from AIXLib [78]. The network is composed of 5 such segments, therefore, it totals 500 m in length. As was the case with the EMC, the thermal losses from pipes in the system are neglected for the purposes of the case study. This is because the MTN is relatively short in comparison to many DE systems, which are typically designed to service entire cities or downtown cores, whereas the ICE-Harvest system in the case study services only 5 buildings.

The building models utilized in the case study only consider the energy use for heating, cooling and electricity. These are modelled as simple energy flows within the corresponding systems of each building. Thermal energy demands are implemented using a model for a simple heater or cooler from AIXLib [78]. This model provides the desired

heat flow based on the nominal value entered in the model and a percentage of this nominal heat flow which is input to the model. This percentage is given by the parameter ***u***, which varies between 0 and 1. This addition or removal of thermal energy due to demand results in a corresponding increase or decrease in temperature of the fluid returning to the ETS. In turn, the heat pumps at the ETS restore the temperature to the setpoint to be supplied back to the building heating or cooling system, which results in the corresponding temperature change in the MTN.

In the case that not all of the heat rejected from cooling can be recovered by the heat recovery heat pump, the cooling tower of the building will reject the remaining heat to the environment. This cools the fluid returning to the cooling heat pump so that it can continue to provide cooling to the building. This cooling tower is represented by a simple cooler model which provides the desired outlet temperature by removing the required amount of heat based on its mass flow rate and inlet temperature. It was assumed for the development of the system model that the cooling towers at each building are designed to handle the maximum amount of cooling the building could require. Therefore, it can be assumed that the cooling tower will always provide the desired temperature to be returned to the cooling system. The electrical energy demands are represented using the generic electrical load model from the Microgrid library. This model receives a real number as input and provides the same amount of electrical power consumption in W. The electricity demand for each building is the combination of plug loads, power consumed by heat pump compressors in the ETSs and power consumed by pumps in the ETS and building thermal systems.

4.3 Multi-Agent System Model

The MAS for the ICE-Harvest system was modelled using components from AIXLib. The library includes component models for heat and cold producer agents, consumer agents and the broker agent. The components utilized are implemented in the system model according to the documentation included within the library [57], [78]. Each agent in the MAS is given an identifier label depending on its type. The broker agent is given 10001, the consumer agent is given 20001, and the producer agents are given 30001-30003. More specifically, the labels 30001, 30002 and 30003 are given to the producer agents representing the CHP, NGB and EMC heat pump, respectively. All of the producer agents within the ICE-Harvest MAS utilize the heat producer agent model, since they control units that provide thermal energy to the hot header. There are no cold producer agents because the MAS is only used to control the EMC, which does not contain chilling units, nor does it provide cooling to the buildings.

The consumer agent represents the hot header temperature at the inlet to the heat exchanger connecting it to the MTN. The agent is connected to the hot header through a PID controller which determines the amount of thermal energy required by the header. Each producer agent is connected to the energy producer it controls, and a cost function model which determines the cost at which the agent provides thermal energy. The upper and lower limits of thermal power output for each agent are specified by parameters within the model. The availability of energy producers can be determined externally via input to the corresponding agent. This input is given by a Boolean function which acts as a conditional switch. The function of this external switch may be to disable the energy producer in the event that the operation is ill-advised. For example, while the heat pump

operates, the temperature of the warm header can decrease depending on the thermal power available from the geothermal field or the heat recovery system. If allowed to continue, this can cause the temperature to become low enough that the water in the warm header will freeze. Therefore, the external switch will disable the heat pump and stop the decrease of temperature before that point to allow the warm header to recover for some time. Since the CHP is unavailable during times when the heat pump operates, the NGB will make up for the temporary outage of the heat pump. The availabilities of the energy producing units are handled by the broker in the execution of the MAS control process.

The MAS controls the ICE-Harvest system through a negotiation process between the consumer and producer agents, which is facilitated by the broker. The negotiation process occurs every five minutes and begins with the consumer agent. The consumer agent receives input from the PID controller connected to the hot header, which is an estimate of the thermal power required to return the temperature to the setpoint. For example, if the difference in temperature between the measured value and the setpoint is 1 °C, the control error seen by the PID controller is 1. The output of the PID controller is then determined by equation 4.12:

$$\boldsymbol{u(t) = K_P\left(e(t) + \frac{1}{\tau_I}\int e(t)\,dt + \tau_D\frac{de}{dt}\right)} \tag{4.12}$$

Where $\boldsymbol{u(t)}$ is the output of the PID controller, $\boldsymbol{e(t)}$ is the control error, $\boldsymbol{\tau_I}$ and $\boldsymbol{\tau_D}$ are the time constants of the integral and derivative parts of the controller respectively, and $\boldsymbol{K_p}$ is the gain of the controller.

The agent communicates the output of this PID controller to the broker, requesting the estimated amount of thermal power from the producer agents. The broker then relays this to the producer agents, requesting the corresponding adjustment in their thermal power

output. Each producer agent responds to the request, either accepting or refusing it based on several criteria. If the current output of a producer is at the upper or lower limit and cannot provide the required change in thermal power, or if the producer is currently unavailable, it will refuse the request. If the producer agent accepts the request, it then responds to the broker with a price for the adjustment in thermal power output based on its cost function.

It is important to note that the cost functions must be adjusted during times when the corresponding energy producer is unavailable to operate. This is required to avoid a situation where the MAS attempts to select a unit which is unavailable, because its cost is the lowest. This is implemented by utilizing two cost function component models that are connected to the inputs of a switch model from the Modelica Standard Library [79]. The output of the switch is connected to the agent, and based on the availability of the unit, it allows the output of either cost function to pass through to the agent. Therefore, in the ICE-Harvest MAS, the cost functions for units that have varying availability are given by piece-wise functions. When a unit is available, its cost function is the product of a binary variable and a linear function. However, when a unit is unavailable its cost function is approximately infinite relative to what the cost would be if the unit were available. This is implemented by increasing the cost per W of the fuel consumed by the unit by several orders of magnitude. These units are the CHP and heat pump, the availabilities of which are related to each other. The cost function for the CHP is given by equation 4.13:

$$\boldsymbol{C_{CHP}} = \begin{cases} \boldsymbol{U_{CHP}}\left(\boldsymbol{p_{CHP}}\dfrac{\boldsymbol{P_{CHP}}}{\boldsymbol{\eta_{el}}}\right), & \boldsymbol{U_{CHP}} = \mathbf{1} \\ \infty \quad , & \boldsymbol{U_{CHP}} = \mathbf{0} \end{cases} \tag{4.13}$$

Where $\boldsymbol{C_{CHP}}$ is the cost of the thermal power adjustment from the CHP, $\boldsymbol{p_{CHP}}$ is the price of fuel per W, and $\boldsymbol{U_{CHP}}$ is the binary variable that represents the availability of the CHP. As mentioned previously, this availability is determined by historical data on the operation of natural gas peaking power plants on the Ontario electrical grid [76]. The CHP in the ICE-Harvest system is available when the peaking power plants are operating and unavailable otherwise. The value of $\boldsymbol{\eta_{el}}$ is used to calculate the amount of fuel consumed by the CHP from the amount of electrical power generated. The electrical efficiency is assumed to vary linearly with increasing part load ratio between the given operating points. This means that the relationship between the electrical efficiency and the part load ratio is another piece-wise linear function, which is given by equation 4.14:

$$\boldsymbol{\eta_{el}} = \begin{cases} \mathbf{0.776}\left(\dfrac{\boldsymbol{P_{CHP}}}{\mathbf{600}}\right) & , \quad \mathbf{0} < \boldsymbol{P_{CHP}} \leq \mathbf{150}\ \boldsymbol{kW} \\ \mathbf{0.284}\left(\dfrac{\boldsymbol{P_{CHP}}}{\mathbf{600}}\right) + \mathbf{0.123} & , \quad \mathbf{150} < \boldsymbol{P_{CHP}} \leq \mathbf{300}\ \boldsymbol{kW} \\ \mathbf{0.148}\left(\dfrac{\boldsymbol{P_{CHP}}}{\mathbf{600}}\right) + \mathbf{0.191} & , \quad \mathbf{300} < \boldsymbol{P_{CHP}} \leq \mathbf{450}\ \boldsymbol{kW} \\ \mathbf{0.092}\left(\dfrac{\boldsymbol{P_{CHP}}}{\mathbf{600}}\right) + \mathbf{0.233} & , \quad \mathbf{450} < \boldsymbol{P_{CHP}} \leq \mathbf{600}\ \boldsymbol{kW} \end{cases} \tag{4.14}$$

Since the heat pump is only available when the CHP is unavailable, the cost function for the heat pump is also influenced by the binary variable $\boldsymbol{U_{CHP}}$. However, there is an additional binary variable that must be included in the cost function of the heat pump. This is because the other determining factor of the availability for the heat pump is the limitation that its source temperature is not allowed to fall below a certain threshold to prevent the water in the warm header from freezing. Therefore, the cost function for the heat pump is given by equation 4.15:

$$\boldsymbol{C_{HP}} = \begin{cases} \infty & , \quad \boldsymbol{U_{CHP}} = \mathbf{1}\ ; \boldsymbol{U_{Temp}} = \mathbf{0} \\ \boldsymbol{U_{Temp}}(\mathbf{1} - \boldsymbol{U_{CHP}})(\boldsymbol{p_{HP}}\boldsymbol{P_{HP}}), & \quad \boldsymbol{U_{CHP}} = \mathbf{0}\ ; \boldsymbol{U_{Temp}} = \mathbf{1} \end{cases} \tag{4.15}$$

Where $\boldsymbol{C_{HP}}$ is the cost of the thermal power adjustment from the heat pump, $\boldsymbol{p_{HP}}$ is the price of electrical power per W, $\boldsymbol{P_{HP}}$ is the electrical power consumed by the heat pump compressor, $\boldsymbol{U_{Temp}}$ is the binary variable which represents the temperature of the medium header in relation to the threshold.

The temperature threshold utilized for the heat pump in this case is 10 °C. Since it is only available when the CHP is not operating, the heat pump at the EMC is only allowed to operate during the off-peak periods on the electricity grid. As stated in Chapter 3, this is because the heat pump in the ICE-Harvest system is utilized to provide thermal energy by consuming off-peak electricity, which is assumed to be generated by carbon-free sources. Additionally, the heat pump can only operate while the temperature of the warm header is greater than 10 °C. In the event that the heat pump becomes unavailable strictly due to the temperature condition, the MAS will dispatch the NGB to meet the entire thermal energy demand from the MTN. The NGB does not have the same changing availability as the CHP and heat pump; therefore, its cost function is much simpler. Since the thermal efficiency of the NGB is assumed to be constant, its cost function is given by equation 4.16:

$$\boldsymbol{C_{NGB}} = \frac{\boldsymbol{p_{NGB}Q_{NGB}}}{\boldsymbol{\eta_{th}}} \tag{4.16}$$

Where $\boldsymbol{C_{NGB}}$ is the cost of adjusting NGB thermal power output, $\boldsymbol{p_{NGB}}$ is the price of fuel per W, and $\boldsymbol{Q_{NGB}}$ is the thermal power being generated by the NGB. The NGB is always available in the ICE-Harvest MAS because it operates as the thermal energy backup for the system. Therefore, it must always be available to supplement or replace the CHP or heat pump depending on the situation. As a result, the cost function for the NGB is not a piece-wise function like those of the CHP and heat pump.

The ICE-Harvest MAS uses the costs provided by the agents to complete the negotiation process. The broker selects the producer that responded with the lowest cost, and signals it to initiate the change in output. The repetition of this process maintains the control of temperature in the system, while also controlling the output of the energy producing units. Therefore, the MAS is balancing the thermal energy supply and demand of the system in order to maintain the temperature near the desired setpoint. However, the inherent function of the MAS is only to provide control of the system for a constant temperature setpoint. In order to change the operating temperature of the system without jeopardizing performance, an upper layer of control is required to strategically provide new setpoints to the MAS at the appropriate times. In the ICE-Harvest MAS, this is accomplished by utilizing the SLCs to switch between discrete temperature setpoints for the MAS. The modelling of the SLCs is discussed in detail in the following section.

4.4 Sequential Logic Controller Models

The upper layer of the modelled ICE-Harvest control framework consists of the three SLCs that were described in Chapter 3. Two of these are the controllers that operate alternately from each other to adjust the temperature setpoint of the hot header. The remaining SLC determines which of the other two is active based on whether the BTES is charging or discharging and adjusts the connection of the BTES to the appropriate header. These are constructed using component models from the StateGraph package of the Modelica Standard Library [79]. As stated previously, each SLC consists of several discrete states, which are modelled with a step and signal component. This component model represents a state that the SLC can be in, and the corresponding output in that state,

which is given by a Boolean variable. The states are connected to each other by another component model called a transition with signal. This model receives an input signal, which is a Boolean function of various measured values from the physical system. This Boolean function is what implements the temperature increase and decrease conditions for each SLC as outlined in Chapter 3. The two controllers used to adjust the temperature setpoint of hot header each have a different set of conditions. The SLC that is active while the BTES is discharging is referred to as SLC 1, and the Boolean functions which represent its increase and decrease conditions respectively, are given by equation 4.17 and 4.18:

$$\boldsymbol{B_{inc} = U_{HH} U_{CHP} U_{Q}} \tag{4.17}$$

$$\boldsymbol{B_{dec} = U_{STES}(1 - U_{CHP}) U_{NGB}} \tag{4.18}$$

Where the binary variables, $\boldsymbol{U_{HH}}$, $\boldsymbol{U_{STS}}$, $\boldsymbol{U_{Q}}$, $\boldsymbol{U_{NGB}}$ represent comparisons of measured values against thresholds for the temperature of the hot header and STES, and thermal power output of the CHP and NGB respectively. It can be seen from these functions that if any factor is equal to 0, the output of the function is also 0. The output becomes 1 only when all of the factors are equal to 1. Therefore, these functions are both logically equivalent to a three-input AND gate. This is implemented in the ICE-Harvest system model using components from the Modelica Standard Library which represent a multi-input AND gate and logical expressions for each factor in the Boolean functions [79]. A schematic representation of this logic circuit is depicted in Figure 4.2.

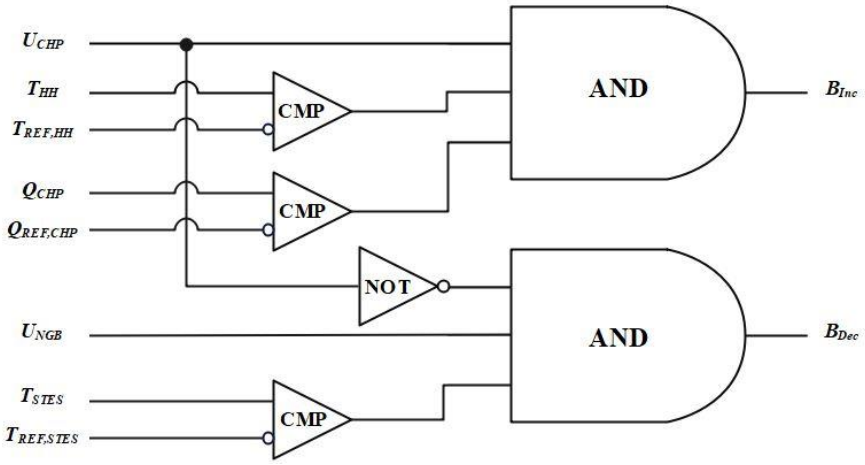

Fig. 4.2. Schematic representation of logic circuit used to change state of SLC 1.

Similarly, the SLC that is active while the BTES is charging is referred to as SLC 2. In the case of this SLC, the Boolean functions utilized are slightly different. Since the operation of the system is focused on charging the BTES, the temperature setpoint of the hot header is adjusted based on the current temperature of the header and the state of charge of the BTES rather than the operation of the energy producers. Additionally, the BTES only switches between the charging and discharging modes when the geothermal field is fully charged or discharged. Therefore, this SLC is only increasing the temperature setpoint during the time it is active. However, the temperature decrease conditions are still necessary for the operation of the control framework since the SLC must return to its original state to begin the charging phase for the following year. For this SLC, the Boolean functions that represent the temperature increase and decrease conditions respectively, are given by equation 4.19 and 4.20:

$$\boldsymbol{B_{inc} = U_{BTES} U_{Charge}} \tag{4.19}$$

$$\boldsymbol{B_{dec} = (1 - U_{BTES}) U_{Discharge}} \tag{4.20}$$

Where U_{BTES} is the binary variable that represents the comparison of the measured temperature of the BTES against its threshold value, while U_{Charge} and $U_{Discharge}$ are the binary variables that represent whether the BTES is charging or discharging, respectively. When the temperature of the BTES is greater than the threshold, the value of U_{BTES} is 1, otherwise it is 0. Therefore, the temperature setpoint of the hot header is increased when the temperature of the BTES exceeds the current threshold and it is in the charging mode. Conversely, the setpoint is decreased when the BTES is in the discharging mode, and its temperature falls to the threshold value or below. These are implemented in the system model in the same way as the set of Boolean functions for the previous SLC. The schematic representation of the corresponding logic circuit is depicted in Figure 4.3.

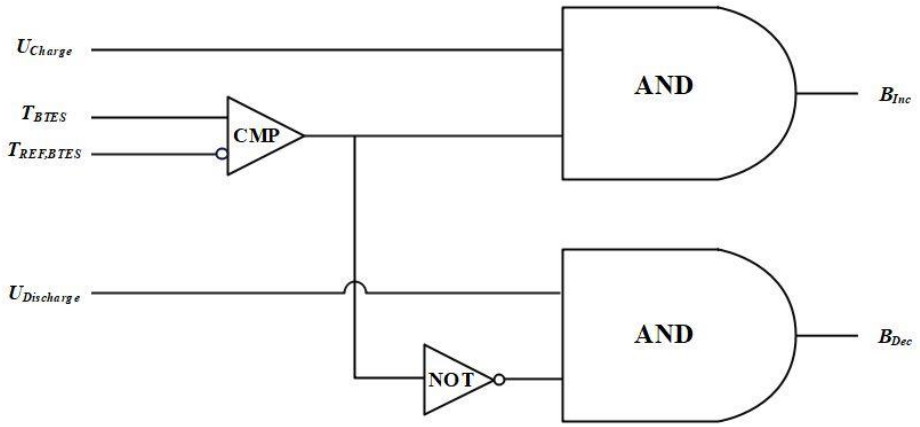

Fig. 4.3. Schematic representation of logic circuit used to change state of SLC 2.

When the output of one of these Boolean functions becomes true, the corresponding transition component is activated. This causes the corresponding SLC to change from the current state to the state it is connected to through the transition component that has just become active. The new state component becomes active and the previous state component becomes inactive, resulting in the corresponding changes in their Boolean outputs. When

a state becomes active, its output becomes true. Since only one state in a single SLC can be active at one time, the remaining states are inactive and their Boolean outputs are all false. Therefore, the output of the controller as a whole can be viewed as a binary value with $\boldsymbol{n}$ bits, where $\boldsymbol{n}$ is equal to the number of states in the SLC. The bit which corresponds to the active state of the SLC is set to 1 while the remaining bits are set to 0. Therefore, the changing of states represents a bitwise shift of this binary value in the corresponding direction. This output from the controller is utilized to determine the appropriate temperature setpoint for the hot header from equation 4.21:

$$\boldsymbol{T_{set,MAS} = \sum_{i=1}^{n} U_i T_{set,i}} \tag{4.21}$$

Where $\boldsymbol{U_i}$ is the binary variable that represents the Boolean output from a given state and $\boldsymbol{T_{set,i}}$ is the temperature setpoint that corresponds to the active state. Since there can only be one active state for any SLC, the terms of this equation are all equal to 0, except for the one which corresponds to the active state. Therefore, the result of this equation is the selection of the appropriate temperature setpoint. This equation is utilized for both of the temperature-changing SLCs. In the system model, this equation is represented by the Real to Boolean and Multi-Sum component models from the Modelica Standard Library [79]. These components convert a Boolean input to the corresponding real number output, and add multiple real number inputs together, respectively. A schematic representation of the resulting circuit is depicted in Figure 4.4.

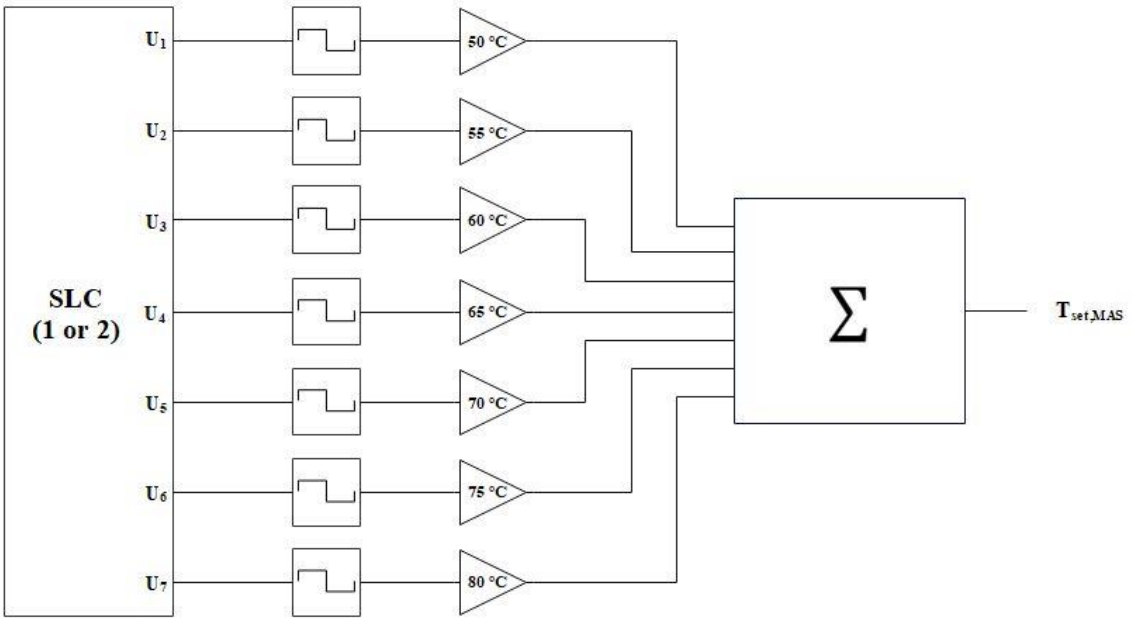

Fig. 4.4. Schematic representation of logic circuit used to provide temperature setpoint to MAS.

The SLC that determines the operation of the BTES is referred to as SLC 3, and is modelled with the same components as SLC 1 and 2. Its two states and transitions are modelled using the step with signal and transition with signal components, respectively. Since the active state of this SLC determines whether the BTES is charging or discharging, the Boolean outputs of the states are the binary variables $\boldsymbol{U_{Charge}}$ and $\boldsymbol{U_{Discharge}}$, which were previously defined. The transitions between the two states are determined solely by the state of charge of the BTES. Switching from discharging to charging occurs when the geothermal field reaches its lower temperature limit, and it switches back to discharging when the high temperature limit is reached. These conditions are described by equation 4.22 and 4.23:

$$\boldsymbol{B_{charge} = U_{LO}} \tag{4.22}$$

$$\boldsymbol{B_{discharge} = U_{HI}} \tag{4.23}$$

Where $\boldsymbol{B_{charge}}$ and $\boldsymbol{B_{discharge}}$ are output of the Boolean functions that represent transition to the charging and discharging phase respectively, and the binary variables $\boldsymbol{U_{LO}}$ and $\boldsymbol{U_{HI}}$ represent the comparison of the measured geothermal field temperature with its respective low and high temperature limits. Since the output of each function is determined by a single binary variable, they are implemented in the model using a single logical expression. Additionally, the outputs of these functions determine the arrangement of the valves connecting the BTES to the rest of the system. When the BTES is discharging and the value of $\boldsymbol{U_{Discharge}}$ is 1, the valves connecting the BTES to the warm header are opened and those connecting the BTES to the hot header are closed. The positions of the valves are then switched when the value of $\boldsymbol{U_{Charge}}$ changes from 0 to 1, and the BTES is connected to the hot header. The pair of valves for each header receive a Boolean input signal from the SLC, fully opening when the input is 1 and fully closing when the input is 0.

The combined operation of the three SLCs within the ICE-Harvest system can be considered a two-stage process to select the appropriate temperature setpoint for the hot header. First, the SLC associated with the BTES determines whether the geothermal field should be charged or discharged based on its temperature. The SLC then manipulates the corresponding valves to connect the BTES with the appropriate header. Simultaneously, the output from this SLC is used to determine which of the SLCs that control the hot header temperature setpoint is active. When the first SLC is in the discharging state, the SLC which prioritizes the operation of the STES is active. The SLC that prioritizes the operation of the BTES is then active when the first SLC is in the charging state. The outputs of both SLCs are connected to the inputs of a switch, the output of which is connected to the PID controller at the input of the MAS. The position of the switch depends on which SLC is

active, and the output of the active SLC is passed through to the MAS. A schematic representation of the interconnection of all three SLCs and the components they interface with is depicted in Figure 4.5.

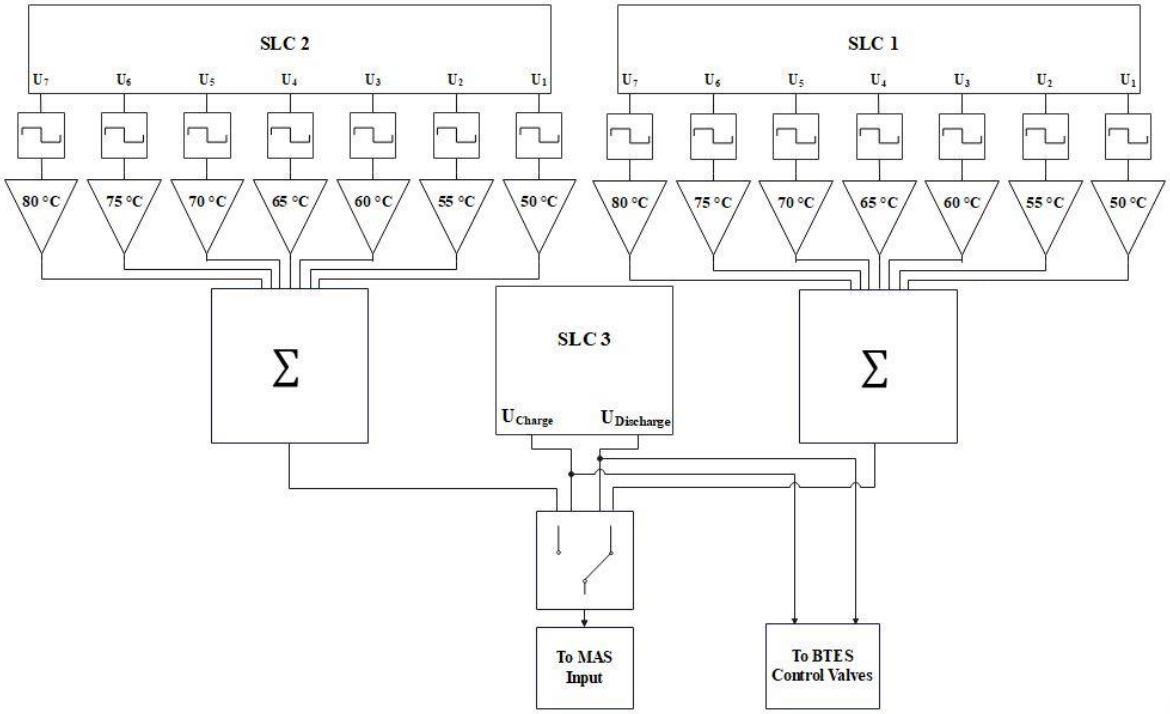

Fig. 4.5. Schematic representation of interconnection of all SLCs to rest of system.

As mentioned previously, the parameters of the case study which were introduced throughout this chapter are summarized by Tables 4.1 – 4.3. Table 4.1 provides the upper and lower limits for variable case study parameters. These represent continuous ranges of possible values for each parameter. Table 4.2 provides the value of all constant case study parameters. Finally, Table 4.3 provides data on the overall energy demand of the set of buildings. These are the minimum, maximum and average demand, as well as the total consumption for heating, cooling and electricity.

Table 4.1: Ranges of Variable Case Study Parameters

Parameter	**Minimum Value**	**Maximum Value**
P_{CHP}	0 kW	600 kW
P_{HP}	0 kW	220 kW
P_{EES}	0 kW	200 kW
E_{EES}	0 kWh	800 kWh
T_{HH}	50 °C	80 °C
T_{WH}	10 °C	50 °C
Q_{CHP}	0 kW	1025 kW
Q_{NGB}	0 kW	3000 kW
Q_{HP}	0 kW	1000 kW
T_{BTES}	16 °C	60 °C
$T_{STES,HH}$	50 °C	80 °C
$T_{STES,WH}$	10 °	50 °C

Table 4.2: Values of Constant Case Study Parameters

Parameter	**Constant Value**
$\dot{m}_{EMC}$	150 kg/s
$\dot{m}_{MTN}$	150 kg/s
f_{EMC}	60 Hz
$V_{EMC,AC}$	600 V
$V_{EMC,DC}$	240 V
T_{MTN}	35 °C
$\eta_{th,NGB}$	0.8
$\eta_{th,CHP}$ *(25% output)*	0.646
$\eta_{el,CHP}$ *(25% output)*	0.194
$\eta_{th,CHP}$ *(50% output)*	0.589
$\eta_{el,CHP}$ *(50% output)*	0.265
$\eta_{th,CHP}$ *(75% output)*	0.565
$\eta_{el,CHP}$ *(75% output)*	0.302
$\eta_{th,CHP}$ *(100% output)*	0.555
$\eta_{el,CHP}$ *(100% output)*	0.325

Table 4.3: Summary of Overall Building Energy Demands

	Minimum (kW)	**Maximum (kW)**	**Average (kW)**	**Total (MWh)**
Heating	0	4362	1234	10808
Cooling	0	3607	838	7342
Electrical	309	1528	838	7344

Chapter 5

Analysis from Multiple Perspectives

5.1 Long-term Results

This section presents results obtained from the simulation of the system model and analysis of the results over the one-year duration of the case study, beginning January 1st, 2017. Analysis of system performance over the long-term can provide useful insight on the merits and potential areas for further innovation of the ICE-Harvest system and the developed control framework. As mentioned in previous chapters, the operation of the ICE-Harvest system can be broken down into two distinct modes corresponding to the charging and discharging of the BTES. The developed control framework operates differently in each mode, which can be observed from the long-term results. The long-term behaviour of the control framework is also influenced by several other factors including seasonal

variations in thermal demand, operation of peaking power plants on the Ontario electricity grid, and the coincidence of building heating and cooling profiles. These affect how the ICE-Harvest control system operates at all levels, and are summarized in Table 5.1 below.

Table 5.1: Summary of Energy Demands on ICE-Harvest System

	Minimum (kW)	**Maximum (kW)**	**Average (kW)**	**Total (MWh)**
Heat removed from MTN	0	3358	981	8593
Heat added to MTN	0	2098	246	2153
Electricity Consumption	381	2438	1169	10633

The MAS responds to the net thermal demand of the buildings by balancing it with thermal energy supplied by the system. The heating and cooling demands of buildings vary significantly with outdoor air temperature and a variety of other factors, which results in seasonal variation of the net thermal demand from the MTN. As a result, the thermal energy producers that are repeatedly dispatched by the MAS, and the magnitude of the corresponding changes in their output are related to this demand. For the performed case study, this behaviour is depicted in Figure 5.1.

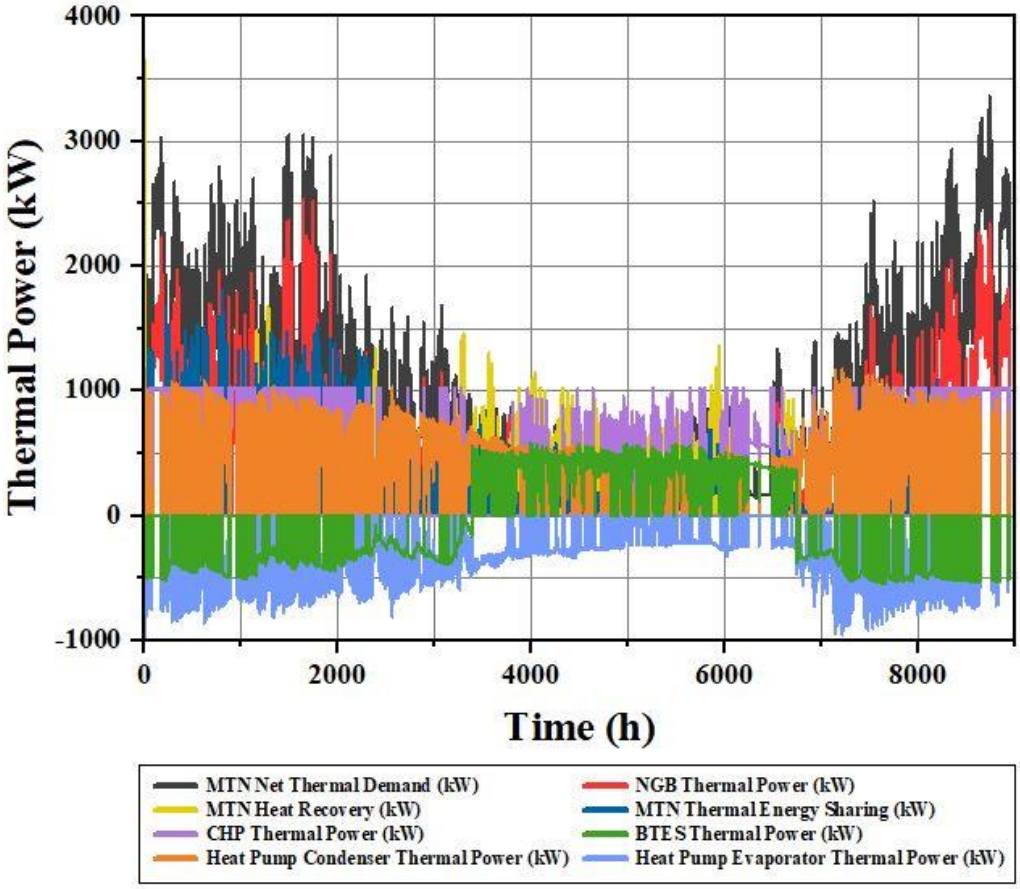

Fig.5.1: Main thermal power flows in EMC and to MTN over the entire year.

It can be observed that during the winter months, when heating demand is the highest, the thermal power output of the NGB follows a similar trend to the net thermal demand of the MTN. This is due to the fact that the CHP and heat pump are preferred over the NGB when they are available. Since the availabilities of the CHP and heat pump are opposite each other due to the electrical peaks, one of them is always available to operate. As a result, the MAS dispatches whichever of the two is currently available, until the point where the unit reaches its maximum thermal power output. Only then does the MAS dispatch the NGB to meet any remaining demand, which results in it following the net thermal demand of the MTN.

Additionally, during the summer months when heating demand is low, either the CHP or heat pump can meet the entire net thermal demand of the MTN, which means the NGB is often inactive and no longer following the same trend. It can also be seen from these results that the thermal power flow of the BTES is related to the heat pump and CHP, depending on whether it is charging or discharging. While in discharging mode (when BTES thermal power is negative), the thermal power flow from the BTES is related solely to that of the heat pump evaporator. When the heat pump begins to operate, BTES begins to discharge to the warm header. The evaporator of the heat pump removes a portion of this thermal energy from the warm header to provide thermal energy to the hot header. Depending on the thermal demand of the MTN, the amount of thermal power which is removed from the warm header varies, and may not be equal to that provided by the BTES unit. This is because the thermal power which flows from the BTES to the warm header is dependent on its own temperature and the temperature of the header.

Simultaneously, the thermal power the heat pump extracts from the warm header, and that which is discharged by the BTES will both influence the header temperature. These factors result in the relationship between the thermal power provided by the BTES and that extracted by the heat pump being coupled to each other by the temperature of the warm header. Therefore, the tandem operation of the heat pump and BTES will cause the temperature of the warm header to fluctuate between the minimum threshold for heat pump operation and the current temperature of the geothermal field. While in the charging mode (when BTES thermal power is positive), the thermal power flow of the BTES is related to that of the CHP or heat pump condenser, depending on which producer is active. Since the BTES is connected to the hot header during the charging phase, its thermal power flow is

no longer directly affected by the temperature of the warm header. However, the heat pump is still connected to the warm header to extract thermal energy. Since the BTES is no longer acting as a source of thermal energy for the heat pump, it utilizes heat recovered from the MTN as its source. The only dependency on the warm header temperature is again the minimum threshold for heat pump operation of 10 °C.

As mentioned in previous chapters, the thermal power drawn from the hot header by the BTES is controlled by manipulating the mass flow rate through a heat exchanger connecting the two. This allows the BTES to consistently draw the amount of thermal power that can be provided by the CHP or heat pump, subtracted by the net demand from the MTN. In this way, the BTES imposes a thermal demand on the hot header which results in the total thermal demand seen by the MAS to increase and be met by the CHP or heat pump. The amount of thermal energy that can be stored in and extracted from the BTES is also related to the operation of peaking power plants. During the discharging phase, thermal energy is only able to be extracted from the geothermal field during off-peak periods on the electricity grid, due to its dependence on the availability of the heat pump. As a result, the system solely relies on carbon-free electricity to extract thermal energy from BTES. If for a given year the grid is peaking power intensive for a significant portion of the discharging phase, then it is possible that not all of the energy that was stored in the geothermal field can be used. In turn, the BTES is forced to hold thermal energy and suffer heat loss to the perimeter of the geothermal field. Conversely, the storing of harvested thermal energy during the charging phase is less influenced by the electricity grid. As mentioned earlier, charging of the BTES is accomplished with both the heat pump and CHP, and one of the two is always available to operate. This means that thermal energy

can be stored in the geothermal field regardless of whether it is an electrical peak or not. However, the difference between the heat pump and CHP lies in the amount of thermal energy they can provide for charging. The CHP can charge the BTES with a consistent amount of thermal power depending on the temperature of the hot header and the geothermal field.

On the other hand, the thermal power that the heat pump can provide depends on the temperature of the warm header and the amount of heat recovered from the MTN as well. Since heat recovery from the MTN is the source for the heat pump, the amount of thermal energy it can charge the BTES with is limited by the amount of heat that can be recovered. If the heat pump draws more thermal power than the heat recovery system is providing, the temperature of the warm header will decrease. This reduces the COP of the heat pump, which limits the thermal energy transferred to the hot header and in turn, that which is transferred to the BTES. Furthermore, if the temperature of the warm header decreases below the minimum threshold, the MAS shuts the heat pump down and the BTES will not be able to charge until it is available again. As a result of these factors, not only does the heat pump provide slightly less thermal power for charging compared with the CHP, it may not be able to operate for the entire time it is available. Therefore, the total time that peaking power plants are online during the charging phase will have some influence on the amount of energy stored in the BTES.

The seasonal variation of thermal demand also has a significant impact on the SLCs since this feature of the control framework both influences and is influenced by the operation of the MAS. As mentioned in Chapter 3, the primary function of the set of SLCs is to adjust the temperature setpoint of the MAS in order to effectively utilize the thermal

energy storage units in the system. In the case of SLC 1, the controller increases and decreases the temperature setpoint to utilize the STES based on the output of the CHP and NGB. As a result, the effect of varying thermal demand on the operation of these units will affect charging and discharging of the STES. For example, if demand is high, there is less thermal energy available to be harvested from the CHP and stored in the STES. Less thermal energy can then be extracted from the STES to offset NGB use when the CHP goes offline. This effect will then be observed in the changing temperature setpoint determined by SLC 1. Similarly, SLC 2 increases the temperature setpoint based on the temperature of the geothermal field to maintain effective charging of the BTES. Over the course of the charging phase, thermal demand has an effect on the amount of thermal energy that can be harvested and stored. As a result, the timing of temperature setpoint increases by SLC 2 are affected, and subsequently, the system may not be able to fully charge the BTES before it is needed as a heat source again. The amount of energy stored over the charging phase coupled with the demand during the next discharge phase will determine how much thermal energy is then extracted from the geothermal field. In turn, this has an effect on the operation of energy producers by the MAS. Therefore, the variation thermal demand over the course of the year can affect the performance of the system not only that year, but the following year as well. The temperature profile of the system over the entire year is depicted in Figure 5.2.

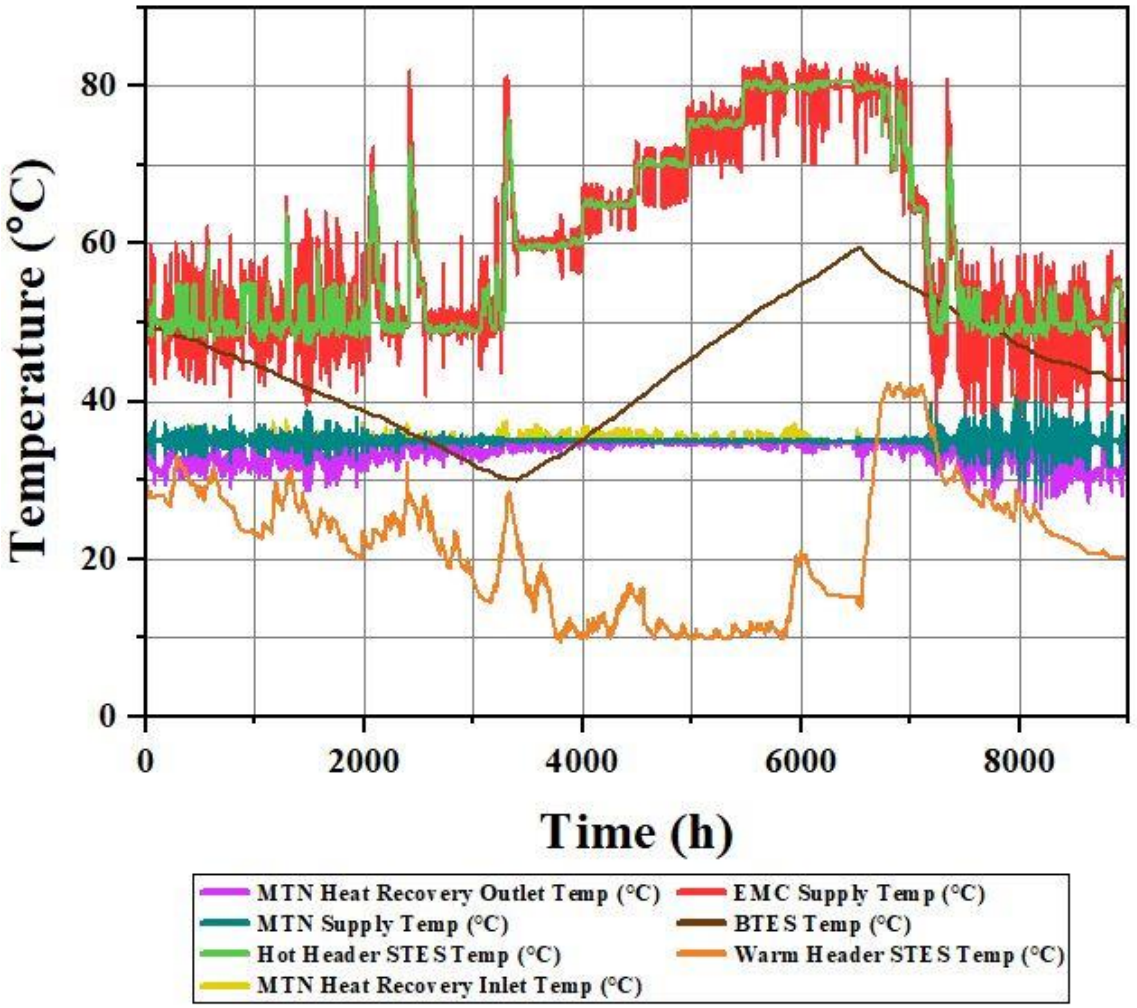

Fig. 5.2: Main temperatures in the EMC and MTN over the entire year.

It can be seen from Figure 5.2 that when the system is operating in the discharging mode (when BTES temperature is decreasing), the temperature setpoint of the hot header rarely increases above 55 °C. This is due in large part to the frequent switching of the CHP and heat pump, which can be observed from Figure 5.1. As stated in Chapter 3, SLC 1 only increases the temperature setpoint of the hot header when the CHP is available and can supply enough additional heat to charge the STES. It only then decreases the setpoint when the CHP is offline and the NGB becomes active, so the thermal energy that was stored can

offset NGB use. For the majority of the discharging phase, high thermal demand results in the system being unable to increase the temperature of the STES beyond 55 °C before it needs to discharge again. Only once thermal demand begins to decrease during the shoulder seasons, can SLC 1 increase the temperature setpoint beyond 55 °C for any significant period of time. In addition to high thermal demand, sporadic operation of the CHP also contributes to this inability to increase the temperature setpoint above 55 °C. This is due to the operation of peaking power plants on the electricity grid.

The electrical peaks are relatively short in duration, which causes frequent switching of the CHP and heat pump. As a result, the STES repeatedly switches between charging and discharging, causing only small amounts of thermal energy to be stored and extracted. During the charging phase (when BTES temperature is increasing) the opposite is true, and SLC 2 is easily able to increase the temperature setpoint for the hot header up to the 80 °C maximum. This is because heating demand is low during this time of the year and there is a large amount of thermal energy that can be harvested from building cooling processes and the CHP. As a result, the BTES is easily able to charge and its temperature increases, causing SLC 2 to increase the setpoint for the hot header. Additionally, both the heat pump and CHP are able to provide the thermal energy for raising the temperature of the hot header, since the heat pump is extracting thermal energy from the heat recovery system instead of the BTES. This means that SLC 2 is able to increase the temperature setpoint of the hot header during both on-peak and off-peak times, which contributes to this ability to reach the maximum temperature.

Seasonal variations in thermal demand have an impact on the operation of the Auxiliary Controllers as well. Naturally, the operation of the controllers in building heating

and cooling systems are directly affected by this, since their function is to accommodate the thermal demands of the buildings. As a result, the controllers associated with building cooling towers and heat recovery systems are affected by thermal demands as well. When operational, the cooling towers are required to reject more heat to the ambient environment when cooling demand is high. Increased cooling demand also means that the heat recovery heat pumps are able to harvest more thermal energy from cooling processes and the associated controllers must adjust their setpoints accordingly. The thermal power setpoints of the heat recovery heat pump controllers are decreased during the cooling season to avoid overheating the MTN if not all of the heat recovered can be transferred back to the EMC. This is because operating the MTN at higher temperatures would decrease the COP of the heat recovery heat pumps and cause the electricity consumption of the system to increase significantly. The collective action of the set of Auxiliary Controllers on the system is depicted in Figure 5.3.

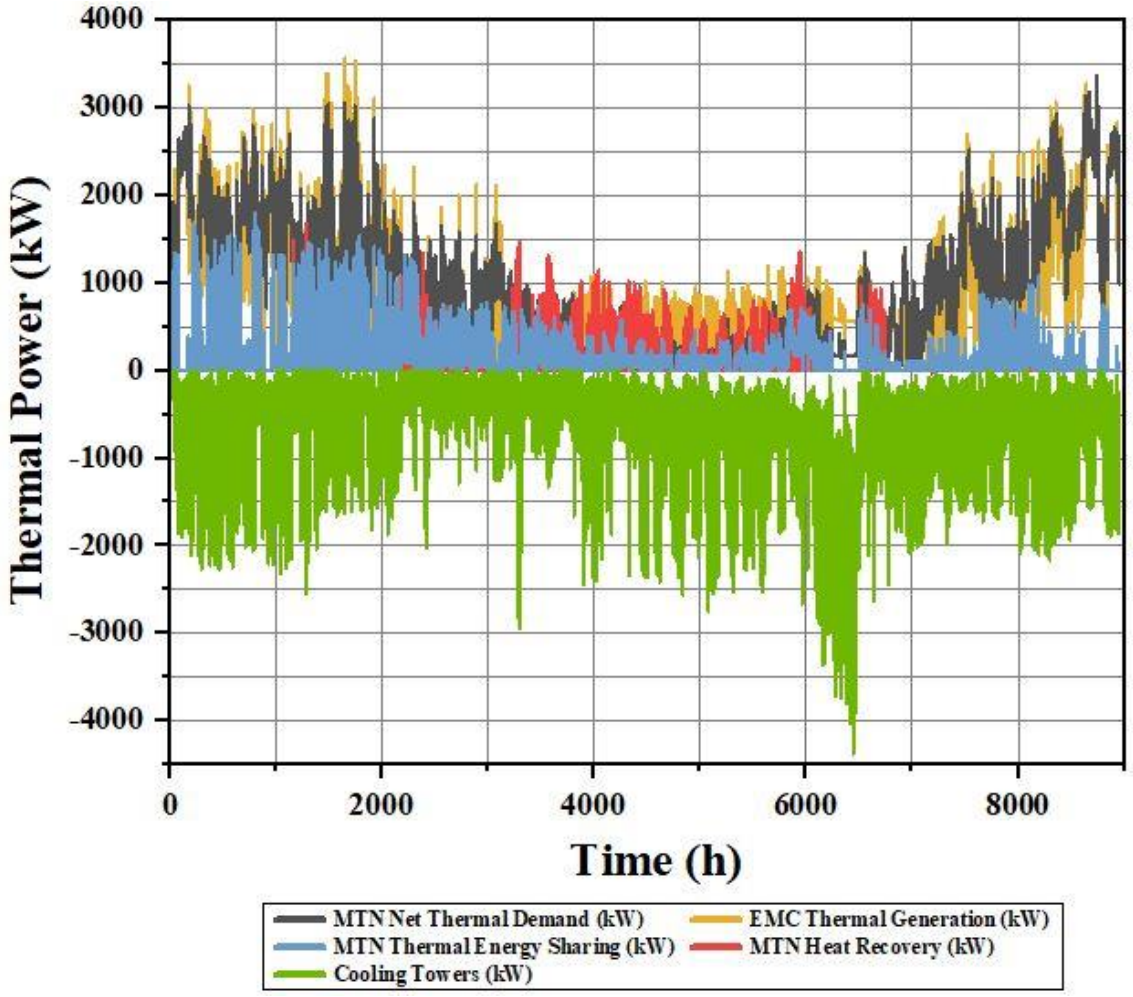

Fig.5.3: Internal and external total thermal power flows of the EMC and MTN.

From Figure 5.3 it can be seen that heat recovery is most prevalent during the period where the net thermal demand from the MTN is low. Simultaneously, thermal energy generation from producers in the EMC is greater than the net thermal demand because the system is in the charging phase and the excess thermal energy is being stored in the BTES. However, a significant amount of thermal energy is still rejected by the cooling towers at the buildings, which indicates some lost opportunity for heat recovery. Thermal energy sharing is prevalent during the periods when the MTN net thermal demand is highest, since there is a significant amount of cooling process heat available, which coincides with high

heating demand. As mentioned previously, the operation of the heat recovery heat pumps is such that the temperature of the MTN does not increase significantly. Therefore, the amount of heat that can be harvested at each building is limited by this temperature constraint.

Thermal energy sharing and heat recovery from the MTN are also limited by the operation of peaking power plants on the Ontario grid. The heat recovery heat pumps in the system are only operational during the off-peak periods to avoid contributing to the peak electrical demand. As a result, the more that the peaking power plants are operational, the lower the amount of heat that can be recovered at buildings. In turn, thermal energy sharing and heat recovery from the MTN are reduced. Lastly, the coincidence of heating and cooling demands has an effect on the amount of thermal energy sharing and heat recovery as well. If periods of high cooling demand are not matched with periods of high heating demand, there is little opportunity for thermal energy sharing between buildings. This causes the amount of heat recovery to increase since thermal energy can still be harvested from cooling processes and captured by the MTN. However, this heat recovery is again limited by the previously mentioned constraint on the temperature of the MTN, resulting in the significant amount of heat rejected by the building cooling towers. The effects of the heating and cooling demand profiles are depicted in Figure 5.4.

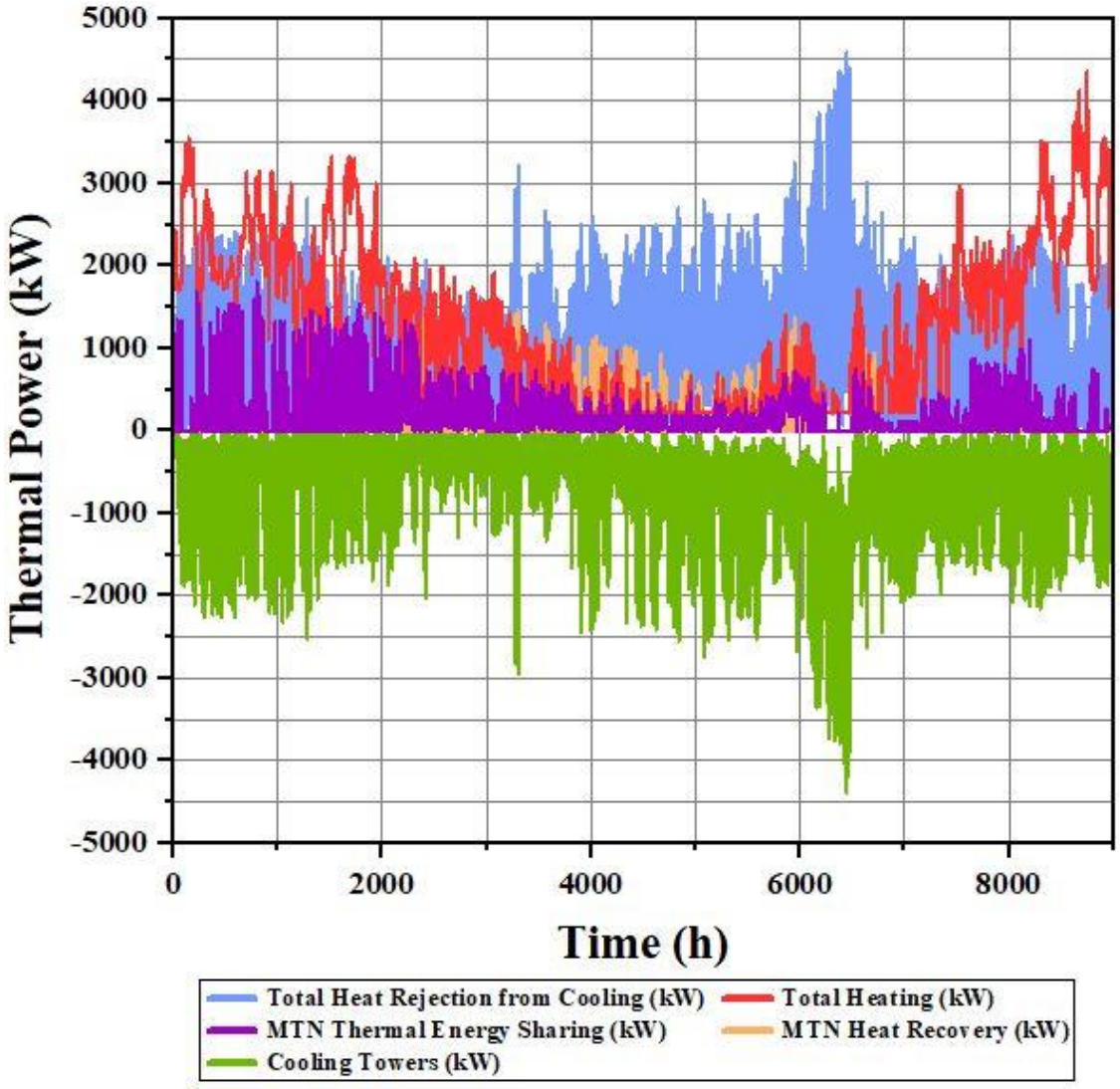

Fig. 5.4: Total thermal power flows of the set of buildings and MTN.

It can be seen from Figure 5.4 that there is a small heating baseload of approximately 200 kW during the charging phase that is fully accommodated by thermal energy sharing when possible. During these periods, some additional thermal energy is able to be recovered from cooling processes and transferred to the MTN and then back to the EMC. Only a portion of the heat rejected from cooling is recovered in this way so that the system is able to maintain a consistent MTN supply temperature of 35 °C, as shown in

Figure 5.3. Even in a limited capacity, these methods of thermal energy harvesting have a tangible impact on the performance of the system. Due to thermal energy sharing and heat recovery, the amount of heat rejected by the cooling towers is decreased in comparison to the amount of heat rejected by building cooling systems. Therefore, thermal energy sharing and heat recovery increase the utilization of otherwise wasted heat.

The analysis presented in this section demonstrates that the long-term performance of the system is heavily impacted by seasonal and cumulative hourly variations of multiple parameters. Seasonal variation of thermal demand and coincidence of heating and cooling demands impact the total thermal energy provided by each energy producer in the EMC and the amount that can be harvested and stored. These energy totals are also influenced by the cumulative effect of hourly variations in thermal demand, coincident heating and cooling loads, and operation of peaking power plants on the electricity grid. It naturally follows that even shorter-term variations can affect the overall performance of the system as well. The short-term dynamics of the system impact the operation of individual energy producing units, which inevitably has an effect on the long-term trends. Therefore, analysis of system performance over the short-term is a critical piece of the overall assessment of the control framework. This analysis is presented in the following section.

5.2 Short-term Results

This section presents the analysis of the obtained results over the short-term. The analysis is based on several short-duration snapshots taken from various periods within the data obtained from the entire year of the case study. The performance of the control framework is assessed based on the dynamic behaviour of the system during steady-state

and transient periods. This assessment is focused on control metrics such as rise time, settling time and the magnitude of overshoot. The dispatch of the energy producers by the MAS and changes in temperature setpoint by the SLCs, as well as their relationship to system dynamics are also discussed in this section. As discussed in the previous section, the operation of the system in the discharging and charging phases differs significantly. As a result, multiple periods from both phases are selected for short-term analysis. The main thermal power and temperature profiles of the system for a selected period of typical winter operation are depicted in Figures 5.5 and 5.6.

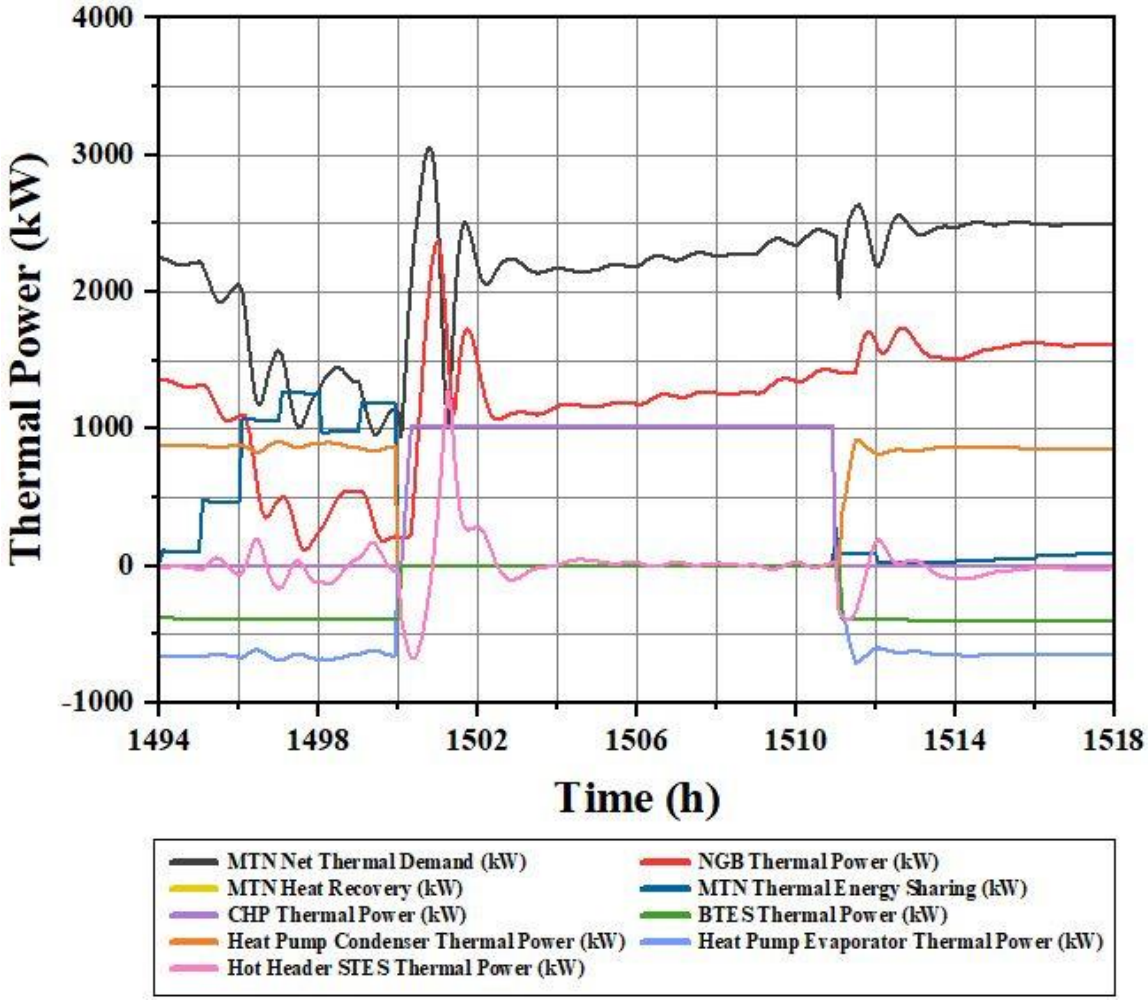

Fig.5.5: Main thermal power flows for selected day during discharge phase

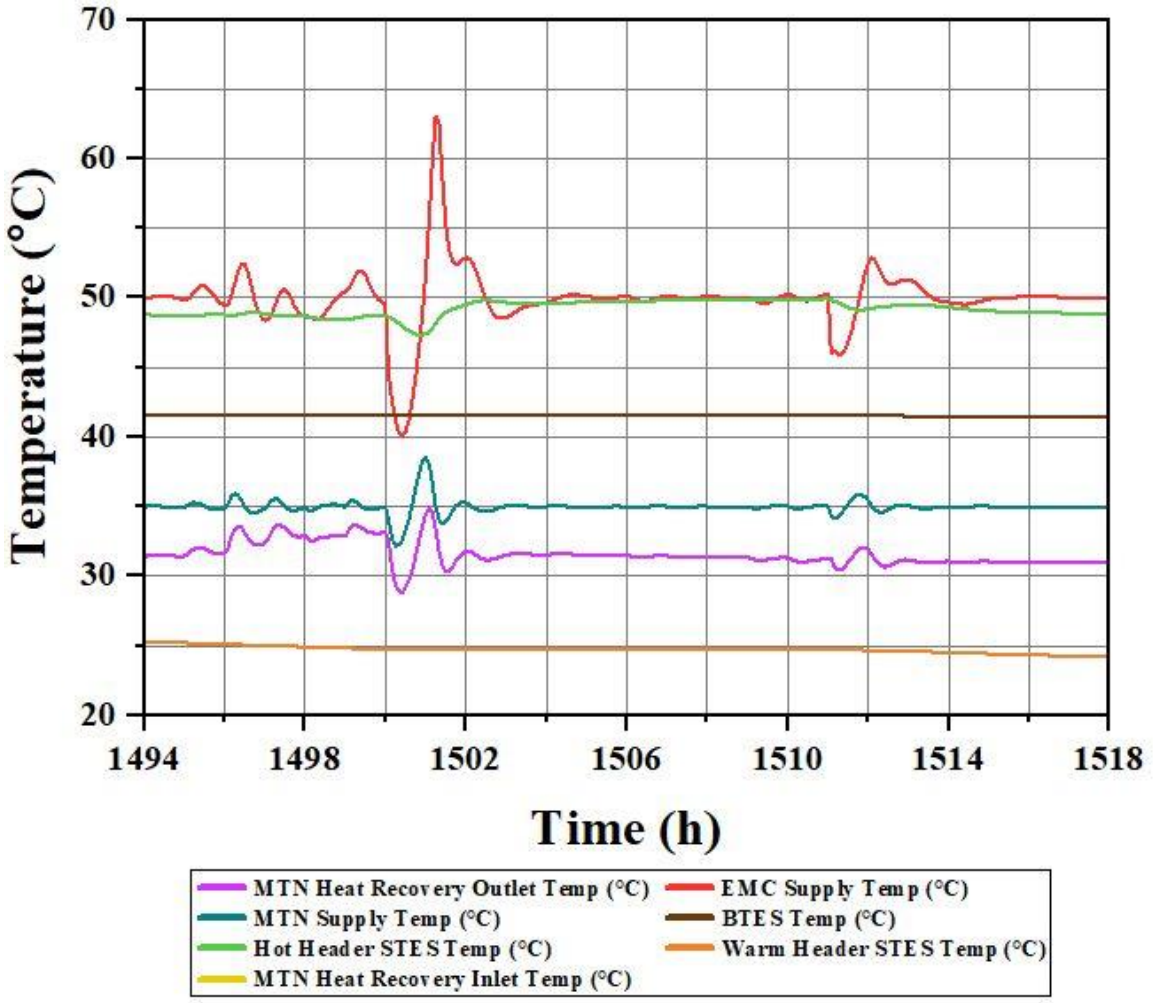

Fig. 5.6: Main temperatures in EMC and MTN for selected day during discharge phase

From above figures, both the steady-state and transient behaviour of the system can be observed. During the time period depicted, two major transient events occur, one at 1500 hours and one at 1511 hours, which are during the discharge phase. From Figure 5.5, it can be seen that these transients are disturbances caused by the switching of the CHP and heat pump due to the electrical peaks. The process is a hard switch, in which the producer that becomes unavailable is taken offline, and then the other producer is dispatched in response to the demand seen by the MAS. Since switching occurs while the EMC is under

thermal load from the MTN, it results in a large mismatch between the demand and the thermal energy provided by producers. The temperature of the hot header then decreases sharply due to the mismatch, which can be seen in Figure 5.6, and the magnitude of the decrease is related to the magnitude of thermal power mismatch. This deviation from the temperature setpoint results in a large thermal energy demand detected by the MAS which responds accordingly. The MAS first dispatches the CHP, and once it has reached its maximum output, then dispatches the NGB. Since the CHP and NGB need time to ramp up their output, there is some delay between when they are dispatched and when they are able to match the demand. It can be seen that the delay is approximately 15 minutes by comparing the curves depicting NGB thermal power and MTN net thermal demand in Figure 5.5. This delay results in the temperature of the hot header continuing to decrease for some time before rebounding and the corresponding rise time of the MAS for both transients is approximately 1 hour.

During the switching process, the STES provides thermal energy to the hot header when its temperature drops below that of the storage tank. This helps to mitigate the temperature decrease of the header and offsets some usage of the NGB during the transient period. The header temperature then overshoots the setpoint by approximately 13 °C (26%) for the first transient and 3 °C (6%) for the second. Additionally, when the temperature of the header surpasses that of the STES, it results in some thermal energy being stored. To allow the temperature to drop from the overshoot, the MAS reduces the thermal power output of the NGB and the STES discharges the stored thermal energy almost immediately. The temperature of the hot header oscillates for some time as it approaches a steady state, corresponding to a settling time of approximately 3 hours in the case of both transients.

From Figures 5.5 and 5.6 the fluctuation of temperature and thermal power during steady state, which are inherent to MAS operation, can also be observed. The magnitudes of these fluctuations are relatively small and represent a maximum deviation from the setpoint of approximately 2.5 °C (5%). Since these fluctuations are part of the proper operation of the MAS, and they result in the temperature moving above and below the setpoint in approximately equal measure, the steady state error of the MAS is 0. The effect of the STES as a buffer can be seen as well, as the thermal power it provides changes between negative and positive values as the hot header temperature fluctuates.

The action of one of the Auxiliary Controllers can also be observed from Figure 5.6. This is a PID controller which manipulates the mass flow rate through the heat exchanger connecting the hot header to the MTN, in order to maintain the MTN supply temperature at 35 °C. It can be seen that the action of his controller mitigates the effect of transients caused by switching of the CHP and heat pump. During the transient responses depicted, the supply temperature of the MTN experiences fluctuations of much lower magnitude than the EMC. During the interruption of thermal energy generation due to switching, the temperature of the hot header decreases, and the Auxiliary Controller attempts to prevent the MTN supply temperature from falling by increasing the flow rate. Similarly, when the temperature begins to overshoot, the controller decreases the flow rate to prevent the temperature from rising. This is because for a given flow rate, the temperature difference between the heat exchanger inlets remains approximately constant. Therefore, without the action of this PID controller, the MTN supply temperature would mirror that of the EMC subtracting the temperature difference. The action of this PID

controller regulates the supply temperature of the MTN, which ensures a more consistent supply temperature to the consumers of the network.

It is important to note that the transient caused by switching from the heat pump to CHP is not equivalent to the inverse. Switching from operating the heat pump to the CHP represents the occurrence of an electrical peak, which means that the heat recovery heat pumps at the buildings will stop operating. This can cause the net thermal energy demand from the MTN to suddenly increase, further contributing to the thermal energy mismatch and resulting temperature decrease. This is apparent from comparing the magnitudes of the transient responses in Figures 5.5 and 5.6. The first transient is caused by switching from heat pump to CHP, and results in an initial temperature drop of 10 °C. The second transient is caused by switching back to the heat pump from the CHP, and results in a significantly smaller temperature decrease. This is approximately 4 °C, which is less than half the magnitude of the previous temperature drop. This corresponds to the difference in thermal demand before and after the respective switches, which can be observed by comparing the transients in Figure 5.5.

During the switching process corresponding to the first transient, the net thermal energy demand from the MTN increases nearly three-fold at its peak, and even after the settling time is reached, demand is greater than double what it was prior to the switch. Conversely, thermal demand does not increase much at all during the second switch, and only increases by approximately 400 kW at peak, and 100 kW once the settling time is reached. This difference in transient responses between switching from CHP to heat pump and vice versa is repeated consistently over the course of the case study. This can be seen

in the multiple instances of this phenomenon during the discharge phase, depicted in Figures 5.7 and 5.8.

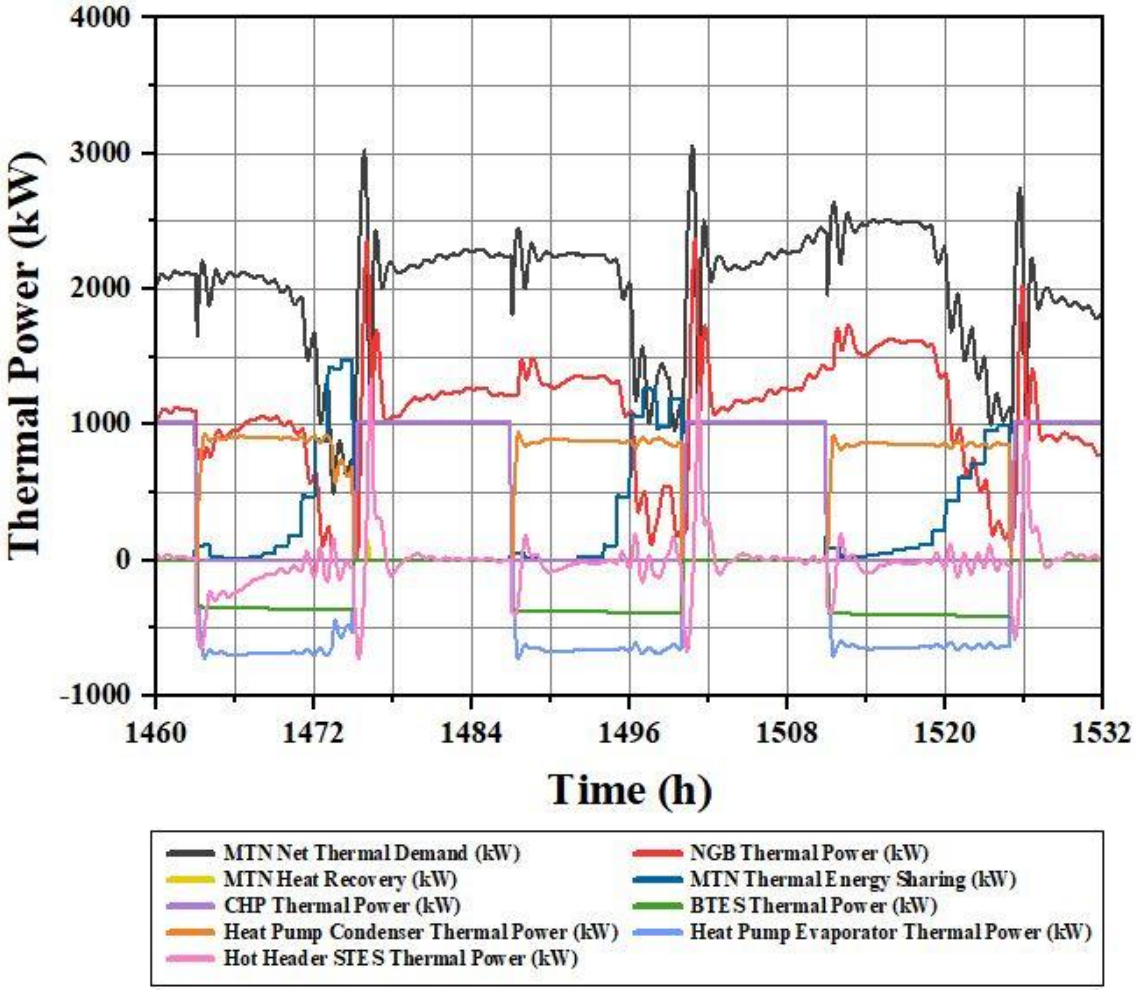

Fig.5.7: Main thermal power flows for multi-day period during discharge phase

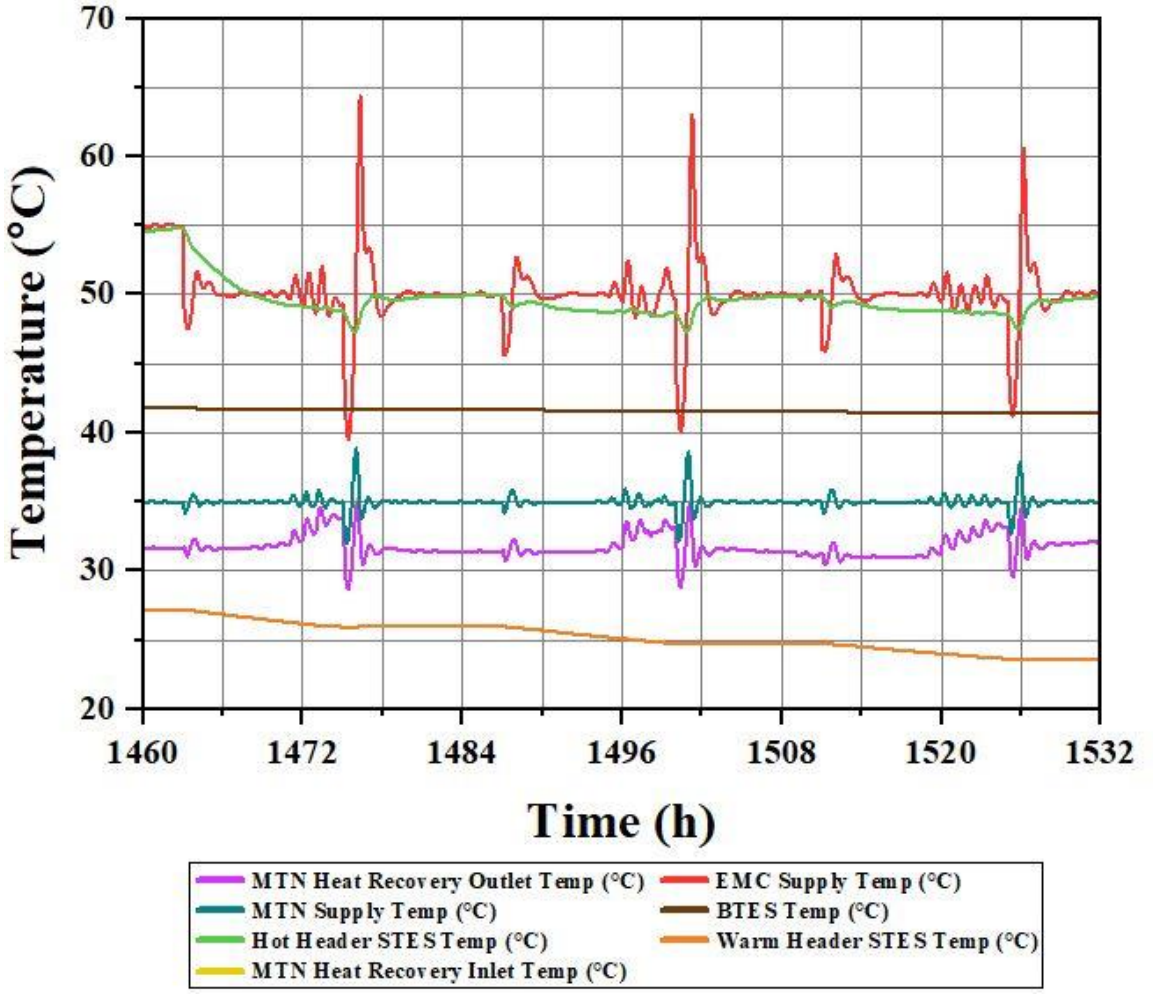

Fig.5.8: Main temperatures in EMC and MTN for multi-day period during discharge phase

The results in shown in Figures 5.5 to 5.8 demonstrate the behaviour of the system during typical operation during the discharge phase. During this period, the control system manages the disturbances caused by switching of the CHP and heat pump, while targeting a single setpoint. As discussed, this is largely handled by the MAS and Auxiliary Controllers, while the involvement of the SLCs is minimal. Since the temperature setpoint does not require adjustment during this period, the state of the active SLC remains the same, which is the extent of its involvement in the control process. The adjustment of temperature setpoint by either of the SLCs is a step change, and the rest of the control

system must respond accordingly. Therefore, the step responses of the system resulting from changes in temperature setpoint are another critical part of assessing the performance of the control framework. The changing of temperature setpoint and the resulting effects on thermal power flows for a selected period are depicted in Figures 5.9 and 5.10, respectively.

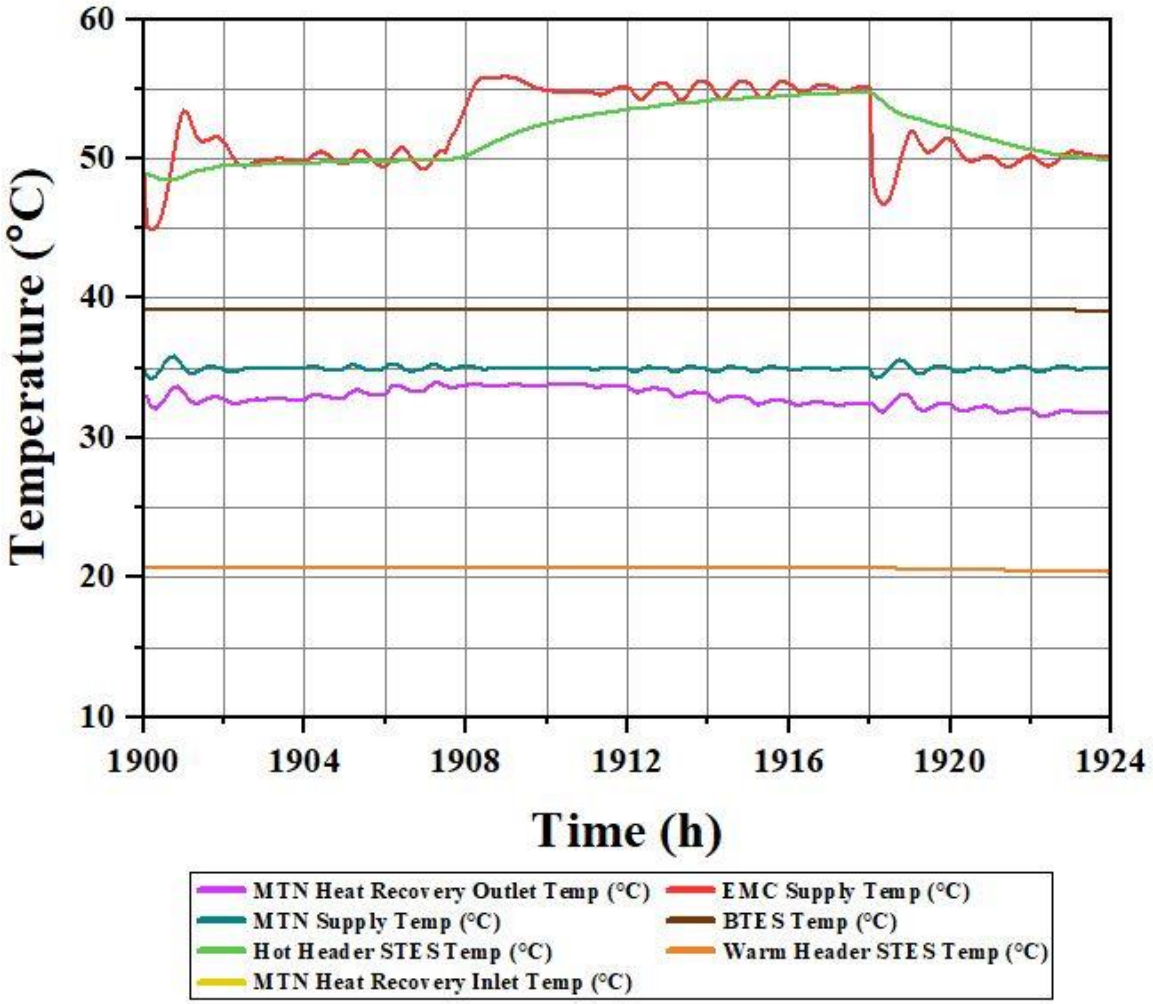

Fig.5.9: Step response of main temperatures due to setpoint change during discharge phase

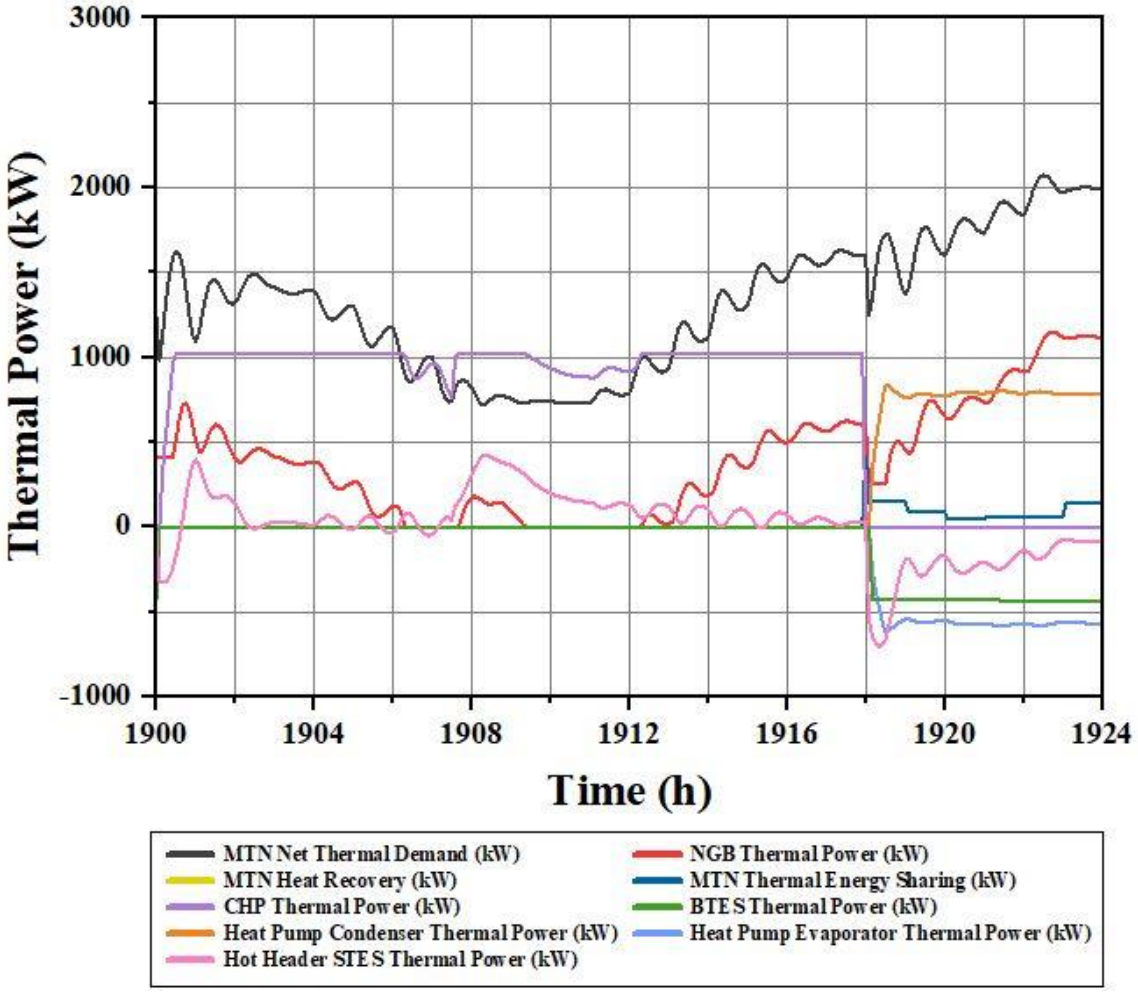

Fig.5.10: Effect on main thermal power flows due to setpoint changes during discharge phase

The above figures show the system response resulting from two changes of hot header temperature setpoint during the discharge phase which correspond to a setpoint increase and decrease during the discharge phase. Additionally, these responses demonstrate the situation in which the system is unable to increase the temperature setpoint beyond 55 °C before discharging the STES. It can be seen that prior to the increase of temperature setpoint at approximately 1907.5 hours, the hot header is at steady state. The temperature of the header begins to rise and reaches the new setpoint just after 1908 hours, corresponding to a rise time of approximately 30 minutes. The temperature then overshoots

the setpoint by less than 1 °C (<1.8%) and reaches steady state at 1910 hours, which results in a settling time of approximately 2.5 hours. Again, the temperature fluctuations that occur during steady state are relatively low in magnitude at less than 1 °C (<1.8%) deviation from the setpoint.

It can also be seen that once the temperature of the hot header rises above that of the STES tank, its temperature begins to rise as well. As the STES stores thermal energy its temperature approaches that of the hot header and the thermal power flow into storage diminishes. As this occurs, the thermal power output of the CHP decreases as well because the STES is not imposing enough thermal load on the system for the MAS to keep the CHP operating at this level. Once its temperature is near that of the hot header, the STES tank again behaves as a thermal buffer and mitigates fluctuation of the header temperature at the new setpoint. This continues until 1918 hours, when the CHP shuts down and the STES must discharge. At this point SLC 1 decreases the hot header temperature setpoint back to 50 °C, and the resulting step response can be observed. When the setpoint is decreased, the header temperature immediately begins to drop due to the switching of CHP and heat pump, while the MAS also allows the temperature to decrease to the new setpoint. The temperature undershoots the setpoint by approximately 3 °C (6%), and reaches steady state after a settling time of approximately 3 hours. While this occurs, the temperature of the STES tank decreases as well and discharges thermal energy to the header, simultaneously offsetting usage of the NGB and mitigating the temperature decrease during the step response. This can be seen in Figure 5.10, at the time when the CHP shuts down. The thermal power output of the NGB at this point decreases from approximately 600 kW to 250 kW, and stays at that level until the temperature of the STES tank nears that of the hot

header. As it discharges, the STES can provide less thermal power, resulting in the NGB increasing its output to meet thermal demand from the MTN. This behaviour represents the desired operation of the STES, albeit when there is only enough excess energy available from the CHP to increase the temperature setpoint once. During times when the CHP can provide significantly more thermal energy to store, SLC 1 can raise the temperature setpoint multiple times consecutively. This results in significantly greater utilization of the CHP and amount of energy stored in the STES. These improvements are depicted in Figures 5.11 and 5.12.

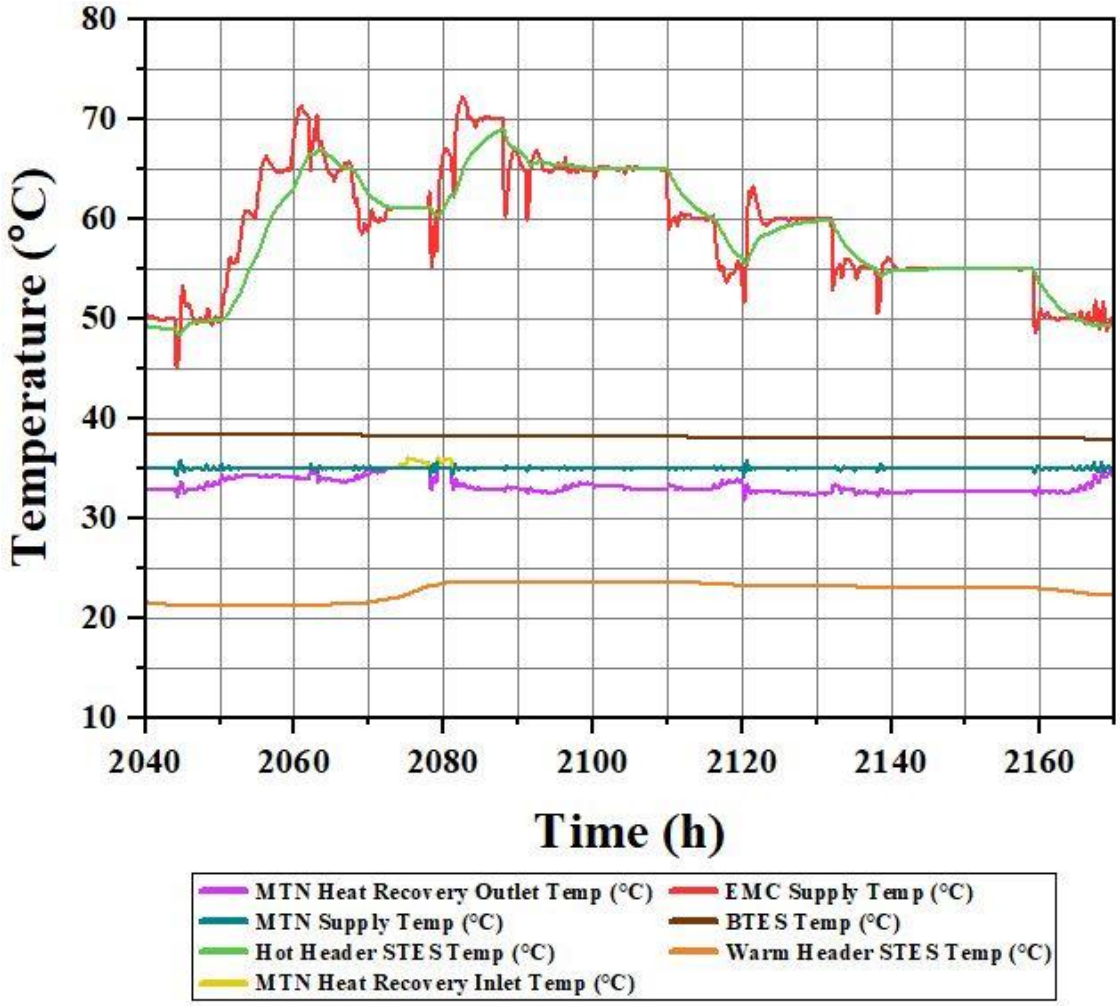

Fig.5.11: Effect of multiple setpoint changes on main temperatures during discharge phase

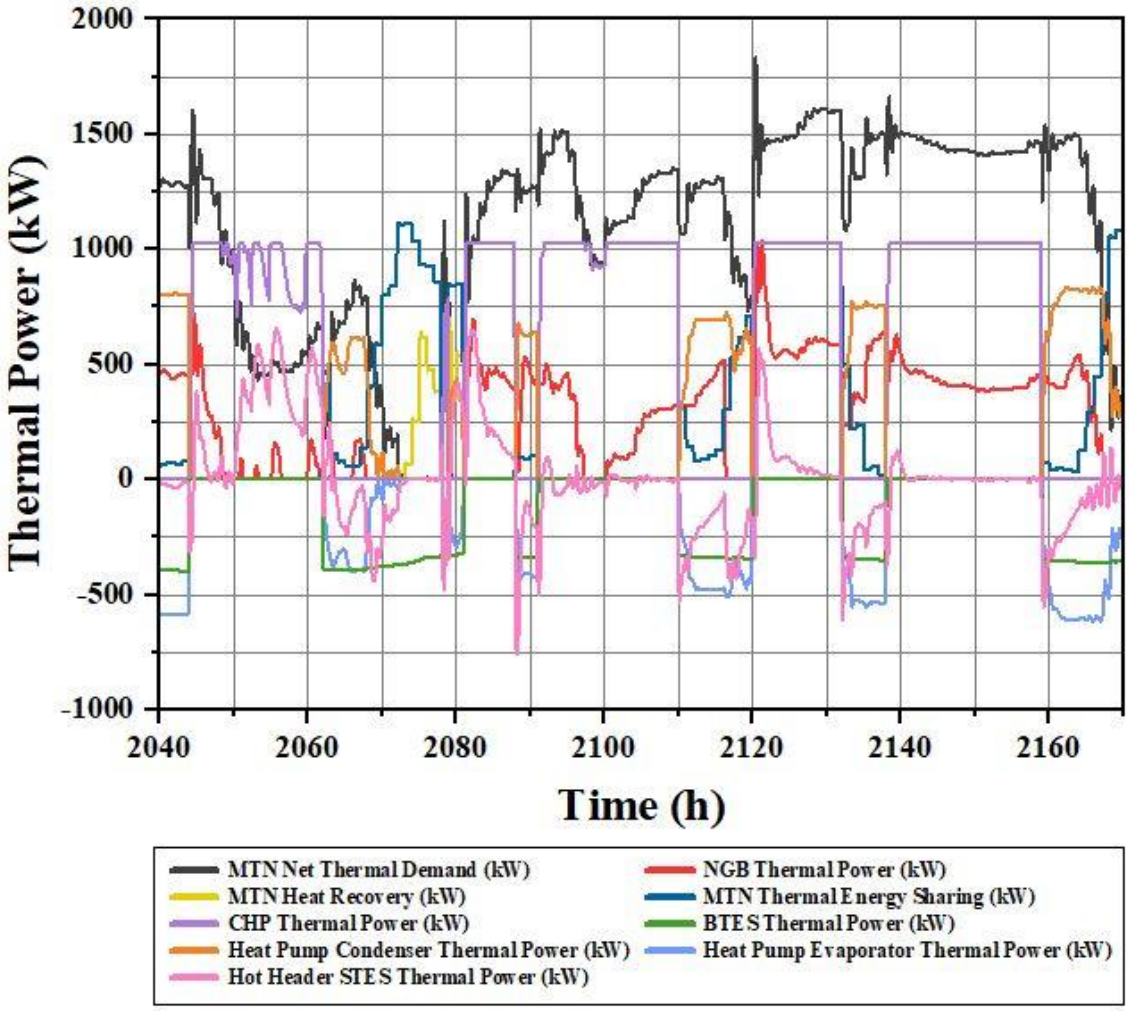

Fig.5.12: Effect of multiple setpoint changes on thermal power flows during discharge phase

From Figure 5.11, it can be observed that the system experiences several changes in temperature setpoint from 2050 hours to 2160 hours. Throughout this period, the setpoint increases and decreases between 50 °C and 70 °C, resulting in the STES tank partially charging and discharging multiple times. It can also be seen from Figure 5.12 that during the initial setpoint increase from 50 °C to 70 °C, the CHP decreases several times and is increased again due to the thermal load imposed by the STES. If the control system did not increase the temperature setpoint in this way, the thermal output of the CHP would follow

the net thermal energy demand from the MTN, which is significantly lower than the capacity of the CHP for most of this period. Therefore, the adjustment of the hot header temperature setpoint simultaneously stores thermal energy and increases the utilization of the CHP. During the decreases of temperature setpoint later in the depicted period, the subsequent discharging of thermal energy from the STES can be observed as well. During these periods, the thermal power provided by the STES affects the output of the NGB in different ways depending on the amount of thermal energy sharing and the net thermal demand from the MTN. In the case that thermal energy sharing is high, typically the net thermal demand is low. As a result, thermal energy from the STES reduces the thermal power output of the NGB. This can be seen in Figure 5.12 at approximately 2116 hours and 2132 hours. On the other hand, when there is little thermal energy sharing and the net demand is high, the energy provided by the storage tank limits the increase of thermal power output from the NGB in response to the net demand. This can be seen by comparing the STES thermal power output to the other thermal power flows depicted in Figure 5.12 during periods from 2110 to 2116 hours, 2135 to 2138 hours, and 2159 to 2164 hours.

The results presented until this point have been focused on the short-term performance of the control framework during different periods throughout the discharge phase. As mentioned repeatedly, the operation of the ICE-Harvest system and the control framework are very different in the discharging and charging modes. Therefore, examining the performance of the control system for short-term durations in the charging phase is another critical part of the analysis. However, during the charging phase, the system spends a significantly greater amount of time in steady-state compared to during the discharging phase. This is due to the fact that temperature setpoint is only increased during the charging

phase, and these increases only occur a handful of times throughout this phase. As a result, the assessment of control performance during this period is greatly simplified and the insights provided from analyzing the system at one temperature setpoint can be extended to others. This can be observed by comparing the system behaviour at each temperature setpoint throughout the charging phase depicted in Figures 5.13 and 5.14.

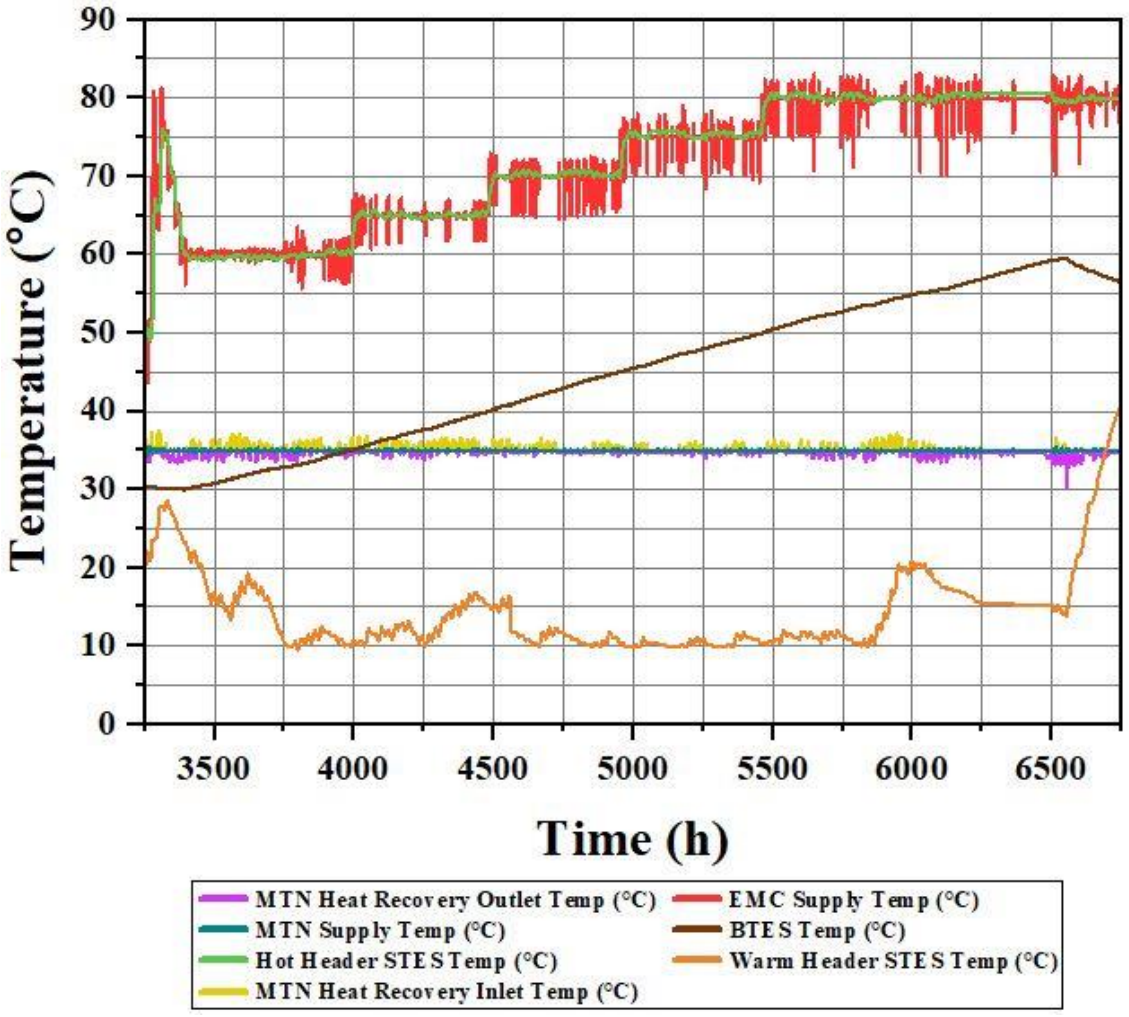

Fig.5.13: Temperatures during operation at all setpoints during the charge phase

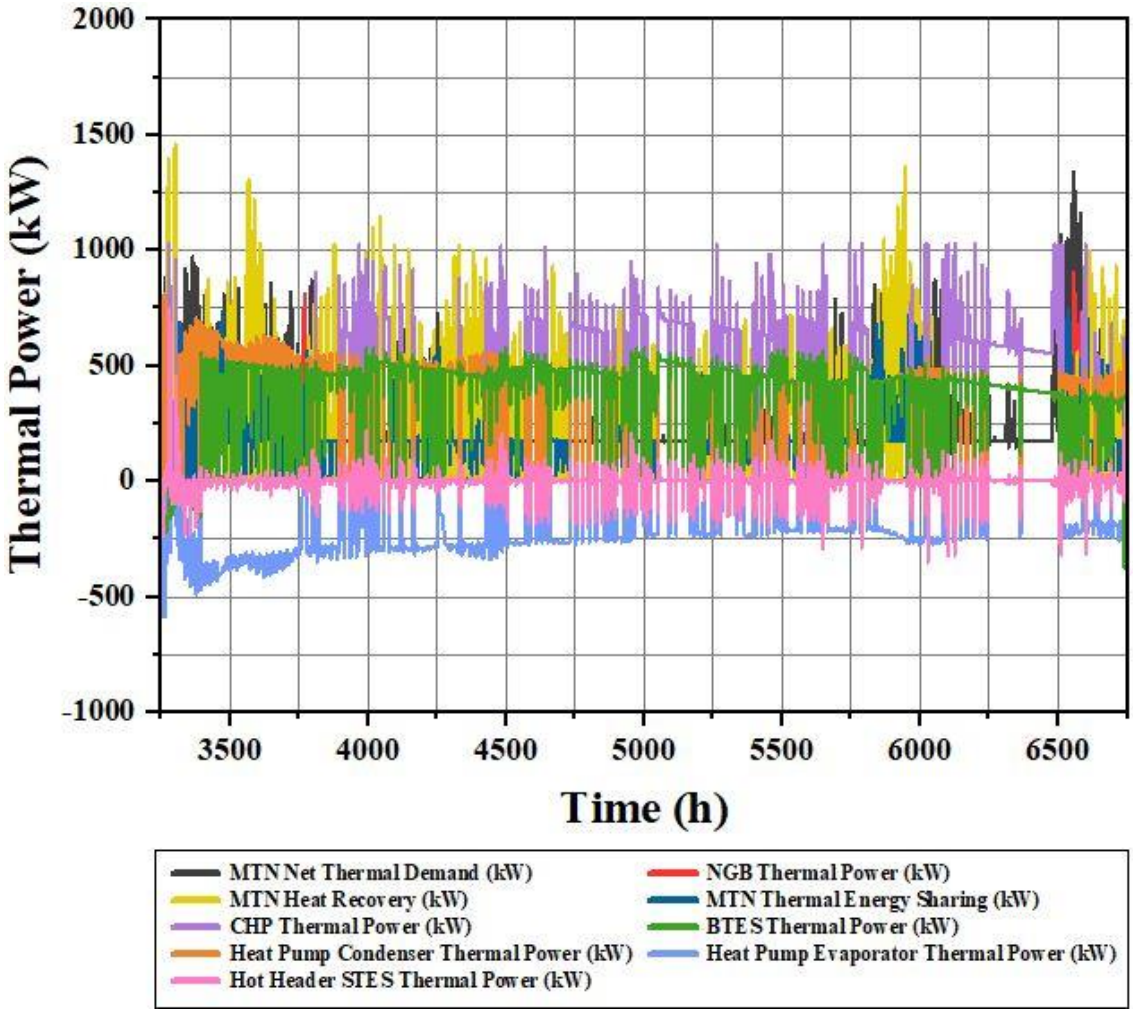

Fig.5.14: Thermal power flows during operation at all temperature setpoints during charge phase

It can be seen from Figure 5.13 that the temperature profile of the system during operation at each setpoint remains relatively consistent, apart from the difference in operating temperature. During each of these distinct periods, the control system targets a single setpoint, with the temperature of the header fluctuating within a small range around it. The magnitudes of steady state fluctuations during each period are similar, at less than 1 °C deviation from the setpoint. The larger deviations from the temperature setpoint correspond to disturbances caused by the switching of CHP and heat pump as discussed

earlier. These are typically 5 °C in magnitude or less, regardless of the temperature setpoint the system operates at. Additionally, it can be seen from Figure 5.14 that the thermal power drawn by the BTES and the resulting thermal power provided by the CHP and heat pump decline slowly over the course of each period. This is due to the increasing geothermal field temperature, which reduces the heat that can be transferred to the BTES as the temperature difference between it and the hot header decreases. These phenomena can be more easily observed by analyzing the temperature profile and thermal power flows during operation at a single setpoint depicted in Figures 5.15 and 5.16.

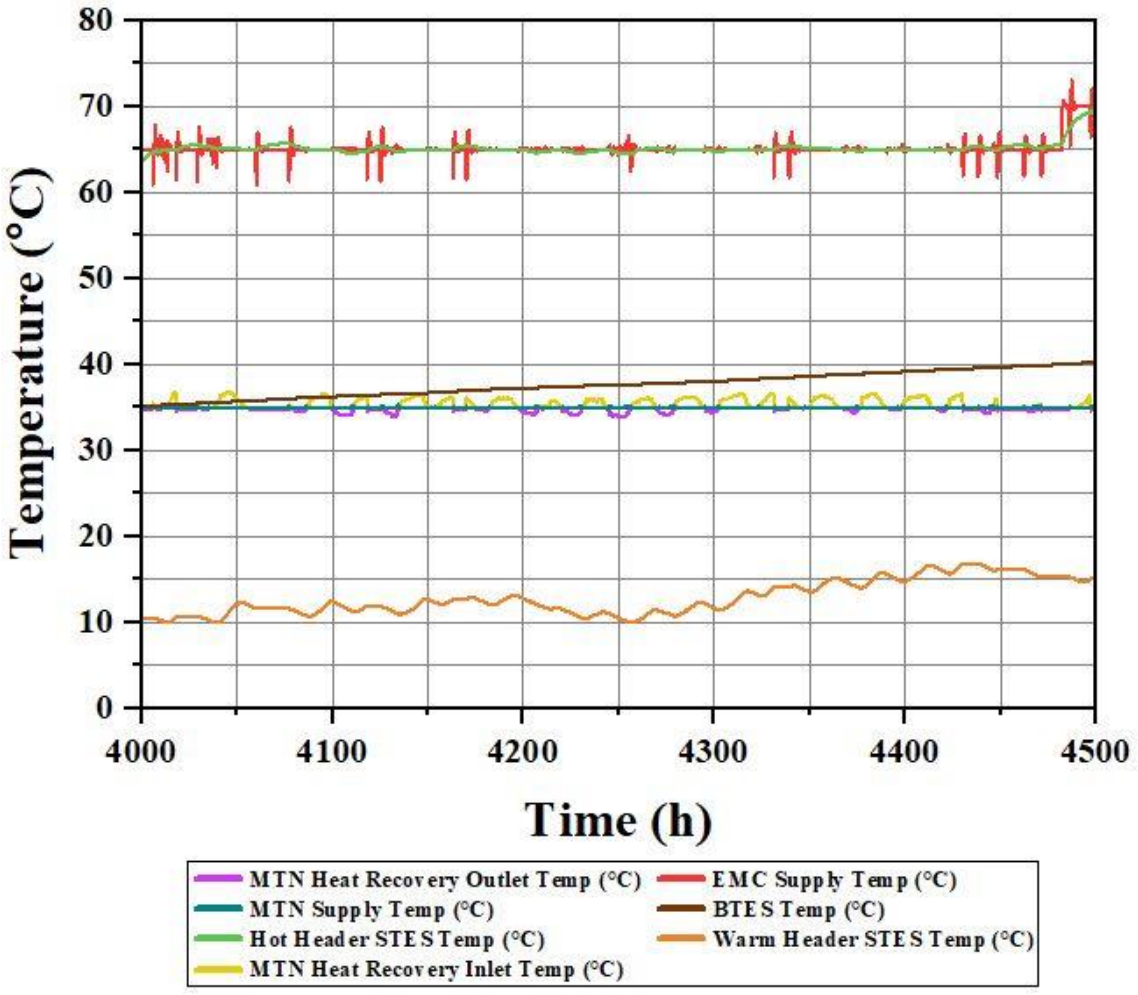

Fig.5.15: Temperatures during operation at single temperature setpoint in charge phase

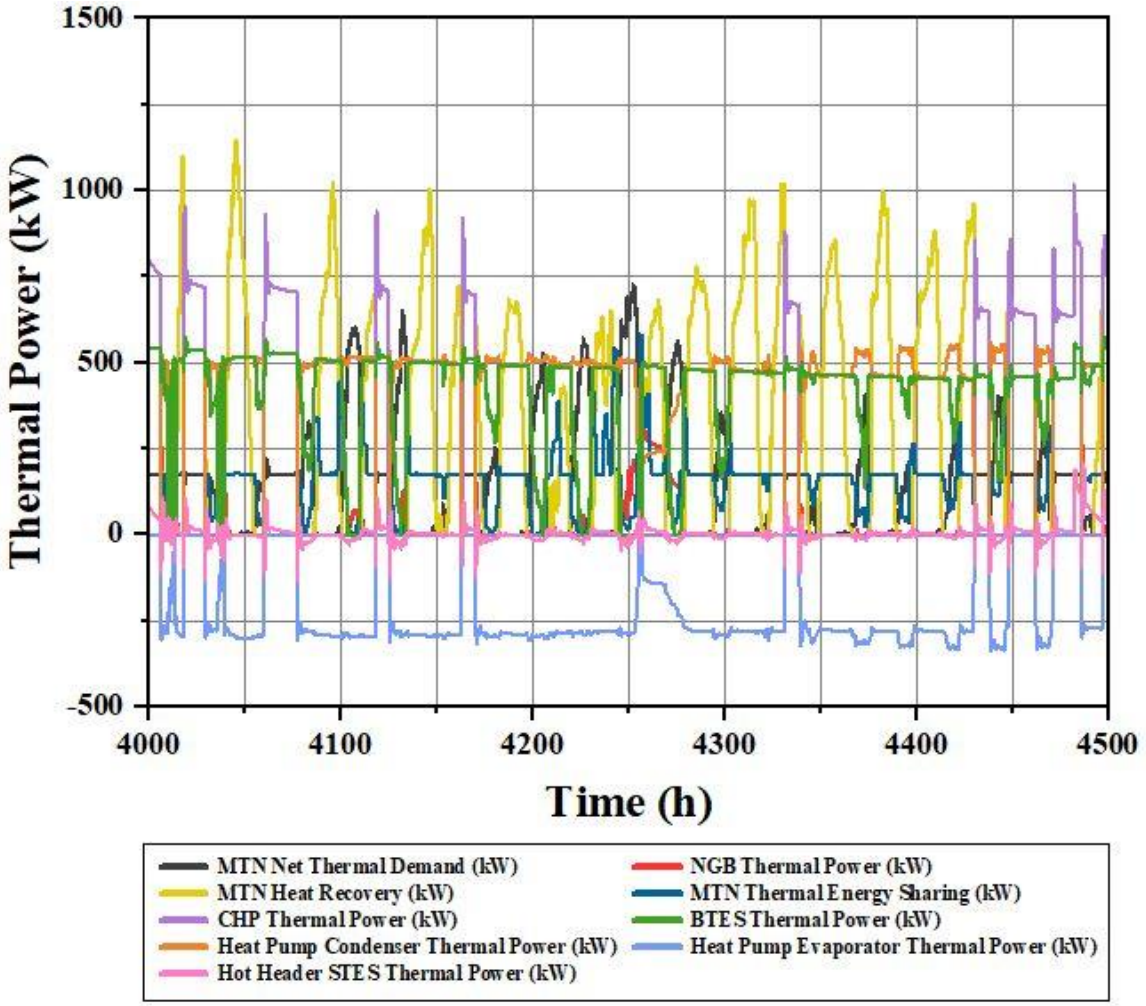

Fig.5.16: Thermal power flows during operation at single temperature setpoint in charge phase

The above figures show the main temperatures and thermal power flows of the system for the entire time it operates at the 65 °C setpoint while in the charge phase. It can be seen from Figure 5.16 that the majority of the disturbances in temperature of the hot header in Figure 5.15 correspond to switches of the CHP and heat pump throughout this period. There are some disturbances which are caused by the temperature of the warm header decreasing below the minimum threshold for heat pump operation. When the threshold is reached, the heat pump immediately ceases operation and the hot header

temperature begins to decrease until either the heat pump can operate again or the NGB takes over. From Figure 5.16 it can also be seen that the amount of thermal power drawn by the BTES decreases over the course of the depicted period, which is again due to the increasing temperature of the geothermal field. Additionally, the thermal power drawn by the BTES decreases when there is thermal energy demand from the MTN. This is accomplished by a PID controller which maintains a thermal power setpoint equal to the difference between the capacity of the CHP or heat pump and the current thermal demand from the MTN. As mentioned previously, this is done to ensure that the NGB is not utilized to charge the BTES.

It can also be seen from Figure 5.16 that during periods when the heat pump is operating, there is typically a significant amount of heat recovered by the heat recovery heat pumps in the MTN. The thermal energy recovered is transferred to the warm header while the heat pump at the EMC charges the BTES. Since the amount of heat recovered varies and is typically either higher or lower than what is drawn by the heat pump, the temperature of the warm header fluctuates, which can be observed from Figure 5.15. There is also thermal energy sharing occurring at the same time, which can be seen in Figure 5.16 as well. This reduces the thermal energy demand from the MTN during these periods and allows more of the thermal energy from the heat pump to be utilized for charging the BTES. Furthermore, throughout this entire period the STES is behaving as a buffer, storing and providing less than 150 kW of thermal power at any given time. This operation helps to maintain the hot header temperature throughout, as shown in Figure 5.15. The transition from the 65 °C to 70 °C temperature setpoint can also be observed from Figure 5.15 and the corresponding effect on thermal power flows from Figure 5.16. At the time when the

setpoint is increased, the CHP is active and its thermal power output increases to accomplish the change in setpoint. The effects of the setpoint change on temperatures and thermal power flows are shown in greater detail by Figures 5.17 and 5.18.

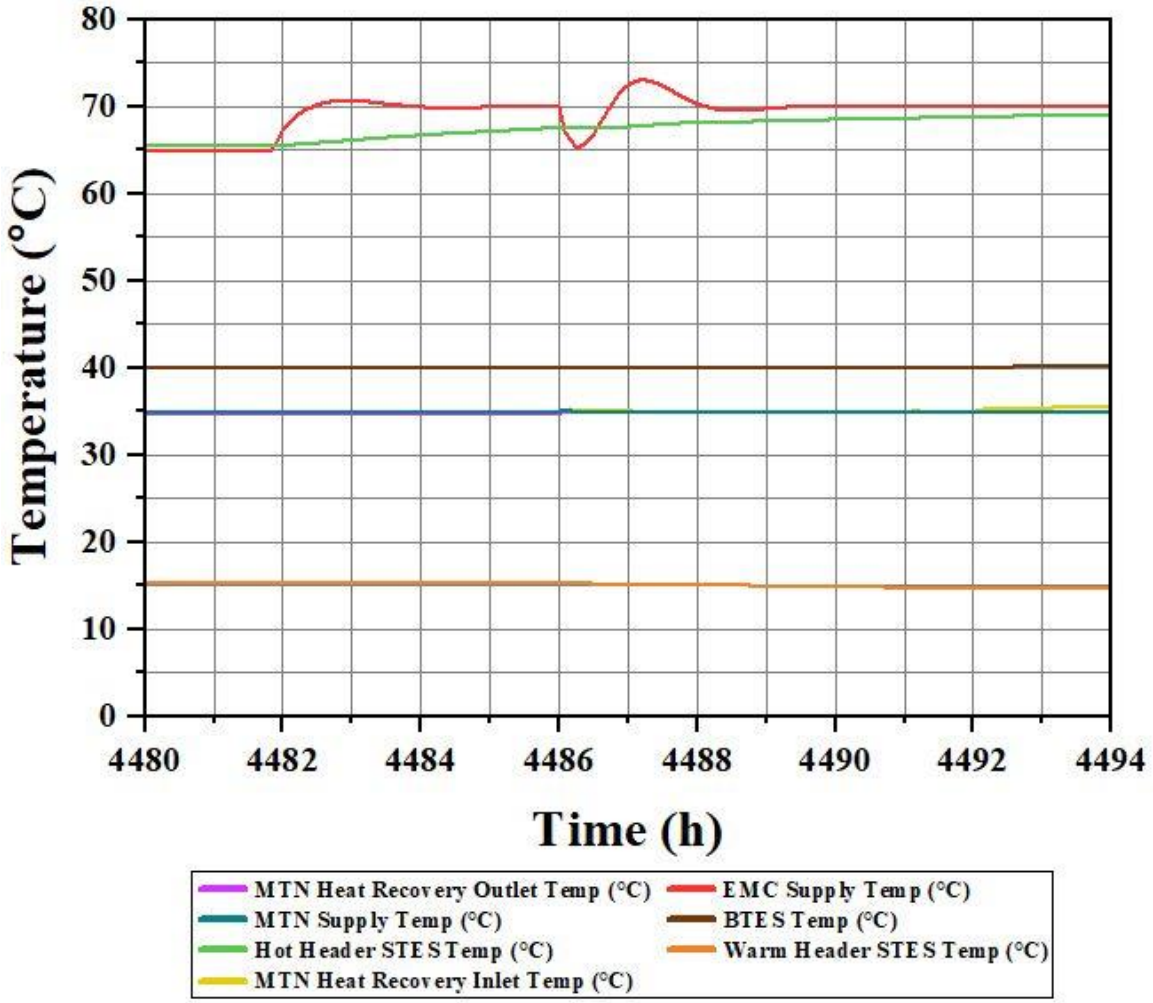

Fig.5.17: Step response of main temperatures due to setpoint change during charge phase

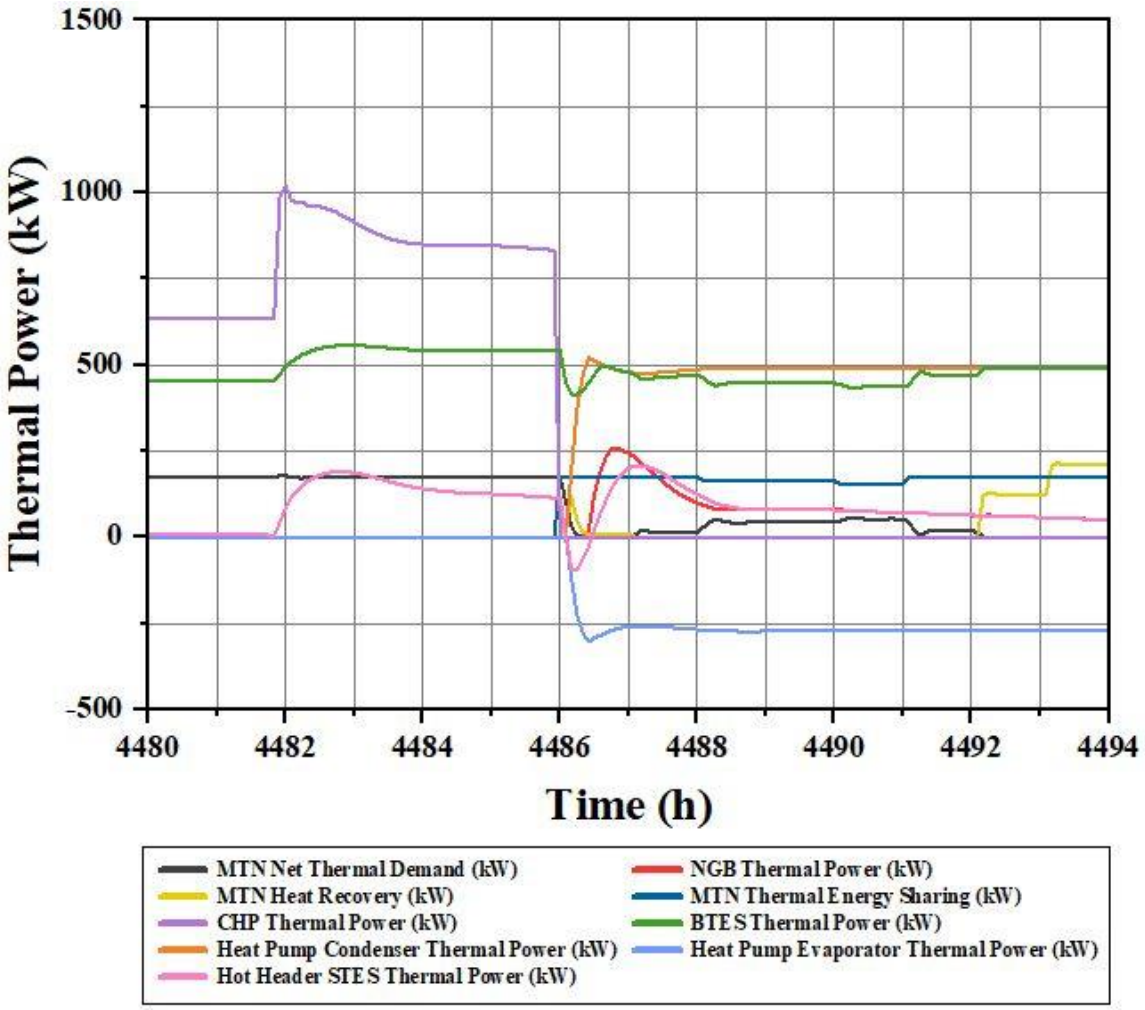

Fig.5.18: Effect on main thermal power flows due to setpoint change during charge phase

From the above figures it can be seen that prior to the change in temperature setpoint, the CHP is consistently providing approximately 650 kW of thermal power. It then increases its thermal power output to its maximum, before settling at 850 kW. This corresponds to an overshoot of temperature by less than 1 °C (< 2%) from the new setpoint. The initial increase in output from the CHP provides the additional thermal power required to raise the temperature of the header, and decreases once the new setpoint is reached. The hot header temperature reaches the settling time after approximately 2 hours, along with

the thermal power output from the CHP. The thermal power produced by the CHP at steady state has increased since the BTES is able to draw greater thermal power at the new setpoint. This causes the BTES to impose a larger thermal load on the hot header, which can be observed from Figure 5.18. This is recognized by the MAS which increases the CHP output to accommodate. It should also be noted that the STES draws thermal power due to the change in setpoint as well. The STES charges as the header temperature increases, and once the setpoint is reached, the STES becomes a thermal buffer again and its temperature follows that of the header.

The results presented in this section demonstrate the short-term performance of the control system. From the analysis performed, it is shown that the developed control framework performs adequately. It can be seen that the developed control framework is able to effectively manage the short-term dynamics of the ICE-Harvest system, as well as operate in consideration of long-term and seasonal requirements. Naturally, the performance over both of these timeframes will impact the ability of the control system to accomplish the goals envisioned for the ICE-Harvest system. Even small impacts on the performance of the control system will result in significant cumulative differences in various important parameters for the ICE-Harvest system. Therefore, in order to fully assess the developed control framework, totalized results must be analyzed as well. This cumulative analysis is presented in the following section.

5.3 Cumulative Results

This section presents the analysis of critical parameters totalled over the course of the case study, as well as outcomes of implementing the developed control framework. This analysis involves the summation of various energy flows and electricity & fuel consumption of the system. These provide insight to the GHG emissions reduction and energy utilization improvement resulting from the operation of the control system. A summary of these metrics is presented in Table 5.2 at the end of this section, in addition to the graphical representations to be presented throughout. Comparison is made between the ICE-Harvest system operating with the developed control framework and business-as-usual (BAU). The BAU case represents the operation of conventional DE systems, in which heating and cooling demands are met entirely by NGBs and electric chillers, respectively, and electrical demands are met only by grid power. The comparison of cumulative thermal energy for heating broken down by source in each case is depicted by Figure 5.19.

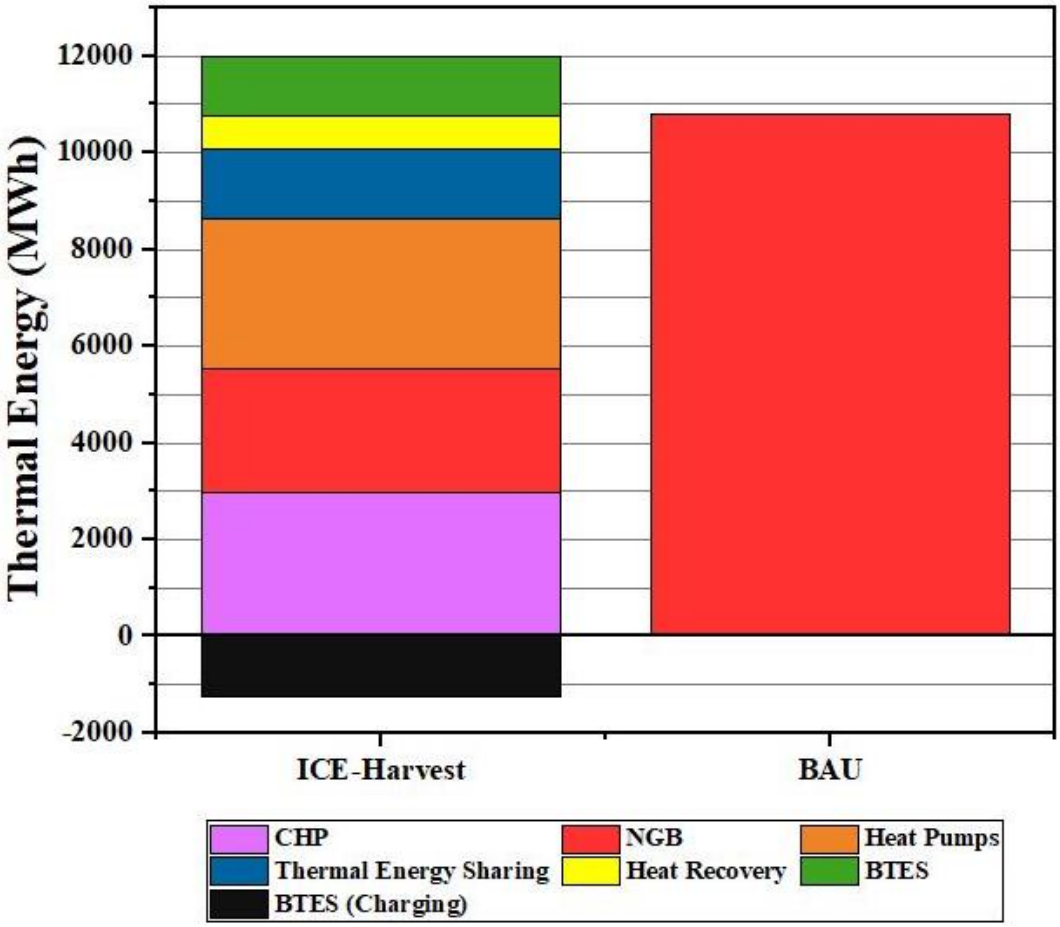

Fig.5.19: Cumulative thermal energy from heating systems in ICE-Harvest and BAU cases

It can be seen from the above figure that the ICE-Harvest system operation results in a significant reduction of NGB heat provided when compared to the BAU case. The total heating demand of the buildings in the system is 10808 MWh, which is entirely supplied by NGBs in the BAU case, since they are the only source of heat in that scenario. To meet the same demand, the ICE-Harvest system provides thermal energy with a variety of sources, which results in only 2550 MWh of heating provided by the NGB. This represents a reduction of thermal energy provided via NGB of over 76%. This reduction is accomplished by the ICE-Harvest system solely through utilizing off-peak electricity to

harvest waste heat from cooling processes and harvesting waste heat from peaking power generation on site.

It can also be observed that in the ICE-Harvest case there is a cumulative thermal energy value which is negative associated with charging the BTES. As mentioned in previous sections, the BTES imposes a thermal energy demand on the system during charging which is equal to the energy that can be provided by the CHP or heat pump beyond what is required by the MTN. Therefore, the total thermal energy demand of the system increases, and the cumulative thermal energy from producers in the ICE-Harvest case increases as well. However, the geothermal storage also provides thermal energy during the winter months when it is discharging, which largely offsets the increase of cumulative demand created by charging. It can be seen from Figure 5.19 that the net effect of the geothermal storage operation is minimal, and thermal energy demand over the course of the year is similar for both cases. It should also be noted that the total amount of thermal energy stored, which is presented in Figure 5.19, does not include the geothermal field energy losses. Therefore, it represents the amount of thermal energy stored which is actually retained by the field and utilized by the system to provide heat.

It is clear from this and previous sections that the ICE-Harvest system differs greatly from conventional DE systems in the way that it provides thermal energy for heating. However, the ICE-Harvest system meets cooling demand in much the same way as in the BAU case. The difference of the ICE-Harvest system operation is that thermal energy is harvested from the heat rejected by cooling processes at the buildings. Therefore, the value of the ICE-Harvest system in this regard is not in how cooling is provided, but in the ability to utilize waste heat and transform it into a valuable thermal energy resource for

the system. A comparison of the cumulative thermal energy flows resulting from cooling process heat for each case is depicted in Figure 5.20.

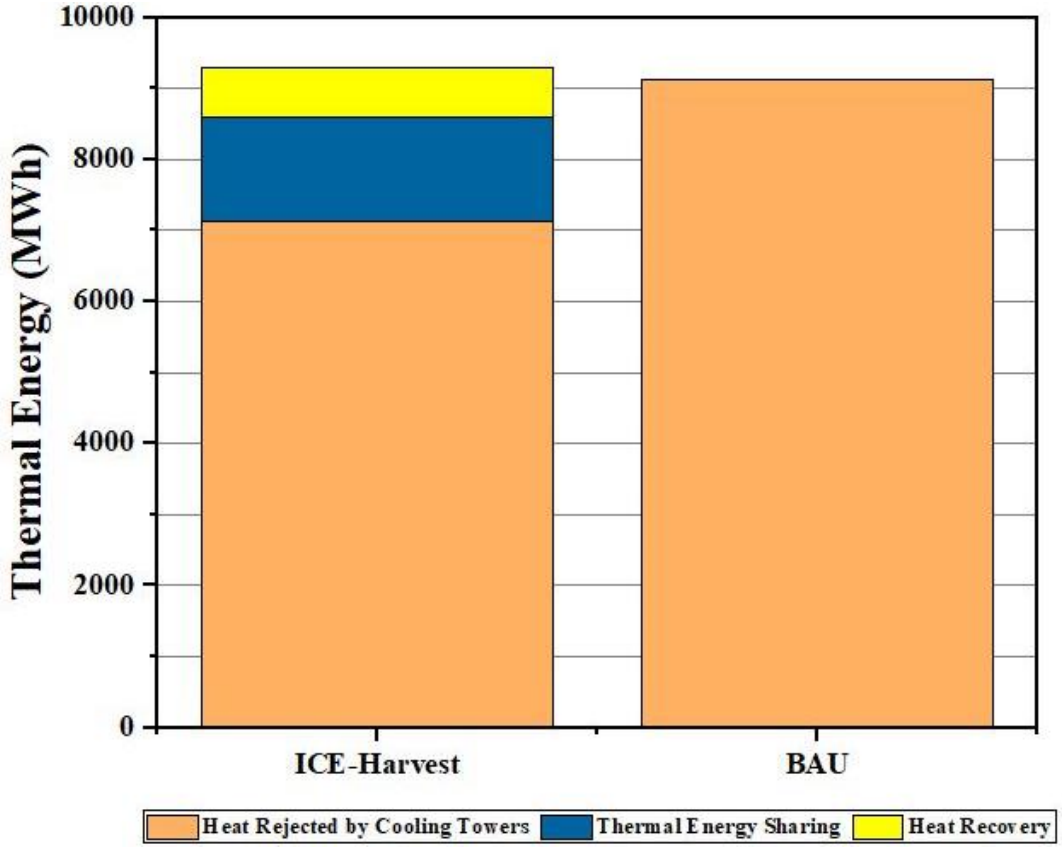

Fig.5.20: Cumulative thermal energy from cooling processes in ICE-Harvest and BAU cases

The above figure demonstrates that the operation of the ICE-Harvest system reduces the amount of heat rejected by building cooling towers by harvesting approximately 2100 MWh of cooling process heat. This represents a reduction in wasted heat by the system of approximately 24%. This harvested thermal energy is first utilized for thermal energy sharing between buildings up to the point at which their heating demands are entirely met. Any remaining heat is then transferred to the warm header of the EMC to be stored in the geothermal field. As mentioned in previous chapters, one of the functions of the developed control framework is to utilize heat pumps to recover as much

thermal energy as possible from cooling processes during off-peak periods on the Ontario grid. However, the majority of cooling process heat still goes unrecovered in the ICE-Harvest case. This is due to multiple factors, including the operation of centralized natural gas peaking power plants and the occurrence of simultaneous heating and cooling demands.

For the reference year used in the case study, natural gas peaking power plants were dispatched for a total of 3369 hours, which also means that cooling process heat could only be harvested for 5391 hours. As a result, the maximum amount of heat that can be harvested is limited to approximately 61.5% of the total cooling process heat available over the course of the year. The amount of heat harvested compared to the available cooling process heat is further reduced by the limitations of thermal energy sharing and heat recovery. Since thermal energy sharing is limited by the overall heating demand of the buildings, the amount of cooling process heat that can be harvested in this way is also limited. Residual thermal energy available from cooling must then be recovered by the MTN and transferred to the EMC, the amount of which is also limited. The amount of heat which can be transferred to the warm header depends on its temperature and the amount of thermal power that the BTES can currently absorb, which is based on its state of charge. The temperature of the geothermal field relative to that of the hot header will determine the thermal power which can be transferred into it. In turn, this influences the amount of thermal power that the heat pump is able to extract from the warm header for charging, which influences the header temperature. Therefore, the state of charge of the geothermal field limits the amount of thermal energy which can be transferred from the MTN to the EMC.

The effect of these limitations can be observed in the thermal power setpoints for the heat recovery heat pumps at each building, which vary throughout the case study

depending on the season. During the heating season, the thermal power setpoint of the heat recovery heat pumps is consistently 60%, while the setpoint varies between 5% and 40% during the cooling season. These selections were made through simulation of the system model in an iterative process to determine the highest thermal power setpoints which would not cause extreme temperature increases in the MTN. The result is that the average thermal power setpoint for the heat recovery heat pumps over the entire year is approximately 48% of the heat available from cooling. This means that the overall limit of thermal energy that can be recovered is approximately 29% of the total available cooling process heat over the entire year.

Comparing the amount of thermal energy harvested from cooling processes over the year with the 29% limit, there is a discrepancy equal to 5% of the total available cooling process heat. This discrepancy results from the variable temperature of the MTN. Since the temperature of the MTN varies not only at the supply and return points, but also at the connection points of each building ETS, the COPs of building heat pumps can be reduced. Depending on the relative magnitudes of overall building heating and cooling demands, the temperature of the fluid in the MTN can increase by variable amounts as it traverses the network. Since the COP of a heat pump degrades as the temperature difference between its inlets increases, higher fluid temperatures on the network side will decrease the COPs of the heat recovery heat pumps accordingly. When this occurs, it is possible for the controllers operating the heat recovery heat pumps to become saturated and hit the upper limit of their control range. This causes the heat pump to recover less thermal energy because it has reached its maximum output. Despite this, the control framework performs well in this regard since it is able to recovery 24% of a possible 29% of the total cooling

process heat that results from building cooling processes. This means that the system is able to harvest over 80% of the cooling process thermal energy which is realistically obtainable within the limitations of the case study and those of the system itself.

From the results presented in this section so far, it is clear that the developed control framework operates as it was designed to. The implemented control principles produce the desired effect and result in a tangible difference in the operation of the ICE-Harvest system when compared to BAU. The unique operation of the ICE-Harvest control system also results in significant differences in energy consumption. This is apparent from the total electricity and fuel consumptions for the entire year, depicted in Figure 5.21.

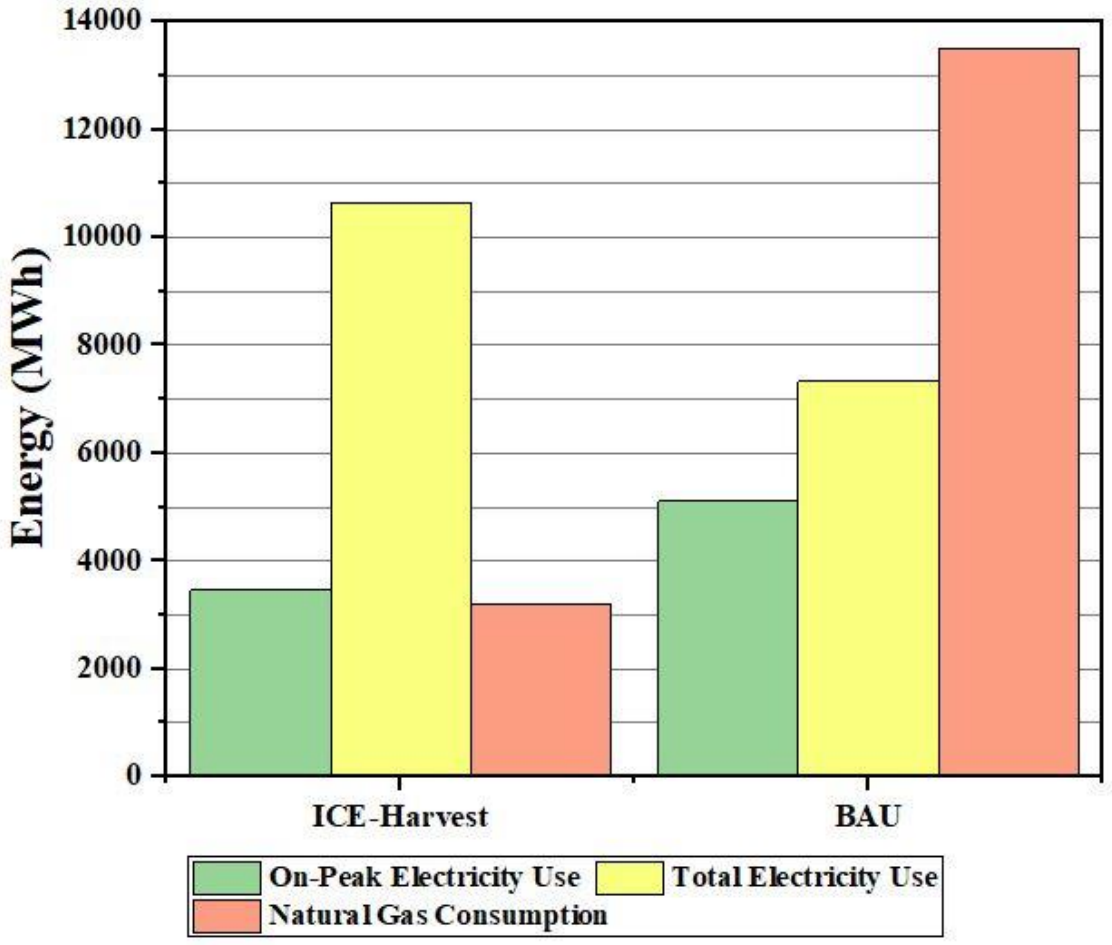

Fig.5.21: Total electricity and fuel consumptions in ICE-Harvest and BAU cases

It can be observed from Figure 5.21 that the ICE-Harvest system operation results in a reduction in all but one of the quantities depicted. The total electricity consumption of the ICE-Harvest system is greater than the BAU case, which is to be expected due to the use of heat pumps at the EMC and building ETSs. However, the on-peak electricity consumption is reduced in the ICE-Harvest case since the ICE-Harvest system primarily uses off-peak electricity to operate its heat pumps and generates electricity during peaks with the CHP. There is still some on-peak electricity consumption in the ICE-Harvest case due to the operation of heating and cooling heat pumps which cannot be shut down and the non-thermal electrical loads of buildings. It can also be seen that the consumption of natural gas is significantly reduced by the operation of the ICE-Harvest system. This is due to the operation of the CHP as a peaking power plant, and the utilization of off-peak electricity in heat pumps to both recover thermal energy from cooling processes and electrify heating at the EMC. Since the CHP produces no additional GHG emissions compared to the status quo of the Ontario grid, the thermal energy harvested from it proportionately reduces the consumption of natural gas by the system.

The harvesting of cooling process heat during off-peak periods accomplishes a similar effect to the operation of the CHP during peaks. The thermal energy sharing and heat recovery resulting from thermal energy harvesting from cooling processes facilitate a reduction in the net thermal energy demand seen by the EMC and MAS. Therefore, the need for heat from the NGB is reduced during the off-peak periods, thereby reducing the consumption of natural gas as well. The overall result depicted by Figure 5.21 is that the ICE-Harvest system increases the total electricity use and operates the CHP as a peaking power plant in order to reduce both natural gas consumption and on-peak electricity use,

as well as take advantage of otherwise curtailed renewable electricity. The ICE-Harvest system delivers the same amount of thermal and electrical energy to the buildings as a conventional system, while consuming approximately 34% less total energy. This represents an increase in energy utilization from 56% in the BAU case to 85% in the ICE-Harvest case. Since the combustion of natural gas and use of on-peak electricity are associated with GHG emissions, these reductions are critical to the goal of the ICE-Harvest system to reduce GHG emissions while considering the impact to the Ontario grid. The total GHG emissions produced by the ICE-Harvest and BAU systems for the proposed case study are depicted in Figure 5.22.

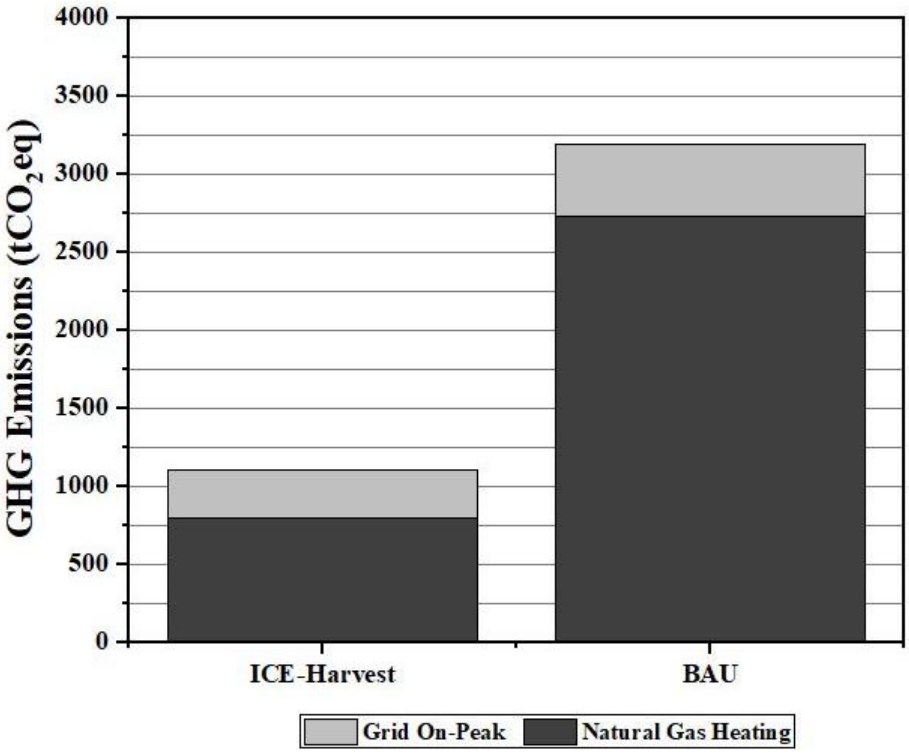

Fig.5.22: Total GHG emissions by source in ICE-Harvest and BAU cases

It can be seen from the above figure that the operation of the ICE-Harvest system results in lower GHG emissions from both on-peak grid power use and natural gas

consumption. This results in the reduction of total GHG emissions from 3192 tCO_2eq to 959 tCO_2eq, which represents a reduction of nearly 70% compared to the BAU system [81], [82]. A reduction in GHG emissions of this magnitude represents a significant step toward reaching Canada's climate targets. With the developed control framework, the ICE-Harvest system not only exceeds the 2030 goal of 40% reduction in GHG emissions, but also provides a pathway to further GHG emissions reductions through the potential for further development of the control system.

Table 5.2: ICE-Harvest System Energy Metrics

Metric	**Value (MWh)**
EMC Thermal Energy Generation	8387
Thermal Energy Delivery to MTN	7145
Thermal Energy Harvested in MTN	2157
Thermal Energy Sharing in MTN	1457
Heat Recovery from MTN	700
Available Cooling Process Heat	9120
Heat Rejected by Cooling Towers	7133
On-Peak Electricity Consumption	3456
Off-Peak Electricity Consumption	7177
Natural Gas Consumption	3187

Chapter 6

Conclusions and Future Work

6.1 Conclusions of the Case Study

This thesis presented the development of an advanced control framework for the ICE-Harvest system and the application of it in a realistic case study. The development process began with a thorough literature review of the structure and control of thermal and electrical energy distribution systems. This included a brief history of DE systems from their infancy to the current state-of-the-art, and the control frameworks that have been utilized in conventional and modern systems. One of the critical outcomes of this review was that the topic of control in modern DE systems has not been extensively researched. As a result, topics in state-of-the-art control algorithms were included in the literature review as well. These included advanced system modelling and optimization techniques,

and various centralized and distributed control structures. From the insights gained through review of the literature, a control structure for the ICE-Harvest system was conceptualized which was primarily based on the concept of MAS. This type of control structure was selected due to its robustness, adaptability and expandability, as well as its ability to be applied to a variety of systems and to implement desirable features. The MAS was combined with sequential logic and conventional methods of control to enhance its performance and provide functions which further the implementation of the ICE-Harvest operating philosophy.

A detailed model of the control framework and ICE-Harvest system was then developed with Dymola and utilized in a case study based on the implementation of an ICE-Harvest system for a set of real buildings in Ontario. The case study involved the simulation of the model using the actual heating, cooling and electricity demands of the buildings and the run-hours of natural gas peaking generators on the Ontario grid for the 2017 reference year as input. The results obtained from the case study were then analyzed in multiple ways. This included analysis over short-term & long-term durations and a comparison of the cumulative performance of the ICE-Harvest system and control framework against the status quo. The analysis provided several key insights to the effect of seasonal phenomena, such as variation in energy demand and peaking power plant operation, as well as the effect of system dynamics on real-time behaviour of the control framework. The comparison between ICE-Harvest and the status quo demonstrated the potential improvements in GHG emissions and energy utilization which are realized by the developed control framework.

Ultimately, the outcome of this work is a blueprint for implementation of an advanced control framework suitable for the ICE-Harvest system. The proposed control system is able to make the principles of the ICE-Harvest system a reality and lays the foundation for commercial deployment and further innovation. As new technological developments are made in the area of community energy systems and the ICE-Harvest methodology is applied to more and more sites in Ontario, the control structure presented in this work can and will continue to grow and change as well.

6.2 Recommendations for Future Work

The control framework developed for the ICE-Harvest system as a result of this research is rife with potential to be further developed. Various additional features which are believed to be desirable for the operation of the ICE-Harvest system beyond those implemented in this work have been identified. Additionally, as the ICE-Harvest system itself continues to develop, the current iteration of the control framework will need to be modified as well, to maintain the level of performance that was achieved in this thesis. These developments have the potential to further improve energy utilization and GHG emissions in future iterations of the ICE-Harvest system.

When considering the potential for additional features in the ICE-Harvest system and control framework, an immediately obvious alternative is to increase use of carbon-free renewable energy sources in the thermal and electrical parts of the system. Naturally, an energy generation mix that is higher in carbon-free renewable sources will contribute to the goal of reducing GHG emissions. Renewable electricity generation can also be utilized to supplement or offset use of the peaking CHP and provide some flexibility to operate

heat pumps during electrical peaks, without the associated increase in GHG emissions. This leads to greater opportunity for harvesting cooling process heat which can reduce GHG emissions even further.

Another potential development for the system is to increase the temperature limit of the BTES. This would allow for direct heat exchange during the early portion of the discharging phase, enabling the BTES to provide thermal energy without the use of the heat pump. As a result, the BTES would be able to offset use of the NGB during the electrical peaks. A larger range of allowable temperatures would also increase the amount of thermal energy which can be stored during the charging phase. To accommodate these changes, the SLCs would require adjustment to effectively manage the connection and operation of the BTES in this case. These improvements would result in further reduction of GHG emissions and increased flexibility, with some additional complexity for the control framework.

The potential future works that have been discussed so far are focused primarily on the EMC and its operation. There are a number of potential developments that can be implemented in the structure and operation of the MTN as well. In this work, the case study focused on the application of the ICE-Harvest methodology to a UTN only. However, the operating principles of the ICE-Harvest system can be applied to BTNs and conventional four-pipe networks. For either of these network topologies, the thermal energy demand of the MTN, as well as the connection of buildings to it will change. This presents different opportunities for thermal energy harvesting in the MTN. The increased number of pipelines associated with these network topologies can provide increased controllability and flexibility to the system. However, the use of multiple pipelines results in a substantial

increase in capital cost for these types of systems. Analysis of the ICE-Harvest system's performance with these types of thermal networks could reveal that the potential financial and non-financial benefits outweigh the increased cost.

In the network topologies discussed, there also exists the potential to operate the network at a variable temperature setpoint. In the case study presented in this thesis, the supply temperature setpoint for the MTN was kept constant at 35 °C, while the temperature is allowed to vary throughout the rest of the network based on the operation of the ETS heat pumps. This limits the typical variation of fluid temperature as it traverses the network to a small range. By allowing the system to change the supply temperature setpoint of the MTN, the range of possible temperatures throughout the pipeline becomes larger. This would facilitate further development of the ETSs by allowing for increased functionality. The ETS of each building could be equipped with both heat exchangers and heat pumps for heating and cooling. If the network temperature setpoint can be adjusted, it is possible to accomplish direct heat exchange at times when it is advantageous. For example, the use of direct heat exchange can reduce the consumption of on-peak electricity required for heating. In addition to heat exchangers, the ETSs could also be equipped with thermal energy storage to provide increased flexibility as well. Adding STES at each ETS would allow for excess thermal energy to be stored and used to offset heating heat pump use during electrical peaks. Therefore, utilizing these technologies in the ETSs would reduce the GHG emissions produced by the system, while increasing the energy utilization.

It naturally follows that the potential future developments of the EMC and MTN discussed would require the ICE-Harvest control system to develop in a similar fashion. The MAS, SLCs and Auxiliary Controllers would require adjustments with each energy

producer or storage unit added to the system, and a major adjustment to utilize a different network topology in the system. There are also several developments to the control framework with the potential to improve the performance of the system analyzed in this work. There is much potential for further development of the control framework on the part of the MAS. For the system presented in this thesis, agents were only utilized to represent the energy producers used for heating. This means that the other units in the system are not being directly controlled by the MAS. The overall operation of the control framework would be improved as a larger portion of energy producing and storage units in the system are communicating within the MAS. This would require the development of agents to represent both short-term and seasonal thermal energy storage. For example, thermal storage units act as either a source or a sink of thermal energy, and the thermal capacity of storage varies based on its temperature relative to that of the connected system. This means that an agent is needed which can provide a sufficiently accurate estimation of thermal power that can flow to or from the storage unit, as well as its state of charge. Any energy producing or storage units with different dynamics to those already in the system would also require the development of agents to represent them as well. For example, to incorporate solar thermal generation in the ICE-Harvest system, the corresponding agent would need to properly communicate its capacity to provide thermal energy, while considering variability of sunlight. To integrate agents such as this into the MAS would require similar work for each new piece of equipment.

Furthermore, agents could also be used to represent the heat recovery heat pumps in the system. These would estimate the amount thermal energy sharing and heat recovery that is possible at each negotiation time for the MAS. This would allow the buildings in

the MTN to bid into the negotiation process to provide thermal energy for their neighbours and the EMC. However, this highlights another modification that would need to be made. Since the temperature setpoint of the EMC and MTN are different, they cannot be controlled by the MAS simultaneously. This is because a single MAS can only target one temperature setpoint. Therefore, an additional MAS would be required to manage the heat recovery heat pumps and control the temperature of the MTN. This functionality could also be expanded to include the potential addition of STES units at each building as mentioned previously. Similar modifications would also be required for the system to utilize a different network topology. Since other topologies use centralized energy producers to provide heating and cooling, these types of system also require multiple MASs to target the temperature setpoints for heating and cooling. The MASs would operate independently from each other, one controlling the heating equipment and the other controlling the cooling equipment.

Naturally, the adaptable nature of the MAS allows for multiple of the aforementioned developments to be accomplished simultaneously in future iterations of the control framework. There are synergies between the various potential features, which when combined, can further improve the performance of the control framework. This represents an interesting direction to pursue for future research and analysis.

As the control framework continues to develop, it is not only the MAS which can be improved through additional features. Various potential developments can be made to the upper layer as well. The SLCs that were utilized in this part of the control framework can be replaced in favour a more sophisticated type of control. The discrete nature of the SLCs results in a finite number of operating points while it is possible that at any given

time, the optimal operating point of the system is somewhere between two of the discrete states of the SLC. Therefore, some form of supervisory control which allows for a continuous range of setpoints for the MAS can be implemented improve the performance and flexibility of the system. The actions of the SLCs are also governed by a predefined set of conditions which do not necessarily result in optimal performance at all times. For example, the threshold for maximum allowable CHP output required for a temperature setpoint increase is a constant value and is not optimal for all situations. Additionally, the possible functionality of each SLC is limited because the conditions for transition between states are limited in complexity. These do not have the ability to incorporate predictions of future behaviour or corrections resulting from past behaviour of the system. As a result of these factors, the ICE-Harvest control system could benefit from a supervisory layer that utilizes optimization, machine learning or other intelligent forecasting techniques.

The potential future works discussed regarding the control framework have focused on the development of new features to increase functionality, and modifications that allow for incorporating a wider variety of energy generation and storage units. In order to realize the potential benefits resulting from these developments, the control framework presented in this work must be implemented in a real ICE-Harvest system and its performance analyzed in this context. The case study presented has demonstrated that the developed control framework can effectively manage the dynamics of the ICE-Harvest system, and provide the potential to improve energy utilization and reduce GHG emissions. However, the control framework presented in this thesis and the ICE-Harvest system must be implemented in communities and continuously innovated to move towards a carbon-free future.

References

[1] IPCC, *Climate Change 2014 Part A: Global & Sectoral Aspects*. 2014.

[2] IPCC, *Climate Change 2014 Part B: Regional Aspects*. 2014.

[3] J. P. Reser and J. K. Swim, "Adapting to and Coping With the Threat and Impacts of Climate Change," *Am. Psychol.*, vol. 66, no. 4, pp. 277–289, 2011, doi: 10.1037/a0023412.

[4] United Nations, "Report of the secretary-general on the 2019 climate action summit and the way forward in 2020," no. December 2019, 2019.

[5] N. Höhne *et al.*, "Wave of net zero emission targets opens window to meeting the Paris Agreement," *Nat. Clim. Chang.*, vol. 11, no. 10, pp. 820–822, 2021, doi: 10.1038/s41558-021-01142-2.

[6] Environment and Climate Change Canada, "2030 EMISSIONS REDUCTION PLAN Canada's Next Steps for Clean Air and a Strong Economy."

[7] W. F. Lamb *et al.*, "A review of trends and drivers of greenhouse gas emissions by sector from 1990 to 2018," *Environ. Res. Lett.*, vol. 16, no. 7, 2021, doi: 10.1088/1748-9326/abee4e.

[8] A. Mathur, U. Singh, Y. K. Vijay, M. Hemlata, and M. Sharma, "Analyzing Performance for Generating Power with Renewable Energy Source using Rice Husk as an Alternate Fuel," vol. 3, no. 2, pp. 64–71, 2013.

[9] J. Milano *et al.*, "Microalgae biofuels as an alternative to fossil fuel for power generation," *Renew. Sustain. Energy Rev.*, vol. 58, pp. 180–197, 2016, doi: 10.1016/j.rser.2015.12.150.

[10] T. A. Semelsberger, R. L. Borup, and H. L. Greene, "Dimethyl ether (DME) as an alternative fuel," *J. Power Sources*, vol. 156, no. 2, pp. 497–511, 2006, doi: 10.1016/j.jpowsour.2005.05.082.

[11] M. C. Lee, S. Bin Seo, J. H. Chung, Y. J. Joo, and D. H. Ahn, "Industrial gas turbine combustion performance test of DME to use as an alternative fuel for power generation," *Fuel*, vol. 88, no. 4, pp. 657–662, 2009, doi: 10.1016/j.fuel.2008.10.027.

[12] S. R. Bull, "Renewable energy today and tomorrow," *Proc. IEEE*, vol. 89, no. 8, pp. 1216–1226, 2001, doi: 10.1109/5.940290.

[13] G. Crabtree *et al.*, "IntegratingRenewableElectricity.pdf," vol. 19, no. 11, 2010.

[14] D. Ürge-Vorsatz, L. D. D. Harvey, S. Mirasgedis, and M. D. Levine, “Mitigating CO2 emissions from energy use in the world’s buildings,” *Build. Res. Inf.*, vol. 35, no. 4, pp. 379–398, 2007, doi: 10.1080/09613210701325883.

[15] A. Allouhi, Y. El Fouih, T. Kousksou, A. Jamil, Y. Zeraouli, and Y. Mourad, “Energy consumption and efficiency in buildings: Current status and future trends,” *J. Clean. Prod.*, vol. 109, pp. 118–130, 2015, doi: 10.1016/j.jclepro.2015.05.139.

[16] Y. Geng *et al.*, “A bibliometric review: Energy consumption and greenhouse gas emissions in the residential sector,” *J. Clean. Prod.*, vol. 159, no. 800, pp. 301–316, 2017, doi: 10.1016/j.jclepro.2017.05.091.

[17] L. D. D. Harvey, “Reducing energy use in the buildings sector: Measures, costs, and examples,” *Energy Effic.*, vol. 2, no. 2, pp. 139–163, 2009, doi: 10.1007/s12053-009-9041-2.

[18] K. Li, X. Xie, W. Xue, X. Dai, X. Chen, and X. Yang, “A hybrid teaching-learning artificial neural network for building electrical energy consumption prediction,” *Energy Build.*, vol. 174, pp. 323–334, 2018, doi: 10.1016/j.enbuild.2018.06.017.

[19] M. Aydinalp, V. Ismet Ugursal, and A. S. Fung, “Modeling of the appliance, lighting, and space-cooling energy consumptions in the residential sector using neural networks,” *Appl. Energy*, vol. 71, no. 2, pp. 87–110, 2002, doi: 10.1016/S0306-2619(01)00049-6.

[20] A. H. Neto and F. A. S. Fiorelli, “Comparison between detailed model simulation and artificial neural network for forecasting building energy consumption,” *Energy Build.*, vol. 40, no. 12, pp. 2169–2176, 2008, doi: 10.1016/j.enbuild.2008.06.013.

[21] J. Moon, S. Park, S. Rho, and E. Hwang, “A comparative analysis of artificial neural network architectures for building energy consumption forecasting,” *Int. J. Distrib. Sens. Networks*, vol. 15, no. 9, 2019, doi: 10.1177/1550147719877616.

[22] J. W. Moon and J. J. Kim, “ANN-based thermal control models for residential buildings,” *Build. Environ.*, vol. 45, no. 7, pp. 1612–1625, 2010, doi: 10.1016/j.buildenv.2010.01.009.

[23] J. E. Braun, “Load control using building thermal mass,” *J. Sol. Energy Eng. Trans. ASME*, vol. 125, no. 3, pp. 292–301, 2003, doi: 10.1115/1.1592184.

[24] M. Rashad, N. Khordehgah, A. Żabnieńska-Góra, L. Ahmad, and H. Jouhara, “The utilisation of useful ambient energy in residential dwellings to improve thermal comfort and reduce energy consumption,” *Int. J. Thermofluids*, vol. 9, 2021, doi: 10.1016/j.ijft.2020.100059.

[25] G. Gao, J. Li, and Y. Wen, “DeepComfort: Energy-Efficient Thermal Comfort Control in Buildings Via Reinforcement Learning,” *IEEE Internet Things J.*, vol.

7, no. 9, pp. 8472–8484, 2020, doi: 10.1109/JIOT.2020.2992117.

[26] J. Ock, R. R. A. Issa, and I. Flood, “Smart building energy management systems (BEMS) simulation conceptual framework,” *Proc. - Winter Simul. Conf.*, vol. 0, pp. 3237–3245, 2016, doi: 10.1109/WSC.2016.7822355.

[27] D. Urge-Vorsatz, K. Petrichenko, M. Staniec, and J. Eom, “Energy use in buildings in a long-term perspective,” *Curr. Opin. Environ. Sustain.*, vol. 5, no. 2, pp. 141–151, 2013, doi: 10.1016/j.cosust.2013.05.004.

[28] EIA Energy Atlas, “World energy statistics & World energy balances,” p. 703, 2020.

[29] “Canada’s Energy Future Data Appendices,” 2017, doi: 10.35002/zjr8-8x75.

[30] B. Rezaie and M. A. Rosen, “District heating and cooling: Review of technology and potential enhancements,” *Appl. Energy*, vol. 93, pp. 2–10, 2012, doi: 10.1016/j.apenergy.2011.04.020.

[31] S. Buffa, M. Cozzini, M. D’Antoni, M. Baratieri, and R. Fedrizzi, “5th generation district heating and cooling systems: A review of existing cases in Europe,” *Renewable and Sustainable Energy Reviews*. 2019, doi: 10.1016/j.rser.2018.12.059.

[32] H. Lund *et al.*, “4th Generation District Heating (4GDH). Integrating smart thermal grids into future sustainable energy systems.,” *Energy*, vol. 68, pp. 1–11, 2014, doi: 10.1016/j.energy.2014.02.089.

[33] H. Lund, N. Duic, P. A. Østergaard, and B. V. Mathiesen, “Perspectives on Smart Energy Systems from the SES4DH 2018 conference,” *Energy*, vol. 190, pp. 4–7, 2020, doi: 10.1016/j.energy.2019.116318.

[34] H. Lund *et al.*, “The status of 4th generation district heating: Research and results,” *Energy*, vol. 164, pp. 147–159, 2018, doi: 10.1016/j.energy.2018.08.206.

[35] S. R. Jones *et al.*, “A system design for distributed energy generation in low-temperature district heating (LTDH) networks,” *Futur. Cities Environ.*, vol. 5, no. 1, pp. 1–11, 2019, doi: 10.5334/fce.44.

[36] A. Revesz *et al.*, “Developing novel 5th generation district energy networks,” *Energy*, vol. 201, p. 117389, 2020, doi: 10.1016/j.energy.2020.117389.

[37] B. Skagestad and P. Mildenstein, *District Heating and Cooling Connection Handbook - Programme of Research, Development and Demonstration on District Heating and Cooling*. 2002.

[38] T. Marlin, *Process Control*, 2nd ed. McGraw-Hill Education, 1995.

[39] S. F. Nilsson, C. Reidhav, K. Lygnerud, and S. Werner, “Sparse district-heating in Sweden,” *Appl. Energy*, vol. 85, no. 7, pp. 555–564, 2008, doi: 10.1016/j.apenergy.2007.07.011.

[40] H. Lund, N. Duic, P. A. Østergaard, and B. V. Mathiesen, “Future district heating systems and technologies: On the role of smart energy systems and 4th generation district heating,” *Energy*, vol. 165, pp. 614–619, 2018, doi: 10.1016/j.energy.2018.09.115.

[41] F. Bünning, M. Wetter, M. Fuchs, and D. Müller, “Bidirectional low temperature district energy systems with agent-based control: Performance comparison and operation optimization,” *Appl. Energy*, pp. 502–515, 2018, doi: 10.1016/j.apenergy.2017.10.072.

[42] L. F. Fuentes-Cortés, J. M. Ponce-Ortega, F. Napoles-Rivera, M. Serna-Gonzalez, and M. M. El-Halwagi, “Optimal design of integrated CHP systems for housing complexes.”

[43] L. F. Fuentes-Cortés and A. Flores-Tlacuahuac, “Integration of distributed generation technologies on sustainable buildings,” *Appl. Energy*, vol. 224, pp. 582–601, 2018, doi: 10.1016/j.apenergy.2018.04.110.

[44] Sargent & Lundy, “Capital Cost and Performance Characteristic Estimates for Utility Scale Electric Power Generating Technologies,” 2020.

[45] A. Arabkoohsar, “Non-uniform temperature district heating system with decentralized heat pumps and standalone storage tanks,” *Energy*, 2019, doi: 10.1016/j.energy.2018.12.209.

[46] L. Brange, J. Englund, and P. Lauenburg, “Prosumers in district heating networks - A Swedish case study,” *Appl. Energy*, vol. 164, pp. 492–500, 2016, doi: 10.1016/j.apenergy.2015.12.020.

[47] A. Hirsch, Y. Parag, and J. Guerrero, “Microgrids: A review of technologies, key drivers, and outstanding issues,” *Renew. Sustain. Energy Rev.*, vol. 90, no. September 2017, pp. 402–411, 2018, doi: 10.1016/j.rser.2018.03.040.

[48] R. Allen *et al.*, “Industrial Waste Heat Recovery Project - An Initiative of the Hamilton Chamber of Commerce,” Hamilton, Ontario, Canada.

[49] O. Miedaner, D. Mangold, and P. A. Sørensen, “Borehole thermal energy storage systems in Germany and Denmark – Construction and operation experiences,” in *GREENSTOCK 2015- The 13th International Conference on Energy Storage*, 2015, pp. 1–8.

[50] F. Ruesch and M. Haller, “Potential and limitations of using low-Temperature district heating and cooling networks for direct cooling of buildings,” *Energy Procedia*, vol. 122, pp. 1099–1104, 2017, doi: 10.1016/j.egypro.2017.07.443.

[51] G. Alva, Y. Lin, and G. Fang, “An overview of thermal energy storage systems,” *Energy*, vol. 144, pp. 341–378, 2018, doi: 10.1016/j.energy.2017.12.037.

[52] P. Nikolaidis and A. Poullikkas, “Cost metrics of electrical energy storage technologies in potential power system operations,” *Sustain. Energy Technol. Assessments*, vol. 25, no. August 2017, pp. 43–59, 2018, doi: 10.1016/j.seta.2017.12.001.

[53] R. Sangi, F. Bünning, J. Fütterer, and D. Müller, “A Platform for the Agent-based Control of HVAC Systems,” *Proc. 12th Int. Model. Conf. Prague, Czech Republic, May 15-17, 2017*, vol. 132, pp. 799–808, 2017, doi: 10.3384/ecp17132799.

[54] F. Bellifemine, G. Caire, and D. Greenwood, *Developing Multi-Agent Systems with JADE*. 2004.

[55] M. Wooldridge and N. R. Jennings, “Intelligent agents: theory and practice,” *Knowledge Eng. Rev.*, vol. 10, no. 2. pp. 115–52, 1995.

[56] A. Kantamneni, L. E. Brown, G. Parker, and W. W. Weaver, “Survey of multi-agent systems for microgrid control,” *Engineering Applications of Artificial Intelligence*, vol. 45. pp. 192–203, 2015, doi: 10.1016/j.engappai.2015.07.005.

[57] F. Bünning, R. Sangi, and D. Müller, “A Modelica library for the agent-based control of building energy systems,” *Appl. Energy*, vol. 193, pp. 52–59, 2017, doi: 10.1016/j.apenergy.2017.01.053.

[58] H. Van Dyke Parunak, “Industrial and Practical Applications of DAIH,” in *Multiagent systems: A Modern Approach to Distributed Artificial Intelligence*, 1999, pp. 377–421.

[59] F. Wernstedt, *Multi-agent systems for district heating management*. 2003.

[60] F. Wernstedt and P. Davidsson, “An agent-based approach to monitoring and control of district heating systems,” *Lect. Notes Comput. Sci. (including Subser. Lect. Notes Artif. Intell. Lect. Notes Bioinformatics)*, vol. 2358, no. June, pp. 801–811, 2002, doi: 10.1007/3-540-48035-8_77.

[61] B. Lacroix, L. Ines, and D. Mercier, “Multi-Agent Control of Thermal Systems in Buildings,” *Agent Technol. Energy Syst. Work.*, no. June 2012, 2012.

[62] S. Kolen, C. Molitor, L. Wagner, and A. Monti, “Two-level agent-based scheduling for a cluster of heating systems,” *Sustain. Cities Soc.*, vol. 30, pp. 273–281, 2017, doi: 10.1016/j.scs.2017.01.014.

[63] K. Gulzar, S. Sierla, V. Vyatkin, N. Papakonstantinou, P. G. Flikkema, and C. W. Yang, “An auction-based smart district heating grid,” *IEEE Int. Conf. Emerg. Technol. Fact. Autom. ETFA*, vol. 2015-Octob, pp. 1–8, 2015, doi: 10.1109/ETFA.2015.7301528.

[64] D. Geysen, P. Booij, and C. Warmer, “A framework for simulation and control of hybrid energy networks,” *ENERGYCON 2014 - IEEE Int. Energy Conf.*, pp. 989–995, 2014, doi: 10.1109/ENERGYCON.2014.6850546.

[65] C. Johansson and P. Davidsson, “Deployment of Agent Based Load Control in District Heating Systems,” *9th Int. Conf. Auton. Agents Multiagent Syst.*, no. April, pp. 75–82, 2010.

[66] H. Li and S. J. Wang, “Load Management in District Heating Operation,” *Energy Procedia*, vol. 75, pp. 1202–1207, 2015, doi: 10.1016/j.egypro.2015.07.155.

[67] A. Reilly and O. Kinnane, “The impact of thermal mass on building energy consumption,” *Appl. Energy*, vol. 198, pp. 108–121, 2017, doi: 10.1016/j.apenergy.2017.04.024.

[68] Z. Wang, L. Wang, A. I. Dounis, and R. Yang, “Multi-agent control system with information fusion based comfort model for smart buildings,” *Appl. Energy*, vol. 99, pp. 247–254, 2012, doi: 10.1016/j.apenergy.2012.05.020.

[69] R. Yang and L. Wang, “Development of multi-agent system for building energy and comfort management based on occupant behaviors,” *Energy Build.*, vol. 56, pp. 1–7, 2013, doi: 10.1016/j.enbuild.2012.10.025.

[70] P. Zhao, S. Suryanarayanan, and M. G. Simoes, “An energy management system for building structures using a multi-agent decision-making control methodology,” *IEEE Trans. Ind. Appl.*, vol. 49, no. 1, pp. 322–330, 2013, doi: 10.1109/TIA.2012.2229682.

[71] O. Van Pruissen, A. Van Der Togt, and E. Werkman, “Energy efficiency comparison of a centralized and a multi-agent market based heating system in a field test,” *Energy Procedia*, vol. 62, pp. 170–179, 2014, doi: 10.1016/j.egypro.2014.12.378.

[72] A. Vandermeulen, B. van der Heijde, and L. Helsen, “Controlling district heating and cooling networks to unlock flexibility: A review,” *Energy*. 2018, doi: 10.1016/j.energy.2018.03.034.

[73] E. Gunnlaugsson, G. Ívarsson, J. S. Friðriksson, and R. Energy, “85 Years of Successful District Heating in Reykjavík , Iceland,” *World Geotherm. Congr. 2015*, no. April, p. 9, 2015.

[74] J. Friedman and J. M. Friefeld, “United States Patent 4146057,” 1979.

[75] H. Xu, W. Y. Lin, F. Dal Magro, T. Li, X. Py, and A. Romagnoli, “Towards higher energy efficiency in future waste-to-energy plants with novel latent heat storage-based thermal buffer system,” *Renew. Sustain. Energy Rev.*, vol. 112, no. June, pp. 324–337, 2019, doi: 10.1016/j.rser.2019.05.009.

[76] "Generator Output by Fuel Type Hourly Report - 2017," 2018.

[77] M. Wetter, M. Bonvini, T. S. Nouidui, W. Tian, and W. Zuo, "Modelica Buildings Library," *J. Build. Perform. Simul.*, pp. 253–270, 2014, doi: 10.1080/19401493.2013.765506.

[78] D. Müller, M. Lauster, A. Constantin, M. Fuchs, and P. Remmen, "Aixlib - an Open-Source Modelica Library Within the IEA-EBC Annex 60 Framework," *Proc. CESBP Cent. Eur. Symp. Build. Phys. BauSIM 2016*, no. September, pp. 3–9, 2016.

[79] M. Otter and H. Elmqvist, "Modelica Language, Libraries, Tools and Conferences," *Simul. News Eur.*, no. June 2001, pp. 3–8, 2002.

[80] J. H. I. Lienhard and J. H. V Lienhard, *A Heat Transfer Textbook*, 5th ed. Cambridge, Massachusetts, USA: Phlogiston Press, 2020.

[81] A. Lorestani, J. Chebeir, M. Narimani, and J. S. Cotton, "Multi-objective Optimization of Integrated Community Energy and Harvesting (ICE-Harvest) System Based on Marginal Emission Factor," *2021 IEEE Int. Smart Cities Conf. ISC2 2021*, 2021, doi: 10.1109/ISC253183.2021.9562882.

[82] TAF, "A Clearer View on Ontario's Emissions: Electricity emissions factors and guidelines," *Atmos. Fund*, pp. 1–26, 2019.